ABSTRACT

Title of Dissertation: FORMATION AND DESTRUCTION
OF CARBON MONOXIDE IN COMETARY COMAE

Donna Michelle Pierce, Doctor of Philosophy, 2006

Dissertation directed by: Professor Michael F. A'Hearn
Department of Astronomy

This dissertation examines the potential impact of chemical reactions and outflow behavior on the chemical development of the coma within one of the most challenging problems in cometary chemistry – identifying the source of extended CO as observed in the comae of some comets. Could chemical reactions and/or outflow behavior contribute significantly to the CO abundance? In these studies, the impact of multiple photochemical processes and two-body chemical reactions are examined within a variety of cases designed to examine the effects of nuclear chemical composition and coma physics, including the dynamics of gas emanating from a region of large-scale negative relief topography.

The results show that two-body chemical reactions can contribute as much as 30% to the formation of CO and as much as 60% of the loss of CO within the inner coma, depending on the production rate. Furthermore, the fractional

contribution of chemical reactions to CO formation and destruction depends on the outflow behavior. However, the overall result suggests that chemical reactions only contribute a small net gain of CO ($\sim$5%) over the CO produced solely by photochemistry. The effects of chemical reactions and outflow behavior are more important, however, to secondary species formed exclusively in the coma.

The results also indicate that H_2CO is the primary contributor to the extended CO source in comet Halley. Observations of H_2CO in comet Halley suggest that it most likely comes from an extended source as well. The extended source problems of CO and H_2CO may be linked, in which case the precursor to H_2CO would gradually produce H_2CO after its release from the nucleus for it to form CO on the observed spatial scale. Such precursors could be large organic molecules, or grains rich in formaldehyde polymers that thermally dissociate upon heating. More difficult to explain, however, is the CO abundance in comet Hale-Bopp, for which the observed H_2CO abundance is insufficient to explain the observed CO abundance.

FORMATION AND DESTRUCTION
OF CARBON MONOXIDE IN COMETARY COMAE

by

Donna Michelle Pierce

Dissertation submitted to the Faculty of the Graduate School of the
University of Maryland, College Park in partial fulfillment
of the requirements for the degree of
Doctor of Philosophy
2006

Advisory Committee:

Professor Michael F. A'Hearn, Chair
Professor Millard H. Alexander
Professor Paul D. Feldman
Professor Douglas P. Hamilton
Professor J. Patrick Harrington
Dr. Michael J. Mumma

DEDICATION

To My $1s^2$ Electrons:

Mom and Dad

ACKNOWLEDGEMENTS

Although this dissertation is primarily my own work, others have left a mark on it in one way or another. My appreciation goes to the following:

Mike A'Hearn, my advisor, who deserves to be thanked many times over for his patience (and funding). I feel truly honored to have been one of his students and to have witnessed the entire *Deep Impact* saga from start to finish. I also want to thank him for being especially good to me throughout my complicated recovery from pulmonary embolism.

Funding from the *Deep Impact* mission (grant NASW00004), part of NASA's Discovery Program.

Mike Combi, for providing me with data from his simulations of the coma of comet Halley and the HST GHRS Lyman α spectra of comet Hyakutake.

Jean-François Crifo, for providing me with the data and interpretive programs from his simulations of the coma around a kidney-bean shaped nucleus.

Mike DiSanti, for providing me with CO data from Hale-Bopp.

Derek Richardson and Bill Jackson, for critically reading through an early version of Chapter 2 and providing me with valuable feedback on modeling.

Committee members Paul Feldman, Doug Hamilton, and Mike Mumma for feedback on the dissertation.

Various colleagues, including Marla Moore, Reggie Hudson, Amy Lovell, Bob Glinski, Steve Rodgers, Steve Charnley, Walter Huebner, and Dominique Bockelée-Morvan for helpful discussions pertaining to the dissertation.

Matthew Knight for helping me submit my final paperwork to the Registrar.

My office partners: Woong-Tae Kim, Ji Hoon Kim, Jianyang Li, Stef McLaughlin, Olivier Groussin, and Jessica Sunshine, for putting up with me, especially in the end when I was hoarding boxes in the office for my move to Texas.

To those who regularly donated food to me, especially Dorothea Zitta and Anne Raugh.

To the departmental staff for keeping the department running smoothly.

The physics and astronomy faculty at the University of Kentucky, especially Keith MacAdam, Mike Cavagnero, and my former advisor, Mike Kovash.

My close friends in Maryland: Liz Tobey, who is *the* definition of altruism. Maria Day, who is always looking for novel projects to try. Leslie Brice, who *really* needs to write a book about her adventures

in Haiti. The wise Ann Wagner, who probably knows everything I don't. Jim Marshall, for allowing me to vent my frustrations over the years.

My other friends and roommates: Evelyn Chia, Julia Yon Lutz, Kathy Tin, Chengbin Yin, and Yanyu Zhou for food, fun, and lively conversations. Also thanks to Gretchen Walker, Laura Woodney, Casey Lisse, Tony Farnham, Boncho Bonev, Linda Newman, and the late Beth Holmes for giving me extra motivation.

Most of all: my parents, for allowing me to indulge all of my interests since childhood, and my brother, William, for his support and lots of fun late-night conversations on my visits home.

Thanks also go to my non-human friends for contributions that are uniquely their own:

- The cats: Morris, Dusty, Tigger, Anouk, Ya-ong-i, Palette, Greygirl, Socks, Dart, and Kirby.
- Liz Tobey's cat, Tartuca, gets special mention for staying by my side for two whole weeks after my hospitalizations. She was one of the very few bright spots from that time.
- The dogs: Tasha, Pepper, Honey Girl, Peanut, and Sebastian.
- My aquatic friends: Halley, Hale-Bopp, Hyakutake, Tempel, Bennett, Encke, Gaspra, Dactyl, Sco the algae eater, and Oort the snail.

TABLE OF CONTENTS

LIST OF TABLES

LIST OF FIGURES

Chapter 1

Introduction

Comets hold a special place in the realm of scientific phenomena because they have both widespread popular appeal and hold potentially valuable scientific information – factors which are intricately linked with history. In the history of human events, comets have often been linked in the public mind with doom and destruction. In natural history, comets are believed to have best preserved a record of the conditions present in the outer Solar System at the time of their formation. It is the latter which forms the basis of cometary science today.

1.1 The Role of Chemistry in Cometary Science

The primary goal of cometary science is understanding the physical and chemical properties of cometary nuclei. However, this goal is exceptionally difficult to achieve due to the small size of the nuclei (a few kilometers to a few tens of kilometers in size), their low albedos (typically a few percent), and the comae which form as the ices are heated when they reach the inner Solar System. As a result, most of what is known about comets comes from studies of comae. Therefore, it is crucial to understand the physical and chemical properties of the

coma in order to understand the chemical and physical structure of the nucleus.

1.1.1 Solar System Formation

Why is it important to understand the properties of cometary nuclei? Throughout the Solar System there is chemical diversity, indicative of the temperature gradient that would have been present in the solar nebula during the Solar System's formation. Because cometary nuclei have small masses, they do not gravitationally collapse to form spherical bodies like the planets, thus their interiors have not been subjected to the physical processes which would significantly alter their chemical composition. Therefore, the chemical composition of the interiors of cometary nuclei should preserve a record of the conditions present at the time and place of their formation.

The more abundant species in cometary comae include water (H_2O), carbon monoxide (CO), carbon dioxide (CO_2), methanol (CH_3OH), methane (CH_4), acetylene (C_2H_2), and ethane (C_2H_6). These species are volatile, having sublimation temperatures of a few tens of Kelvins, suggesting a cold formation environment. It is generally believed that comets formed in the region of the giant planets and beyond, which is consistent with a volatile-rich composition. Many of the comets were then dynamically ejected from this region, and the fraction of cometary material that remained bound to the Solar System is found in two reservoirs today: the Kuiper Belt and the Oort Cloud (Gladman 2005; Gomes et al. 2005). Subsequent dynamical perturbations by passing stars or collisions with other bodies can bring these objects back to the inner Solar System, where we observe them. However, if some comets were dynamically ejected to interstellar space, is it possible that some comets in our own Solar System may have come

from other solar systems that experienced the same phenomena? While an interstellar source for comets is plausible, to date such comets have not been observed (Sekanina 1976; McGlynn & Chapman 1989; Francis 2005).

1.1.2 The Chemical Puzzle

Chemical studies of comae have been conducted across multiple wavelength regimes and have detected many tens of atomic and molecular species. However, these observed species alone do not represent the exact chemical composition of the nucleus. When species are released from the nucleus, solar radiation causes them to photodissociate and photoionize, and the interaction of the solar wind with the outer coma can also alter the chemical composition of the gas (Huebner et al. 1987). It is well established that the presence of the hydroxyl radical (OH) in the cometary coma is due mostly to the photodissociation of H_2O (Weaver et al. 1981). Because H_2O is difficult to observe from the ground, OH is often used to determine H_2O production in comets (Schleicher & A'Hearn 1983). It wasn't until the 1986 apparition of comet Halley that H_2O was definitively detected in the infrared (Mumma et al. 1986; Combes et al. 1986) and in mass spectra from flyby missions (Krankowsky et al. 1986). The photodissociation of H_2O, OH, and CO_2 is also responsible for the $O(^1D)$ emission seen in comets, which is observed at 6300 and 6364 Å (Festou & Feldman 1981; Fink & Johnson 1984; Magee-Sauer et al. 1988; Fink & Hicks 1996; Cochran & Cochran 2001). Two abundant species in the ion tails of comets, H_2O^+ and CO^+, are photoionization products of H_2O and CO, respectively (Magnani & A'Hearn 1986), and the strong emission of the

$A - X$ bands of CO^+ is responsible for the bluish color of the ion tail[1] (Herzberg 1950). Other observed species, such as the cyano radical (CN) and imidogen (NH), are also generally regarded as photodissociation products, at least partially from hydrogen cyanide (HCN) and ammonia (NH_3), respectively (Mumma et al. 1993). However, there are several other species observed in comets for which there is no obvious origin, such as the carbon trimer (C_3), and nitrogen sulfide (NS), thus demonstrating less than complete understanding of coma processes, nuclear composition, or both.

Even when all chemical species released directly from nuclei are identified, understanding the chemical nature of comets will not be complete. When cometary nuclei are in "dynamical storage" in the Oort Cloud or Kuiper Belt, they could experience multiple phenomena leading to processing of the ice to depths as much as tens of meters below the surface. For Oort Cloud comets, the radiation from high-mass stars could cause significant processing of the surface and bring about the selective removal of supervolatile species such as neon and argon (Stern & Shull 1988). Further processing from heating by supernovae and high-energy particle bombardment can also cause existing chemical bonds to break and form new ones, but these processes are not as likely to penetrate as deep as heating by high-mass stars (Moore 1981; Moore et al. 1983; Stern & Shull 1988; Johnson 1991). Surface processing could also be brought about by bombardment of grains from the interstellar medium (ISM), resulting in the loss of 1-20 m of surface material since the formation of the Oort Cloud (Mumma et al. 1993; Stern 2003). The Kuiper Belt objects (KBO) are thought to experience surface processing by

[1]These are sometimes referred to as the comet-tail bands, since they were seen in comets before they were seen in the laboratory.

collisions with other KBOs, thus heating the nuclei to depths of several tens of meters (Stern 2003). Therefore, the process of understanding the composition of the nuclear interior will not only require relation of coma species back to the nuclear surface, but ongoing laboratory studies of ices undergoing multiple types of processing.

1.2 Carbon Monoxide in Comets

Studies of the spin temperatures of H_2O in comets Halley (Mumma et al. 1988) and Hale-Bopp (Crovisier 1999) have indicated the formation temperatures of these nuclei are ~25 K. At this temperature, condensing water vapor forms amorphous ice. If other gases are present, they can adhere to the walls of pores in the ice via van der Waals forces and remain there as water ice continues to build the amorphous structure around them, and they would remain trapped until the structure of the ice changes in such a manner as to allow their release (Bar-Nun & Kleinfeld 1989; Notesco et al. 2003). Although amorphous ice can form at temperatures as high as 120 K, the amount of other volatiles trapped in the ice decreases exponentially with increasing temperature, thus making such species sensitive indicators of the region of nucleus formation. Studies by Notesco et al. (2003) and Notesco & Bar-Nun (2005) have shown that for the ice to trap 10% CO relative to H_2O, an amount seen in comets such as Hyakutake and Hale-Bopp, the formation temperature of the nucleus would have to be 22-27 K.

One of the most frequently studied molecular species in comets is CO. Abundances of CO in comets range widely from practically nonexistent to ~25% relative to H_2O, as seen in comets Hale-Bopp and Hyakutake (DiSanti et al. 2001). When present, CO often ranks second or third in abundance after H_2O. Because

CO is one of the more abundant volatiles and fairly easy to observe, it is an excellent molecule to gauge the formation temperature of cometary nuclei, thus allowing constraints to be placed on models of Solar System formation.

1.2.1 Observations of CO

The first detection of cometary CO via rocket ultraviolet observations of comet West (1976 VI) indicated that CO is an important chemical component of comets (Feldman & Brune 1976; Feldman 1978). These observations yielded abundances of CO at 20 - 25% with respect to the abundance of H_2O. Subsequent observations of other comets with the International Ultraviolet Explorer (IUE) yielded CO abundances of only a few percent, such as the observation of CO in comet Bradfield (1979 X) (A'Hearn & Feldman 1980), and the abundances varied greatly among the comets observed (Festou & Feldman 1987; Tozzi et al. 1998). Although it is possible that comets may exhibit different CO abundances due to the vast range in heliocentric distances over which they could have formed, another proposed explanation for this is the difference of aperture sizes of the IUE observations and the rocket-based observations (DiSanti et al. 2001), coupled with CO not being solely a parent molecule. The latter explanation is especially plausible, in light of *in situ* measurements of CO as well as more recent ground-based observations of CO in other comets, yielding abundances from 1% to 17% as seen at infrared wavelengths (Gibb et al. 2003).

1.2.2 Discovery of Extended CO

During the *Giotto* spacecraft flyby of comet Halley in 1986, the Neutral Mass Spectrometer (NMS) gathered data on several chemical species, including CO,

as it flew through the coma. An analysis of the 28 amu peak at a distance of 1,000 km from the nucleus yielded an abundance of CO at 3.5% relative to H_2O, but analysis of the data taken at 20,000 km showed the CO abundance was 11% (Eberhardt et al. 1987; Eberhardt 1999). Furthermore, the profile of the data at $r < 20{,}000$ km is significantly flatter than r^{-2}, suggesting a strong source in the coma in addition to a nuclear source, a so-called "extended source" (See Fig.1.1a). There are other species that could be responsible for the 28 amu signal, dinitrogen (N_2) and ethylene (C_2H_4), but analysis of data taken simultaneously in other modes indicates that C_2H_4 is negligible and that $n(N_2)/n(CO) < 2$ (Eberhardt et al. 1987). Therefore, CO is the dominant source of the 28 amu peak.

Halley is not the only comet believed to have had an extended source of CO in its coma. Observations of comet Hale-Bopp (C/1995 O1) show evidence of both nuclear and extended sources for CO, with projected extended source strengths ranging from 50% (DiSanti et al. 2001) to 90% of the total CO abundance (Brooke et al. 2003). Figure 1.1b shows a result from the DiSanti et al. observation, demonstrating the strong change in production rate of CO within 5000 km of the nucleus.

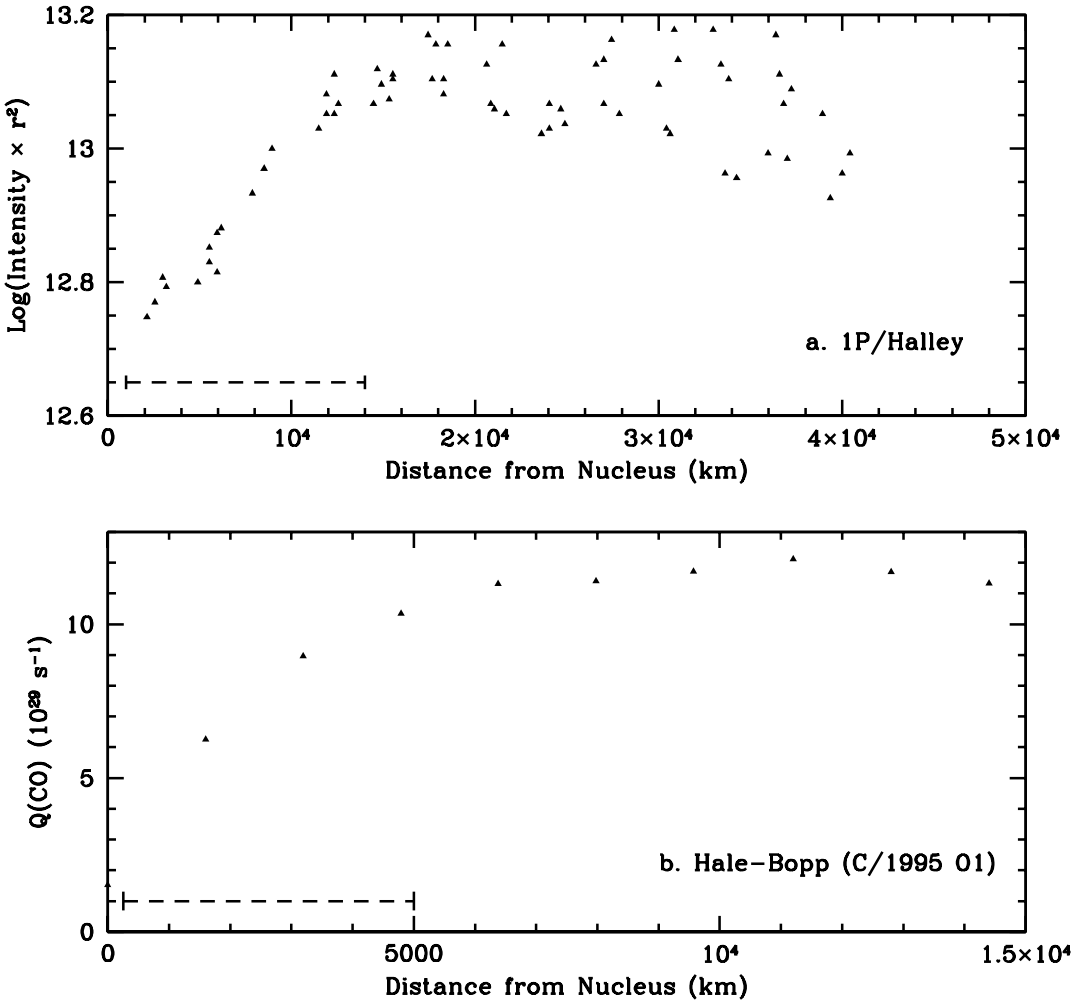

Figure 1.1 – a. Plot of Intensity $\times$ r^2 (in km) as a function of r, showing the data from the 28 amu channel of the *Giotto* NMS data. The non r^{-2} behavior of the data inside 20,000 km (region indicated by the dotted bar) strongly suggest an extended source of CO. Data derived from Figures 1 and 2 of Eberhardt et al. (1987). b. Plot of Q(CO) as a function of distance from the surface of comet Hale-Bopp, with the region of CO formation indicated as in Fig. a. Data originally shown in Figure A4 of DiSanti et al. (2001).

Several explanations for extended CO have been proposed. Given the substantial dust content of these comets, the CO could be coming from grains in the coma. Other proposed explanations involve the release of CO from the photodestruction of one or more unidentified organic compounds. These compounds may photodissociate almost immediately after their release from the nucleus, creating a region of enriched CO that would appear to come from an extended source, as seen in the flyby data (Boehnhardt et al. 1990). On the other hand, recent re-analysis of Hale-Bopp data, although preliminary, suggest that the extended CO source in Hale-Bopp may not actually exist, and that opacity and temperature variations in the coma may have caused the CO to appear to come from an extended source (Bockelée-Morvan et al. 2005). While all of these ideas are possible, they all have problems as well, and the source of extended CO in comets still remains unsolved.

1.3 Chemical Reactions in Cometary Comae

In the earliest references on the subject, Oppenheimer (1975) and Shimizu (1975) considered the possibility of chemical reactions in cometary comae, proposing that a variety of chemical reactions, particularly those involving ions, could take place on much shorter timescales than many photochemical processes. Following on this idea, the first chemical models of the coma to incorporate chemical reactions revealed that many species could be produced in the coma at varying levels depending on the assumptions made in the models (Giguere & Huebner 1978; Huebner et al. 1980; Mitchell et al. 1981). With the discovery of CHON grains and extended sources of CO, formaldehyde (H_2CO), and the cyanogen radical (CN) in comet Halley (Krankowsky et al. 1986; Eberhardt et al. 1987), chemical

reactions were then generally regarded as minimal contributors to the chemical development of the coma.

However, studies of several species in recent years have prompted chemical reactions to be revisited as important contributors to the chemical development of the coma. One of the more intriguing chemical species found in comets is HNC, the isomer of HCN. Rodgers & Charnley (1998) have conducted extensive numerical studies to determine the origin of this species. They have thus far concluded that HNC may come from chemical reactions taking place in the near-nucleus coma or from the photodissociation of large HCN polymers (polyaminocyanomethylene (PACM)) (Rodgers & Charnley 2001b). A'Hearn et al. (2000) studied emission of the sulfur dimer (S_2) in comet Hyakutake (C/1996 B2) and found that the presence of S_2 could be explained by a reaction between carbonyl sulfide[2] (OCS) and metastable-state sulfur produced by the photodissociation of carbon disulfide (CS_2). Another species of interest to Hale-Bopp observers was the formyl cation (HCO^+), and the multiple studies done on this species all showed that its presence is due to chemical reactions (Lovell et al. 1999; Womack et al. 1999; Milam et al. 2004).

Given the possibilities for chemical reactions to produce some observed species, could they also contribute to the abundances of such major species as CO? In the present study, the potential for chemical reactions to produce CO in the coma is examined. This study incorporates widely used photochemical processes as well as chemical reactions involving neutral-charge species and ions. While some of the chemical reactions used here are included in other chemical models, other reactions used in this study are only just starting to be considered in coma chem-

[2]OCS was first observed in comet Hyakutake by Woodney et al. (1997).

istry. Specifically, these reactions involve species such as high-velocity hydrogen and metastable-state oxygen. These reactions have large rate constants and involve some of the more abundant cometary species, making them potentially important mechanisms for species formation and destruction in the coma.

Because chemical reactions depend on the collision rates of the reactants, factors influencing the collision rate of species are also examined. Most notably, the impact of nuclear shape on the outflow behavior of the gas could have an additional impact on coma chemistry if gas species are brought together in high rates of collision, which could happen if the material emanates from a concave surface feature. Currently, such features are not widely incorporated into coma modeling. The models presented here represent a first-order attempt to examine the impact of topography on coma chemistry.

This study is the first to seriously consider all of these phenomena in coma chemistry, particularly as applied to the CO extended source problem. Chapter 2 describes the physical and chemical features incorporated in the numerical studies. Chapter 3 presents studies of physical phenomena that may influence the chemical reaction contribution to CO in the coma. Chapter 4 examines the effects of nucleus composition on the formation of extended CO. Conclusions and ideas for future work are presented in Chapter 5.

Chapter 2

Modeling CO Chemistry in the Coma

2.1 Introduction

Attempts to reproduce the observed cometary coma go back nearly a century. The earliest model representing the coma was the fountain model (Eddington 1910). This model treated the coma as a collection of small emitters of light emanating from a point source, such that their density would fall as r^{-2} from the source. These emitters were also subject to a uniform acceleration pushing them from the sunward direction. This model produces a coma shape represented by a paraboloid of revolution along a line parallel to the acceleration, which passes through the point source.

Haser (1957) built on this idea, using a spherical nucleus with constant uniform outflow having a r^{-2} density dilution profile with distance from the nucleus. Additionally, he considered the work by Wurm (1943) and Swings (1943), indicating that radicals and ions were unstable and had to be formed by release of larger molecular species from the solid constituents of comets. The parent molecules photodissociate to produce daughter species, which were assumed to have one

parent and to move strictly radially away from the nucleus. The column density of species along the line of sight is then represented by a series of modified Bessel functions. This model is still popular today because it is computationally simple and yields plausible results in a number of cases (Combi & Delsemme 1980; Cochran 1985; Combi et al. 2004).

However, the Haser model does not contain much actual physics, and it fails to reproduce the observations of several important molecular species, such as C_2, which has been shown to have a flat profile close to the nucleus (Cochran 1985). Furthermore, it is possible for a daughter species to have more than one parent, and it is also possible that these daughter species may have excess velocity on formation and may not move in a strictly radial manner away from the nucleus. Newer models have been developed to account for these features, such as the vectorial model (Festou 1981) and the Monte Carlo model (Combi & Delsemme 1980). The vectorial model builds on the Haser model by considering additional factors such as the release direction of the daughter species and its velocity on release. In this case, integration over all parameters included in the problem is required. The Monte Carlo model, on the other hand, is more generally applicable to a broader range of cometary phenomena, including variable flow velocity and non-spherically symmetric comae. Monte Carlo models have been used for a variety of studies of the outflow behavior of comet Halley (Bockelée-Morvan & Crovisier 1987; Combi & Smyth 1988; Combi 1989; Ip 1989; Hodges 1990), including comparisons of isotropic and anxisymmetric cases (Xie & Mumma 1996a,b).

Meanwhile, other classes of models apply the physics of gas kinetic theory to reproduce the observed coma. The models of Marconi & Mendis (1983, 1984) and

Gombosi et al. (1985) numerically solve the equations of mass, momentum, and energy conservation for the cometary coma for a variety of cases with differing levels of gas and dust content. Other models, such as those developed by Skorov & Rickman (1998, 1999) have examined gas flow and acceleration in the cometary Knudsen layer[1], examining the behavior of the flow as the gas thermalizes.

Despite the tremendous advances in modeling the coma, few models have examined the behavior of the gas around a non-spherical nucleus. Flyby data of comets Halley, Borrelly, Wild 2, and Tempel 1 reveal irregularly-shaped nuclei with jet-like features emanating from small portions of their surfaces (Keller et al. 1987; Boice et al. 2002; Newburn et al. 2004; A'Hearn 2005). Simulations of the temperature distribution and mass-loss rates of concavities in ice have shown that such features exhibit higher mass-loss rates due to secondary heating mechanisms, may be responsible for some jet-like features in the coma, and may be partially responsible for nuclear breakups (Colwell & Jakosky 1987; Colwell et al. 1990; Gutiérrez et al. 2000, 2001).

The simulations of Crifo & Rodionov (1997, 1999) represent the first major hydrodynamic simulations of the inner coma around a non-spherical nucleus. In their simulations they use a kidney-bean shaped nucleus, containing a large-scale concavity at the subsolar point. The outflowing gas and dust produce features in the near-nucleus coma resembling jets and fans, which emanate from the concavity. While their models do not contain heating from the photodissociation of H_2O or the secondary heating mechanisms that should be present in the concav-

[1]The layer of gas and dust immediately surrounding the nucleus, where the velocity distribution is non-Maxwellian. This layer encompasses ~10 collisional mean free paths with an outer boundary of less than one meter above the surface.

ity, their models do incorporate much of the gas dynamics that is expected to be present in the near-nucleus environment. If topography can cause jet-like features in the coma, this could be an additional mechanism contributing to the chemical development of the coma as chemical species are brought together in high rates of collision, setting up an environment potentially rich in chemical reactions.

Models of coma chemistry in which chemical reactions are examined have been developed before. Some are based on the chemistry expected to take place in hot cores in the ISM, with networks containing tens to hundreds of reactions, while others consist of smaller networks designed to study one specific chemical problem. The large networks have the advantage that they are more complete, having more indirect sources and sinks of chemical species incorporated into them. The big disadvantage of large networks is that they contain many unobserved chemical species. While these species may be present but currently remain undetected, these studies often don't consider the effects of removing these species from the networks. Furthermore, it is more difficult to break down the network to examine individual reaction rates in the coma. Smaller reaction networks, while less complete in reactions, are easier to break down for the purpose of examining individual reaction contributions, and they tend to incorporate fewer unobserved species.

The models presented here will focus on the formation and destruction of CO, one of the most abundant chemical species in comets. There are multiple mechanisms by which CO can theoretically be created and destroyed, making it a subject of potentially rich chemistry. As discussed in Chapter 1, there is evidence that CO is formed in the comae of some comets, but the exact mechanism by which this is done is not definitively known (Eberhardt et al. 1987; Combi

1987; Greenberg & Li 1998). If indeed chemical reactions are important, and the presence of topography influences chemical reaction rates in the coma, these mechanisms may contribute not only to additional CO production but also to the production of other chemical species in comets which currently lack explanation.

2.2 The Behavior of the Outflow

The outflow cases to be examined are arranged in a "bottom-up" manner – in other words, these studies start with the simplest assumptions and build up to incorporate more phenomena. The following cases are considered in these studies:

2.2.1 Case 1: Constant Temperature and Velocity

The simplest assumptions for the behavior of the outflowing gas from a cometary nucleus are the assumptions of constant gas temperature and constant flow velocity, with a density dilution factor of r^{-2}. While these conditions are not actually seen in cometary comae, they represent first-order approximations for most of the middle coma. These assumptions are still widely used in coma chemical modeling, owing to the computational simplicity and reliability of the Haser model. When this case is used, the gas temperature is typically assumed to be 200 K or less, and the flow velocity ranges anywhere from 0.3 km s^{-1} to 1 km s^{-1}.

This case is useful because it allows the chemical reaction behavior to be monitored independent of the variation of temperature-sensitive reaction rates and added dilution of species concentrations by acceleration. This is not valid for the innermost coma where the acceleration is large and the gas is coupled to the dust, nor is it accurate in the outer coma where photodissociative heating

and solar wind interactions must be considered. However, it is a reasonable first-order representation in the middle coma, provided the flow velocity and gas temperature are appropriately tailored to the production rate and the comet's heliocentric distance.

2.2.2 Case 2: Varying Temperature and Velocity

To reproduce the behavior of the gas over the entire region of the coma surveyed here, a model reproducing more of the physical phenomena is needed to generate appropriate profiles for gas temperature and flow velocity. In the innermost coma, the gas and dust are coupled to one another on their release from the nucleus, and they act as a compressible fluid for the first tens of kilometers. This case is an intermediate to Cases 1 and 3, permitting the effects of temperature and acceleration to be examined separate from further deviations from r^{-2} density dilution that may be caused by large-scale topographic features.

The computational code for these models does not perform the gas dynamic calculations but instead draws upon existing results from other models. In this case, the profiles for gas temperature and flow velocity are based on the Monte Carlo simulations of Bockelée-Morvan & Crovisier (1987) and Combi et al. (1993) (See Fig. 2.1). The two Monte Carlo models use different assumptions for nuclear size and production rate, as well as dust content. However, the near-nucleus acceleration is present in both models, as well as photodissociative heating from H_2O, causing the increase in gas temperature beyond the first few hundred kilometers.

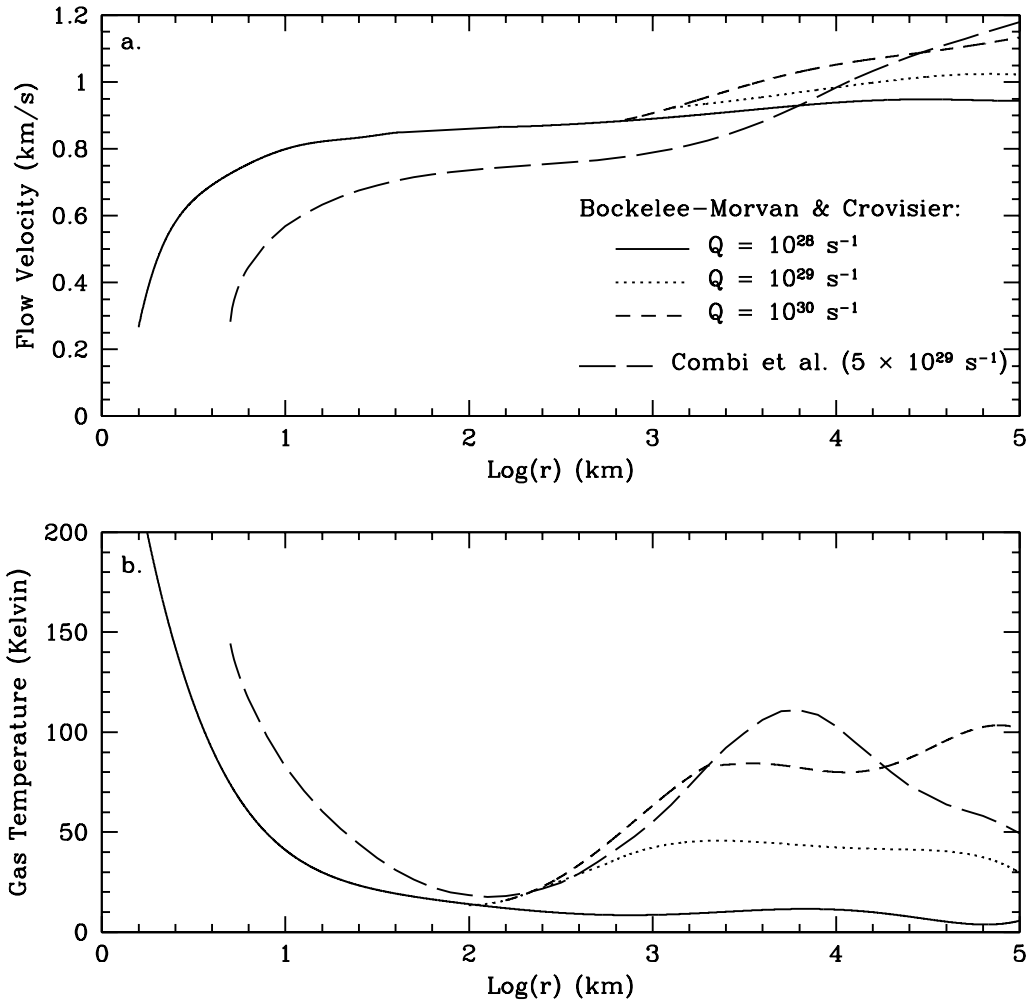

Figure 2.1 – Physical properties of the gas derived from the simulations of Bockelée-Morvan & Crovisier (1987) and Combi et al. (1993): a. flow velocity,and b. gas temperature.

2.2.3 Case 3: Outflow from a Concavity on a Non-Spherical Nucleus

In order to examine the potential impact of outflow behavior of gas from a large-scale concave surface feature, a gas dynamic model with a non-spherical nucleus is required. This case examines the widest range of near-nuclear phenomena and their influence on the chemistry. Similar to Case 2, information about the behavior of the gas is taken from other models. The simulations of Crifo & Rodionov (1997) provide the results needed to study this case (See Fig. 2.2 and Fig. 2.3).

For this study, the profiles for number density, gas temperature, and flow velocity were extracted along the major gas flow line along the center of a fan-shaped feature emanating from the bottom of the concavity, which is the subsolar point in this simulation. While these simulations contain many phenomena generally regarded as important in the near-nucleus environment, they do not contain the secondary heating mechanisms expected to be present in large-scale concavities – namely reflections and further insolation from radiation released from within the concavity, factors that have been shown to have an impact on nuclear mass-loss rates (Colwell & Jakosky 1987; Colwell et al. 1990; Gutiérrez et al. 2000, 2001). Furthermore, the simulations focused on examining potential near-nuclear phenomena, the profiles extracted from this simulation are only valid within 1,000 km of the nucleus. Photodissociative heating from H_2O is also not included in the simulations, and as a result, these results have the gas temperature approaching zero at 1,000 kilometers, which does not actually occur. To compensate for this, the gas temperature and flow velocity from Case 2 is used instead to provide more reasonable conditions beyond the region covered by these near-nucleus profiles.

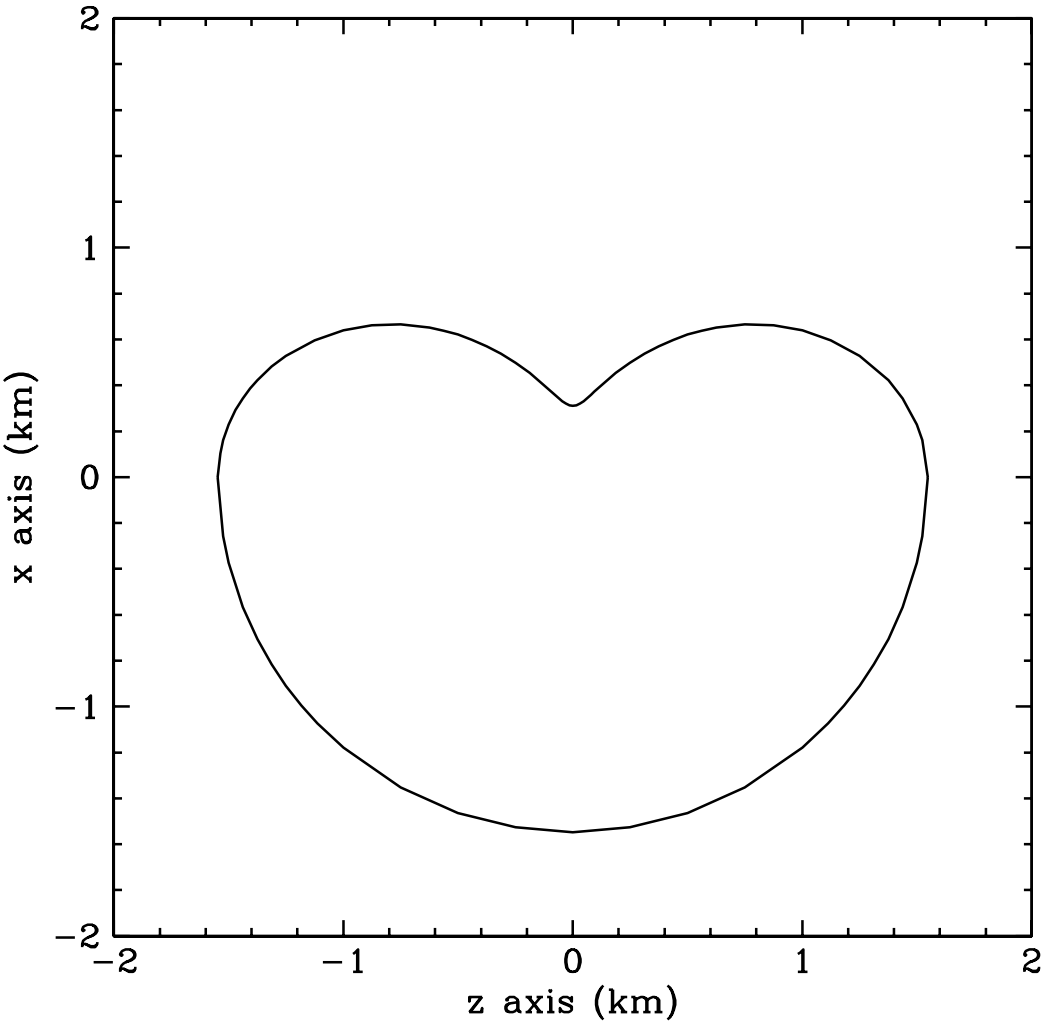

Figure 2.2 – A plot of the z-x plane of the nucleus shape model used in the simulations of Crifo & Rodionov (1997), showing the large-scale concavity on the surface.

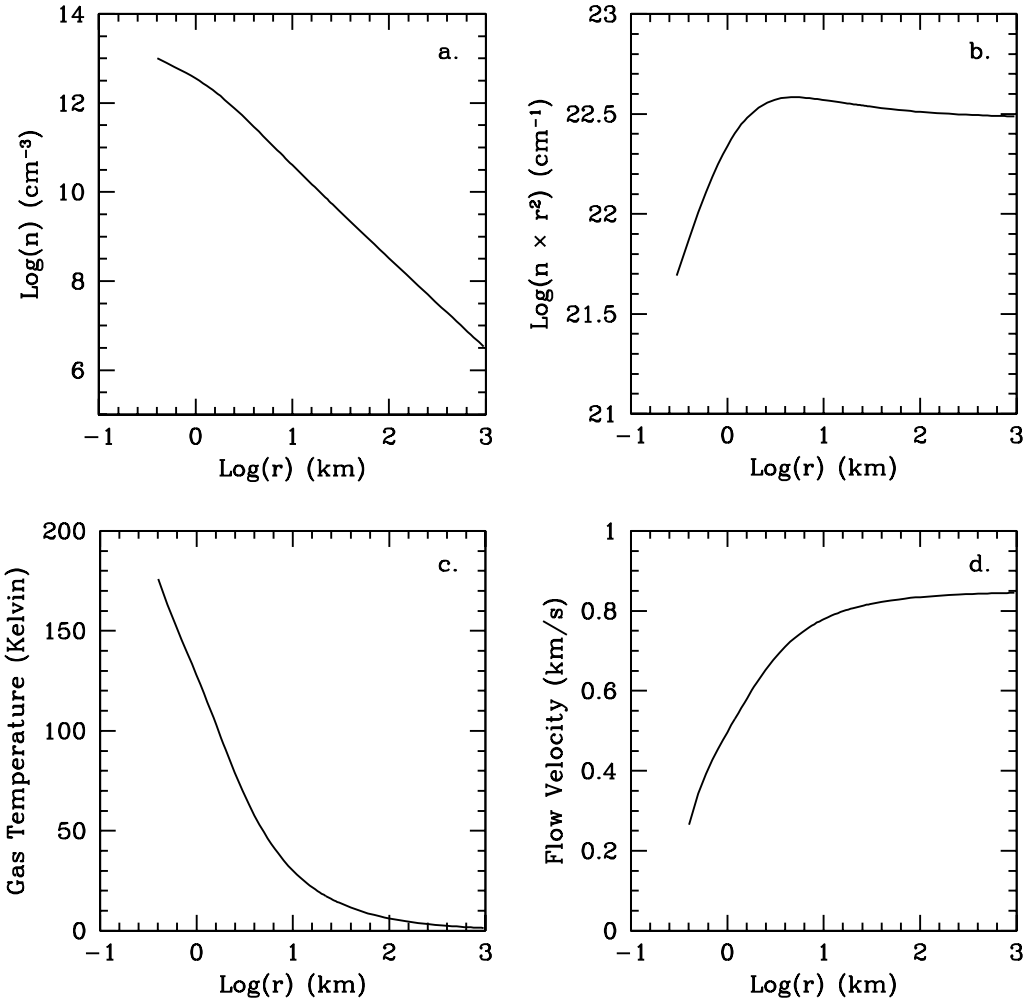

Figure 2.3 – Physical properties of the gas in the center of the jet-like feature emanating from the bean-shaped nucleus shown in Fig. 2.2: a. number density, b. n(r) $\times$ r^{-2} showing the significant near-nucleus deviation from r^{-2}, c. gas temperature, and d. flow velocity. Note that the gas temperature approaches zero in these models. Instead, results from Case 2 are substituted to keep the temperature in the simulations above absolute zero.

2.3 The Chemical Reaction Network

Several processes are thought to contribute to the chemical development of the coma. As discussed in Chapter 1, it is well-known that photochemical processes play an important role in breaking down parent species coming directly from the nucleus, thereby producing simpler species further out in the coma. While establishing the role of chemical reactions in coma chemistry has been more problematic, the potential contributions to CO from multiple photochemical and two-body chemical reactions will be demonstrated here.

Chemical reactions, particularly those involving exclusively neutral-charge species, will most likely occur in the inner coma, where the concentration of species is highest. Chemical reactions between species could rival the photochemistry rates for some of the more abundant species (Oppenheimer 1975; Giguere & Huebner 1978), particularly if the relevant photodissociation lifetimes are long. Reactions involving ionic species, however, may occur several orders of magnitude further out in the coma, given their large collisional cross-sections, coupled with their increased relative abundances upon photoionization of their parent species.

In order to understand how reaction rates are determined, consider the following photodissociation of chemical species A:

$$A + h\nu \rightarrow B + C \, . \tag{2.1}$$

The rate of formation of species C can be written as

$$\frac{d[C]}{dt} = \gamma_A \, [A] \tag{2.2}$$

where $[C]$ is the number density of species C, $[A]$ is the number density of species A, and γ_A is the photodissociation rate of species A into B and C.

For an elementary[2] chemical reaction involving species A and B:

$$A + B \rightarrow C + D \tag{2.3}$$

the rate of formation of species C in this process is written as

$$\frac{d[C]}{dt} = k_{AB}\,[A]\,[B] \tag{2.4}$$

where $[C]$ once again is the number density of species C, $[A]$ and $[B]$ are the number densities of species A and B, respectively, and k_{AB} is the rate constant of the reaction between A and B. Buried within the rate constants is information about the reaction energetics which determine the likelihood of a reaction taking place upon each encounter of the reactants.

Two-body reactions were chosen for the network using the criteria of large k in the temperature range below 200 K and ample quantities of reactants, which were required to be species observed in comets. Table 2.1 lists all of the chemical reactions included in the network, with rate constant data given by the UMIST 1999 astrochemistry database (Le Teuff et al. 2000) and photodissociation data for average solar activity from Huebner et al. (1992). Chemical reactions involving O(^{1}D) use rate constant data given by Heidner et al. (1973) and Tully (1975). The photodissociation rate of HCO is not available, and was estimated using the spatial profile of the transition at 4833 Å as observed by Cosmovici & Ortolani (1984) in comet IRAS-Araki-Alcock (See Section 2.3.1 for additional discussion).

[2]This discussion refers to two-body reactions that follow the general behavior of rate constants as determined by collision theory and activated complex theory, $k = A\ T^m\ \exp(-E'/RT)$, where A is a constant, T is temperature, R is the ideal gas constant, E' is a quantity related to the activation energy, E_a, by E_a - mRT, and m is usually an integer or half-integer exponent ($m = 0$ yields the Arrhenius relation), which is generally the case with the reactions included here.

Reactions involving hot hydrogen, H^* require special treatment (see Section 2.5.1 for further explanation), and their rate constants are given in Table 2.2. To convert the data for two-body reactions in Table 2.1 from coefficients into a rate constant, k, the following equation is used:

$$k = \alpha \left(\frac{T}{300}\right)^{\beta} e^{-\gamma/T} \tag{2.5}$$

where T is the gas temperature in Kelvins and k has units of s^{-1} for photochemical reactions and $cm^3\ s^{-1}$ for the two-body chemical reactions (Le Teuff et al. 2000). The α term contains information on the collisional cross section, β is the pre-exponential temperature dependence of the reaction, and γ (not to be confused with γ in Equation 2.2) contains information about the minimum energy required for a collision to result in reaction. A reaction network diagram of the processes leading to the creation and destruction of CO, showing the interrelationships of the species involved, is shown in Figure 2.4. The contributions to the network coming from H_2O are represented in Figure 2.5.

Table 2.1. Chemical Reactions and Rate Constant Coefficients

Reaction	α[1]	β[1]	γ[1]
Photochemical Processes:[2]			
$H_2O \rightarrow H^* + OH$	$\mathcal{A}$[3]	...	...
$H_2O \rightarrow H_2 + O(^1D)$	1.0×10^{-6}	0.0	0.0
$H_2O \rightarrow H_2O^+ + e^-$	5.8×10^{-7}	0.0	0.0
$CO \rightarrow C + O(^1D)$	5.6×10^{-7}	0.0	0.0
$CO \rightarrow CO^+ + e^-$	6.7×10^{-7}	0.0	0.0
$CO_2 \rightarrow CO + O(^1D)$	1.2×10^{-6}	0.0	0.0
$CO_2 \rightarrow CO + O(^3P)$	4.6×10^{-7}	0.0	0.0
$CO_2 \rightarrow {CO_2}^+ + e^-$	1.2×10^{-6}	0.0	0.0
$CH_3OH \rightarrow H_2CO + H_2$	1.4×10^{-5}	0.0	0.0
$CH_3OH \rightarrow CH_3OH^+ + e^-$	7.5×10^{-7}	0.0	0.0
$H_2CO \rightarrow CO + H_2$	1.2×10^{-4}	0.0	0.0
$H_2CO \rightarrow HCO + H$	6.7×10^{-5}	0.0	0.0
$H_2CO \rightarrow CO + H + H$	3.8×10^{-5}	0.0	0.0
$HCOOH \rightarrow HCO + OH$	6.4×10^{-4}	0.0	0.0
$HCO \rightarrow CO + H$[4]	1.3×10^{-3}	0.0	0.0
$OH \rightarrow O(^3P) + H$	1.3×10^{-5}	0.0	0.0
$OH \rightarrow O(^1D) + H$	1.2×10^{-5}	0.0	0.0
Neutral-Neutral Reactions:			
$H_2CO + OH \rightarrow HCO + H_2O$	2.2×10^{-12}	1.42	−416.0
$CO_2 + H^* \rightarrow CO + OH$	$\mathcal{B}$[3]	...	...
$CO + H^* \rightarrow C + OH$	$\mathcal{C}$[3]	...	...
$CO + OH \rightarrow CO_2 + H$	1.2×10^{-13}	0.95	−74.0
$OH + HCO \rightarrow H_2O + CO$	1.7×10^{-10}	0.0	0.0
$O(^1D) + CO_2 \rightarrow O_2 + CO$	2.0×10^{-10}	0.0	0.0
$HCO + HCO \rightarrow H_2CO + CO$	3.0×10^{-10}	0.0	0.0
$CO + O(^1D) \rightarrow CO_2$	8.0×10^{-11}	0.0	0.0
$C + OH \rightarrow CO + H$	1.1×10^{-10}	0.5	0.0
$H_2O + O(^1D) \rightarrow OH + OH$	2.2×10^{-10}	0.0	0.0
$O + HCO \rightarrow CO + OH$	5.0×10^{-10}	0.5	0.0

Table 2.1—Continued

Reaction	α[1]	β[1]	γ[1]
Electron Recombination:			
$H_2O^+ + e^- \rightarrow O + H + H$	2.0×10^{-7}	-0.5	0.0
$H_2O^+ + e^- \rightarrow O + H_2$	3.3×10^{-8}	-0.5	0.0
$H_2O^+ + e^- \rightarrow OH + H$	6.3×10^{-8}	-0.5	0.0
$HCO^+ + e^- \rightarrow CO + H$	1.1×10^{-7}	-1.0	0.0
$CO^+ + e^- \rightarrow C + O$	2.0×10^{-7}	-0.48	0.0
$CO_2^+ + e^- \rightarrow CO + O$	3.8×10^{-7}	-0.5	0.0
$H_3O^+ + e^- \rightarrow O + H_2 + H$	1.0×10^{-8}	-0.3	0.0
$H_3O^+ + e^- \rightarrow OH + H + H$	4.8×10^{-7}	-0.3	0.0
$H_3O^+ + e^- \rightarrow OH + H_2$	1.8×10^{-7}	-0.3	0.0
$H_3O^+ + e^- \rightarrow H_2O + H$	3.3×10^{-7}	-0.3	0.0
$H_3CO^+ + e^- \rightarrow CO + H_2 + H$	2.0×10^{-7}	-0.5	0.0
$H_3CO^+ + e^- \rightarrow HCO + H + H$	2.0×10^{-7}	-0.5	0.0
$H_3CO^+ + e^- \rightarrow H_2CO + H_2CO + H$	2.0×10^{-7}	-0.5	0.0
$CH_3OH_2^+ + e^- \rightarrow CH_3OH + H$	3.0×10^{-7}	-0.5	0.0
Ion-Neutral Reactions:			
$H_2O^+ + CO \rightarrow HCO^+ + OH$	5.0×10^{-10}	0.0	0.0
$CO_2^+ + H_2O \rightarrow H_2O^+ + CO_2$	2.0×10^{-9}	0.0	0.0
$CO^+ + H_2O \rightarrow H_2O^+ + CO$	1.0×10^{-9}	0.0	0.0
$CO_2^+ + H \rightarrow HCO^+ + O$	2.9×10^{-10}	0.0	0.0
$CO^+ + H_2CO \rightarrow HCO^+ + HCO$	1.7×10^{-9}	0.0	0.0
$H_2 + H_2O^+ \rightarrow H_3O^+ + H$	3.4×10^{-9}	0.0	0.0
$OH + H_2O^+ \rightarrow H_3O^+ + O$	6.9×10^{-10}	0.0	0.0
$H_2O + H_2O^+ \rightarrow H_3O^+ + OH$	2.1×10^{-9}	0.0	0.0
$C + H_3O^+ \rightarrow HCO^+ + H_2$	1.0×10^{-11}	0.0	0.0
$H_2CO + H_3O^+ \rightarrow H_3CO^+ + H_2O$	3.4×10^{-9}	0.0	0.0
$CH_3OH + H_3O^+ \rightarrow CH_3OH_2^+ + H_2O$	2.5×10^{-9}	0.0	0.0
$H_3CO^+ + H_2O \rightarrow H_2CO + H_3O^+$	2.3×10^{-10}	0.0	0.0
$OH + CO^+ \rightarrow HCO^+ + O$	3.1×10^{-10}	0.0	0.0
$H_2O + HCO^+ \rightarrow H_3O^+ + CO$	2.5×10^{-9}	0.0	0.0
$H_2CO + HCO^+ \rightarrow H_3CO^+ + CO$	6.9×10^{-10}	0.0	0.0
$CH_3OH + HCO^+ \rightarrow H_3OH_2^+ + CO$	2.7×10^{-9}	0.0	0.0
$CO_2 + CO^+ \rightarrow CO_2^+ + CO$	1.0×10^{-9}	0.0	0.0

Table 2.1—Continued

Reaction	α [1]	β [1]	γ [1]
De-Excitation Rates:			
$O(^1D) \rightarrow O(^3P) + h\nu$ [5]	7.5×10^{-3}	0.0	0.0
$H_2O + O(^1D) \rightarrow H_2O + O(^3P)$ [6]	2.3×10^{-10}	0.0	0.0

[1]Rate coefficients for two-body reactions are converted to rate constants using Equation 2.5.

[2]Photodissociation rates given in this table are applicable at 1 A.U. They scale as r^{-2} elsewhere.

[3]These reactions depend on H^*, which has a distribution of velocities. See Table 2.2 for a list of reaction rates for each velocity bin of H^*.

[4]Estimated using the spatial profile of the transition at 4833 Å as observed by Cosmovici & Ortolani (1984) in Comet IRAS-Araki-Alcock.

[5]From Glinski et al. (2004).

[6]From Streit et al. (1976).

Table 2.2. Rate Constants for Reactions Involving Hot Hydrogen

Bin	$\mathcal{A}$ (s^{-1}) [1]	$\mathcal{B}$ $(cm^3\ s^{-1})$ [1]	$\mathcal{C}$ $(cm^3\ s^{-1})$ [1]
1	5.1×10^{-7}	1.1×10^{-10}	7.9×10^{-13}
2	5.3×10^{-6}	1.3×10^{-10}	2.8×10^{-12}
3	1.2×10^{-6}	1.5×10^{-10}	8.0×10^{-12}
4	6.6×10^{-8}	1.8×10^{-10}	2.0×10^{-11}

[1]The values given here are the actual rate constants and are not to be used in Equation 2.5.

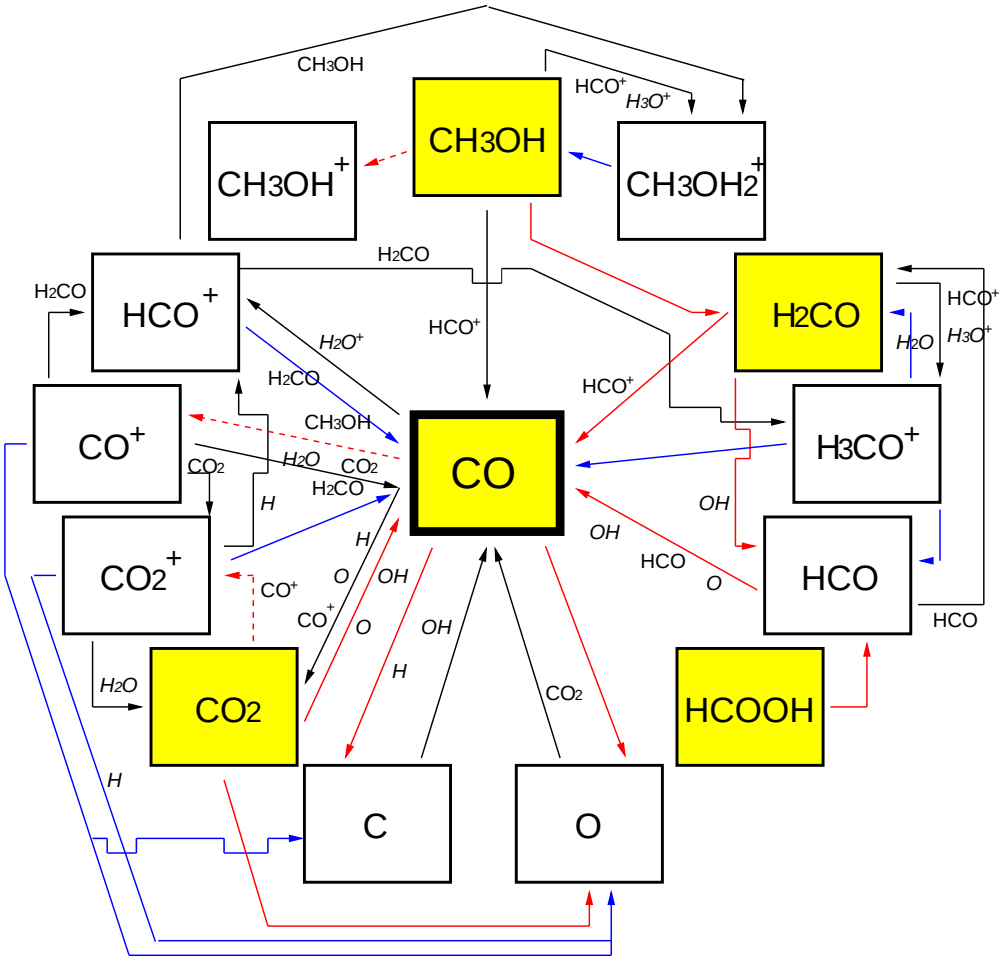

Figure 2.4 – Reaction network diagram showing formation and destruction of CO. The yellow boxes represent molecular species present in the nucleus. Photochemical processes are represented by red arrows (photodissociation by solid lines and photoionization by dotted lines). Blue arrows indicate a reaction with an electron. Black arrows indicate two-body chemical reactions. If a reactant is present next to a red or blue arrow, it indicates there is a chemical reaction that creates the product *in addition to* the other process. Reactants in italics come from the H_2O network, shown in Fig. 2.5.

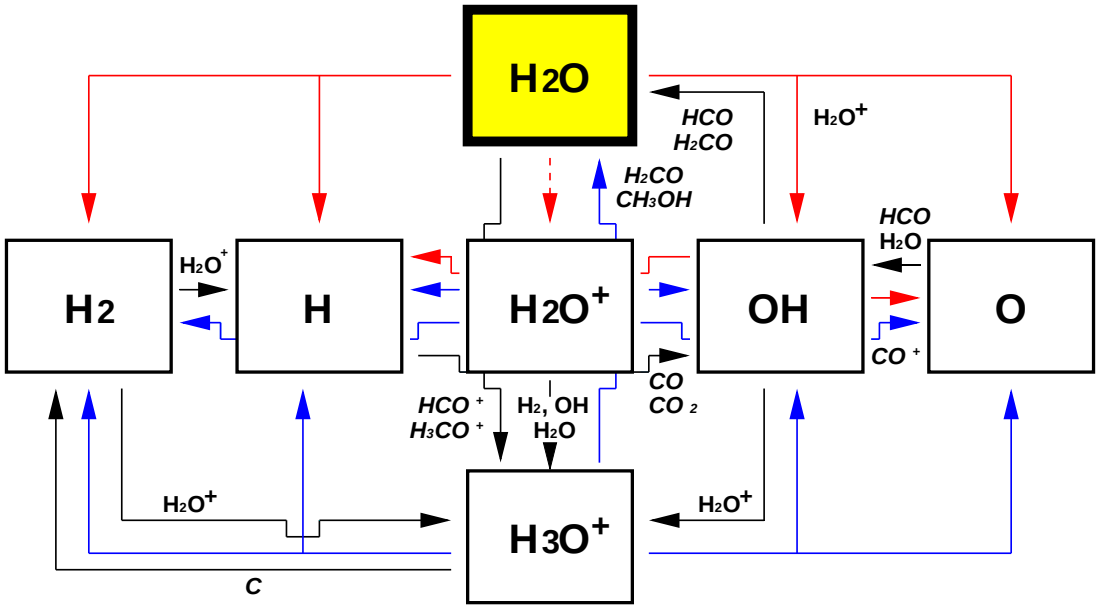

Figure 2.5 – Reaction network diagram showing the photodissociation products of H_2O, which play key roles as reactants in the CO reaction network. Colored boxes and arrows have the same meaning as those in Fig. 2.4. Reactants in italics come from the CO network, shown in Fig. 2.4.

2.3.1 Photochemistry

There are multiple photochemical paths ultimately leading to CO. One direct path is the photodissociation of CO_2 to form CO and O. This process is known to happen because the CO produced in this process emits prompt emission in the ultraviolet, contributing to the Cameron bands at 2000 Å (Weaver et al. 1994). Additionally, H_2CO has a relatively short photodissociation lifetime and is generally thought to be a contributor to the extended CO source, potentially contributing as much as 66% of the extended CO (Eberhardt et al. 1987). It is also thought that H_2CO may have an extended source, possibly from grains in the coma. However, the studies here are being exclusively performed on known major gas species, and in these studies, the photodissociation of CH_3OH serves as an extended source for H_2CO, which has been shown to have relative abundances in comets as much as 5% or more (Mumma et al. 1993; Eberhardt 1999). Another species, formic acid (HCOOH), is not as abundant as the other parent species involved in these photodissociation sequences, yet it is still potentially important in the near-nucleus coma since its photodissociation rate is extremely fast, photodissociating $\sim$1500 s after leaving the nucleus (Huebner et al. 1992). Furthermore, H_2CO, CH_3OH, and HCOOH also produce the formyl radical (HCO) in the coma through one or more photodissociation paths.

The reported detection of HCO in comets by Cosmovici & Ortolani (1984) in comet IRAS-Araki-Alcock (1983 d) is weak and has been met with skepticism by most researchers (A'Hearn, private communication). The authors even admit that the transition showing the strongest case for detection (4833 - 4838 Å) could have contamination from CO lines at 4835 Å. Given that there is no published photodissociation lifetime for HCO (Rodgers, private communication),

the lifetime had to be estimated.

The photodissociation rate was estimated based on the spatial profile of the line at 4833 Å, assuming the parent was HCOOH[3]. This yields a photodissociation lifetime of ~800 s. However, even with the uncertainties of the detection and the derived lifetime, HCO should not last long in the solar radiation field. HCO is a classic example of a bent triatomic molecule which is highly susceptible to the Renner-Teller Effect, which lifts the degeneracy of an electronic state when there is a coupling between molecular bending and electronic motion (Herzberg & Teller 1933; Renner 1934; Herzberg 1950). For HCO, this can lead to predissociation of the molecule at visible wavelengths (Goldfield et al. 1993). The derived 800 s photodissociation lifetime is consistent with the fact that two of its parents, H_2CO and HCOOH, are also short-lived and photodissociate at significantly higher energy (Okabe 1978). Given the uncertainty of the HCO detection and lifetime, the impact of HCO lifetime on CO is examined in Chapter 4.

2.3.2 Two-Body Chemical Reactions

Several processes in the reaction network are particularly interesting because they involve atomic species in transient states (H^* and $O(^1D)$). Chemical reactions involving such species are not frequently studied in cometary chemical reaction networks. However, they could be potentially more important than some reactions which have been studied previously.

[3]Cosmovici & Ortolani (1984) claim the parent is most likely H_2CO with HCOOH secondary, but it is the opinion of this author that it is inconsistent with the profile. With an outflow velocity of ~0.5 km s^{-1}, HCOOH is more consistent with the profile. Furthermore, if the primary parent was H_2CO, their detection of HCO should have been stronger.

Oxygen in the ^{1}D State

The ground-state configuration for atomic oxygen is ^{3}P. However, the photodissociation of species such as H_2O and CO_2 produce atomic oxygen in metastable ^{1}D and ^{1}S states (Huebner et al. 1992), giving rise to [O I] emission in comets. Because the level lifetime for ^{1}D is short compared to the photodissociation lifetimes of H_2O and OH, observations of transitions coming from the ^{1}D state at 6300.304 and 6363.776 Å (Cochran & Cochran 2001) are often used in addition to OH to track H_2O in the coma (Fink & Hicks 1996).

Knowing the level excitation of a species is also important because the electron configuration can influence the rate at which it is likely to react with another atom or molecule. For example, the reaction $O + H_2O \rightarrow OH + OH$ has a rate constant of $\sim 10^{-26}$ cm^3 s^{-1} if oxygen is in the ^{3}P state (Lifshitz & Michael 1991), but the rate constant becomes $\sim 10^{-10}$ cm^3 s^{-1} if oxygen is in the ^{1}D state (Heidner et al. 1973). Other reactions involving O(^{1}D) in the chemical reaction network experience similarly large order-of-magnitude differences if O were in the ^{1}D state instead of the ^{3}P state.

Studies of oxygen and hydrogen chemistry in the near-nucleus coma have been examined by Glinski et al. (2004). Their studies have shown that O(^{1}D) reactions can have an impact on the abundances of H_2O products in the coma, despite the short level lifetime for O(^{1}D) (130 s (Glinski et al. 2004)) and significant collisional de-excitation by H_2O. Furthermore, their studies indicate that O(^{1}D) reactions may play a significant role in the formation of O_2 and O_2^+ in the coma, neither of which has been definitively identified in comets, but may be responsible for some of the unidentified features seen in the plasma-tail spectra of comets Hyakutake (Wyckoff et al. 1999) and Ikeya-Zhang (C/2002 C1) (Kawakita & Watanabe 2002)

at 4950, 5300, and 6000 Å (Glinski et al. 2004).

In addition to radiative decay of $O(^1D)$ to $O(^3P)$, there is significant collisonal de-excitation of $O(^1D)$ to $O(^3P)$, particularly in the inner coma where the collision rate with H_2O is high. In this study, the $O(^1D)$ and $O(^3P)$ level excitations of O are treated as separate chemical species. The radiative decay of $O(^1D)$ to $O(^3P)$ is included in the chemical reaction network, shown in Table 2.1. The collisional de-excitation rate for $O(^1D)$ to $O(^3P)$ with H_2O is also considered, with the rate data taken from the work of Streit et al. (1976). Oxygen has also been observed in comets in the $O(^1S)$ state leading to the "green line" at 5577 Å, but the level lifetime is short (0.6 s (Festou & Feldman 1981)), and no chemical reaction rate data involving this excitation are available. Furthermore, $O(^1S)$ would come primarily from H_2O, CO_2, and CO. The $O(^1S)/(^1D)$ production ratio for H_2O is 0.1 (Festou & Feldman 1981; Cochran & Cochran 2001), and both CO and CO_2 are slow to photodissociate. Therefore, $O(^1S)$ is not considered in this network.

High-Velocity Hydrogen

It has long been known that atomic hydrogen in comets comes from the photodissociation of a parent species and is not likely to be found in significant amounts in the cometary nucleus because of its extreme volatility and high diffusion rate (Biermann 1968). The hydrogen coma is vast, and it produces substantial Lyman-α emission at 1216 Å. It took multiple observations, however, to identify sources of hydrogen in the coma. Early observations of [O I] by Biermann & Trefftz (1964) suggested the source of hydrogen should be the photodissociation of H_2O, thus demonstrating that atomic hydrogen could be produced in great abundance in the coma. Keller (1971) argued that the hydrogen should have high veloc-

ities upon release from its parent species, thus observations to determine the velocity of the hydrogen should indicate the parent. Because the solar Lyman-α radiation pressure acts against hydrogen atoms moving in the sunward direction, the deviations from circular isophotes would reveal the velocity of the hydrogen. The Lyman α images of comet Tago-Sato-Kosaka (1969 IX), taken by the Orbiting Astronomical Observatory, revealed an outflow velocity of hydrogen of 8 km s^{-1} (Code et al. 1972), which Keller (1971) showed was too slow to be associated with direct photodissociation from H_2O and suggested that the low velocity could be explained by collisional cooling of the hydrogen with slower-moving heavier species. It was speculated that the 8 km s^{-1} outflow speed might belong to H produced by an electron recombination reaction with H_3O^+ ($H_3O^+ + e^- \rightarrow OH + H + H$) (Shimizu 1975), but a subsequent study by Keller (1976) showed that the 8 km s^{-1} velocity could be explained by hydrogen atoms freshly photodissociated from OH. Subsequent observations of comet Bennett (1970 II) by Keller & Thomas (1975) revealed a high-velocity component of hydrogen with $v > 16$ km s^{-1}, consistent with the photodissociation of H_2O. Later, a low velocity component of hydrogen with $v < 4$ km s^{-1} was found in an observation of comet Kohoutek (1973 XII), attributed to the thermalization of hydrogen atoms upon repeated collisions with other species in the inner coma (Carruthers et al. 1974; Meier et al. 1976).

Chemical reactions involving fast-moving hydrogen, or "hot" hydrogen (H^*) have been proposed to explain chemical phenomena throughout the Solar System and the ISM, including the formation of organic molecules in the atmosphere of Titan (Chang et al. 1979), as well as the depletion of deuterium cyanide (DCN) and the formation of phosphorus mononitride (PN) in the hot cores of giant

molecular clouds (Charnley & Millar 1994; Herbst & Talbi 1998). Talbi & Herbst (2002) have investigated the importance of the reaction $H^* + CO_2 \rightarrow CO + OH$ in the ISM and have determined that it could be an important mechanism in the destruction of CO_2. On the other hand, chemical reactions in the coma involving hot hydrogen are only now beginning to be investigated. Rodgers & Charnley (1998) proposed that hot hydrogen could contribute to the formation of HNC, whereby $H^* + HCN \rightarrow HNC + H$. Additionally, Pierce & A'Hearn (2003) have proposed the aforementioned $H^* + CO_2$ reaction as a possible contributor to extended CO in comets. A subsequent study of hot hydrogen reactions by Rodgers & Charnley (2005) confirmed the CO result for high-activity comets but failed to produce sufficient quantities of HNC to explain observations.

The reaction of $H + CO_2$ is highly endothermic, requiring H to have a velocity > 14 km s^{-1} (Oldershaw & Porter 1969; Rice & Baronavski 1991). Atomic hydrogen with a temperature the same as that of the coma lacks the kinetic energy to overcome this barrier. However, the photodissociation of H_2O often imparts excess translational energy to the hydrogen atom due to its small mass. These newly dissociated "hot" hydrogen atoms have an average velocity of 18 km s^{-1} (Keller & Thomas 1975), giving them sufficient kinetic energy to react with CO_2 to form CO. At these energies, hot hydrogen reacting with CO_2 has a rate constant $k \sim 10^{-10}$ cm^3 s^{-1}, which is about the highest order of magnitude that rate constants for neutral-charge two-body reactions can have under cometary conditions. In theory, this reaction could produce nearly twice as much CO as is formed from the photodissociation of CO_2.

Laboratory studies of this reaction are extensive (Rice & Baronavski 1991; Nickolaisen et al. 1992; Marshall et al. 2003). There are multiple reasons for

the extensive work done on this reaction, both scientific and logistic. First, the reverse of this reaction is the dominant pathway for the formation of CO_2 in the combustion of hydrogenous systems, and it plays a role in upper-atmospheric chemistry (Nickolaisen et al. 1992). Second, the species involved are fairly light, allowing for ease in generating a potential energy surface to examine the reaction dynamics and test theories of product formation (Flynn 1989; Rice & Baronavski 1991). Additionally, the H-atom reactant can be produced fairly easily in a monoenergetic state, and OH is easy to detect (Rice & Baronavski 1991).

The energy required to dissociate one hydrogen atom from a water molecule is 5.1 eV (Okabe 1978). Ultraviolet photons with wavelengths between 1216 - 1856 Å are primarily responsible for this dissociation (Huebner et al. 1992). These photons can produce hydrogen atoms with velocities ranging from 15 - 30 km s^{-1}. Upon collision with other molecules, the hydrogen atoms slowly lose momentum. It takes several tens of collisions for a typical hot hydrogen atom to thermalize after dissociation from H_2O (Combi & Smyth 1988). Although it doesn't take long for the hydrogen atoms to re-thermalize in the inner coma, these atoms do have an opportunity to chemically react with CO_2 before thermalization takes place. Because the rate of formation of CO from hot hydrogen and CO_2 is dependent on the velocity of the hydrogen atoms, it is necessary to consider the cooling of the hydrogen as it collides with other particles in the coma. This places a more realistic constraint on the rate of formation of CO by hot hydrogen. In this case, the most likely collision to cool the hydrogen is a collision with H_2O, since H_2O is the most abundant species.

In order to estimate the collisional cooling of hot hydrogen, the velocity distribution of the hydrogen is partitioned into bins chosen such that the hydrogen

atoms undergo the same number of collisions in each bin. The collision frequency, Z, of atomic hydrogen with H_2O is represented by

$$Z \;=\; \sigma \;<v>_{rel}\; n_{H_2O} \tag{2.6}$$

where σ is the collision cross section between H^* and H_2O (1.89×10^{-15} cm^2 (Hodges 1990)), $< v >_{rel}$ is the average relative velocity between H^* and H_2O, and n_{H_2O} is the number density of H_2O. Furthermore, the number of collisions the hydrogen will undergo in a given timeframe t, N_{coll}, is represented by

$$N_{coll} \;=\; Z\,t\;. \tag{2.7}$$

The equation for the energy loss of H^* per collision, as obtained by Huxley & Crompton (1962), is

$$\Delta E \;=\; -\,\frac{2\,m_{H^*}\;m_{H_2O}}{(m_{H^*}\;+\;m_{H_2O})^2}\,(E_{H^*} - E_{H_2O})\;. \tag{2.8}$$

From this equation, an equation to determine the widths of the velocity bins can be derived:

$$\frac{\Delta v_{H^*}}{v_{H^*}} \;=\; -\,\frac{m_{H_2O}}{(m_{H^*}\;+\;m_{H_2O})^2}\left[m_{H^*}\;-\;m_{H_2O}\left(\frac{v_{H_2O}}{v_{H^*}}\right)^2\right]\;. \tag{2.9}$$

For a description of how Equations 2.8 and 2.9 were obtained, see Appendix A.

Because a hydrogen atom with a velocity slower than 14 km s^{-1} is not energetic enough to undergo a reaction, all hydrogen thermalized down below this velocity is treated as cold hydrogen and not binned. The binning of hydrogen starts at 14 km s^{-1} and goes up to 25 km s^{-1}. The photodissociation rates for H_2O at wavelengths shorter than Lyman α drop off by several orders of magnitude, and their contribution to the abundance of hot hydrogen is small, so they are not included here. Furthermore, the reaction rates for H^* with CO_2 and CO

are extremely small for $v_{H^*} < 16$ km s^{-1}, and these bins are not actually included in the model. Furthermore, in these studies, only H* produced by the photodissociation of H_2O is actually considered to be hot hydrogen. The 8 km s^{-1} hydrogen produced by the photodissociation of OH is considered cold hydrogen here.

The photodissociation rates to produce hot hydrogen from H_2O to be used in this model are derived from Figure 76 of Huebner et al. (1992) in the range of 1856-1216 Å, which give the wavelength dependence of the photodissociation rate of H_2O. These data are modified here using the results of Wu & Chen (1993) to account for the partitioning of energy between the H* and OH fragments, as well as the energy going to the internal excitation of OH (which ranges from a few percent at 1850 Å to nearly 50% at Lyman α). Figure 2.6 contains a histogram of the velocity bins above 15 km s^{-1} and the formation rate of newly-dissociated hot hydrogen from H_2O in each bin. The exact range of velocities in each bin is given in Table 2.3. The bins incorporate multiple values of k as given by the Huebner et al. data. The value of k for these velocity bins was determined by summing all k values falling in each bin. Under this scheme, a hot hydrogen atom will change bins after two collisions. For comparison, the velocity bins are shown against a Lyman α profile from comet Hyakutake (see Fig. 2.7), obtained with the Hubble Space Telescope (HST) Goddard High-Resolution Spectrograph (GHRS) (Combi et al. 1998). The bins have been normalized around the 17.8 km s^{-1} peak in the velocity distribution. The distribution does not exactly reproduce the observed distribution of the highest velocities, indicating the H* abundance is underestimated. While this would be partially reconciled by including data from wavelengths shorter than 1216 Å from Huebner et al.'s distribution, it has been shown in studies by Brown & Spinrad (1993) that models incorporating the

Table 2.3. Velocity Bins for Hot Hydrogen

Bin	Velocity Range (km s^{-1})
1	16.11 - 17.69
2	17.69 - 19.46
3	19.46 - 21.40
4	21.40 - 23.54

results of Wu & Chen (1993) can easily underestimate the high-velocity element of the cometary Lyman α profile above 20 km s^{-1}.

With each integration of the chemical reaction network, there are multiple gains and losses of hydrogen in each bin:

- H_2O is photodissociating to produce new hot hydrogen atoms.
- Collisions with H_2O cause the hydrogen to cool, thereby causing hydrogen atoms to move into lower velocity bins.
- The hot hydrogen reacts with CO_2 and CO.

The different bins of hydrogen are treated as separate species, and each bin's reaction with CO and CO_2 is treated as a separate chemical reaction. Data on the reactions involving H^* are taken from the UMIST astrochemistry database.

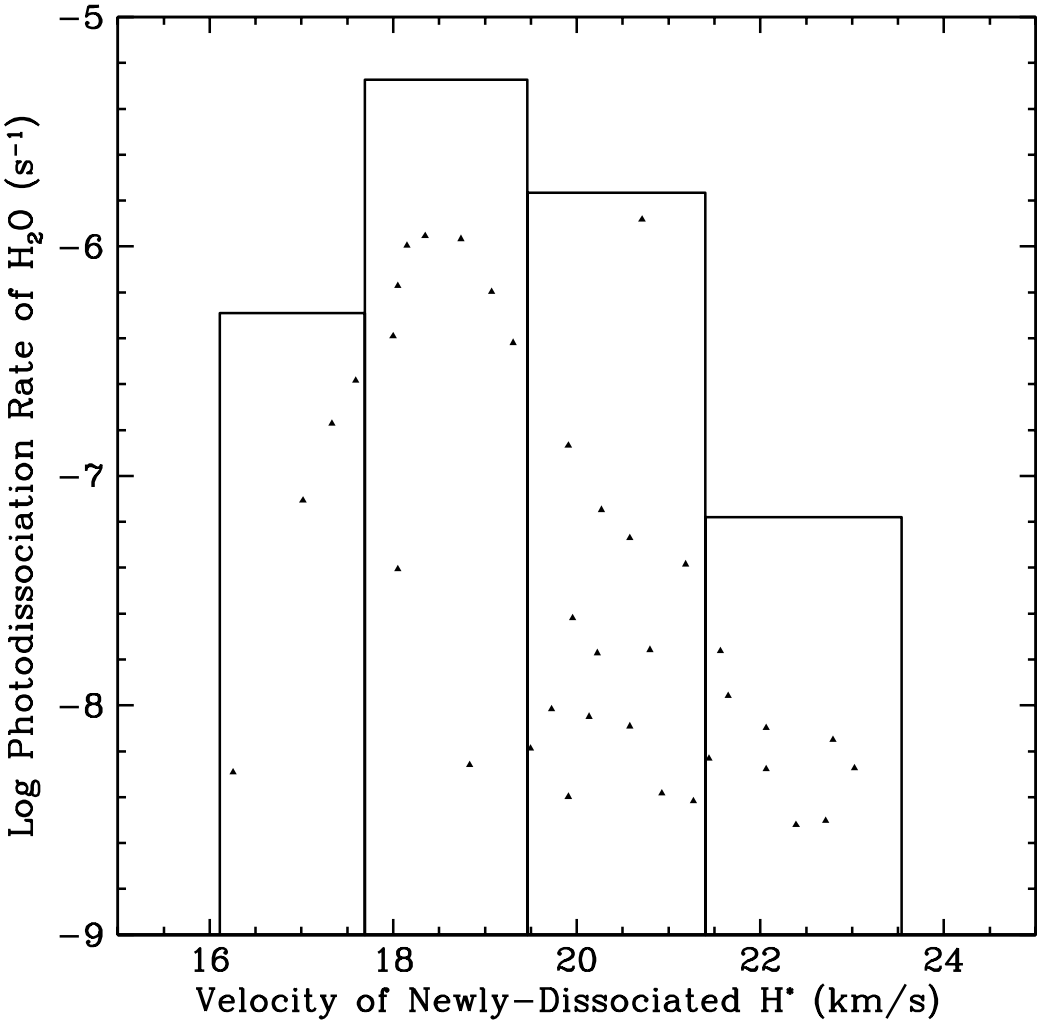

Figure 2.6 – The distribution of velocities above 14 km s^{-1} of H produced in the photodissociation of H_2O. The bins of the histogram are partitioned such that hydrogen atoms undergo the same number of collisions in each bin. The dots are data derived from Fig. 76 of Huebner et al. (1992), adjusted here for the energy partitioned to the OH product.

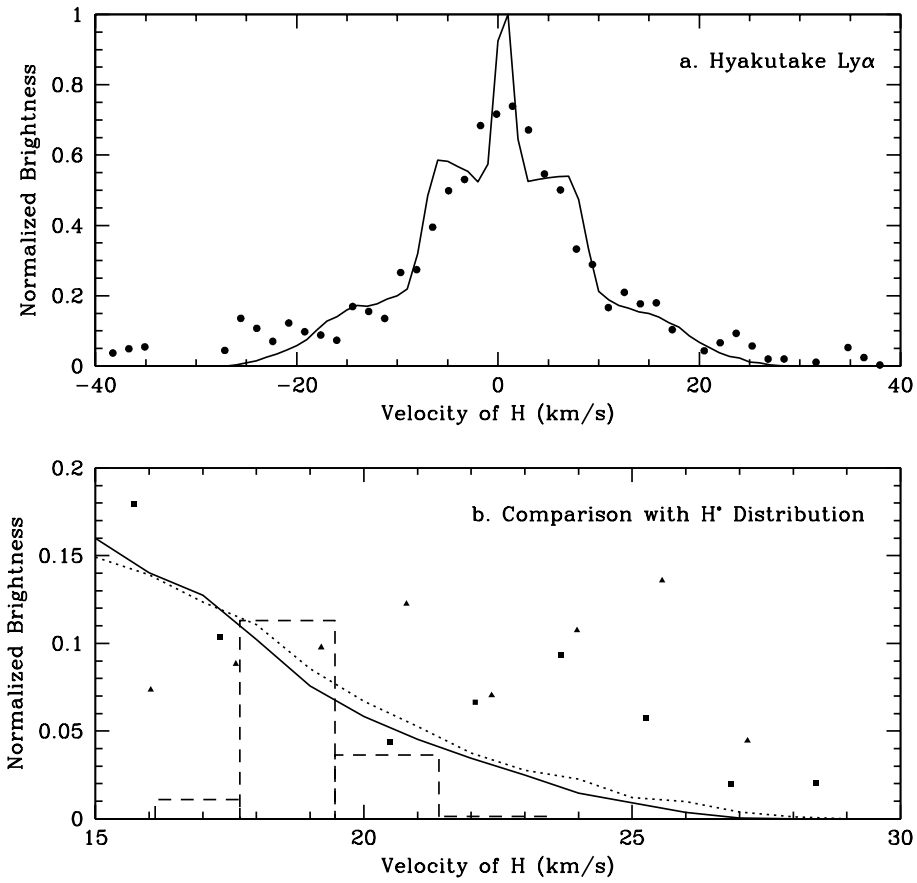

Figure 2.7 – Comparison of the H* distribution with observations: a. The Lyman α profile of comet Hyakutake, taken with the HST GHRS, displaying shoulders due to the production of H* from OH ($\pm$ 8 km s^{-1}) and H_2O ($\pm$ 18 km s^{-1}). The dots are HST GHRS data, and the line is the modeled line profile. b. Comparison of the H* distribution derived for chemical modeling (See Fig. 2.6) with the high-velocity wings of the profile shown in Fig. a. The bins have been normalized around the 17.8 km/s peak of the distribution. The solid line and squares represent the positive-velocity wing, and the dotted line and triangles represent the negative-velocity wing. Data originally shown in Combi et al. (1998).

2.4 Numerical Methods

Because chemical species can have multiple means of creation and destruction, the differential equations describing their change in number density can contain many terms, making it difficult to find analytic solutions except under certain limiting cases. Therefore, these equations must be solved numerically. For each species i in the chemical network, an equation can be obtained to describe the net change in number density by adding and subtracting all of the sources and sinks. In the most general form, this is represented by

$$\frac{dn_i}{dt} = \sum_j \mathcal{R}_{ji} - \sum_k \mathcal{R}_{ik} \, , \tag{2.10}$$

where $\mathcal{R}_{ji}$ is the rate of formation of species i due to species j, $\mathcal{R}_{ik}$ is the rate of destruction of i due to k, and n_i is the number density of i.

In this model, a volume element of gas will be tracked as it travels away from the nucleus. At each spatial step, the gas profiles derived from Giguere & Huebner (1978), Bockelée-Morvan & Crovisier (1987), Combi et al. (1993), or Crifo & Rodionov (1997) will be used to scale the number densities of all of the species, the temperature of the gas, and the velocity at which the volume element is moving away from the nucleus. Once the physical conditions are scaled, the differential equations describing the rates of change of the number densities of all of the species (Equation 2.10), are solved to account for the chemistry that has occurred over that spatial step. Once completed, the volume element will be moved out to the next point of integration, and the calculations will be repeated at the new distance. The code performs the calculations using a modified Bulirsch-Stoer routine with adaptive stepsize control. A detailed description of this method is provided in Appendix B.

Chapter 3

The Impact of Physical Phenomena on CO Chemistry in the Coma

3.1 Introduction

The chemical reaction network described in Section 2.3 contains several two-body reactions. The rates of these reactions greatly depend on the frequency of collisions of the gas species. It is therefore necessary to examine the potential impact of various physical phenomena on the chemical reaction rates. As described in Sections 2.1 and 2.2, the outflow behavior of the gas is potentially complex, having acceleration and temperature variations throughout the coma. The rates of CO formation and destruction, as well as the abundances of all species, will be examined under the following scenarios:

- Comparison of the results from tests using the three different outflow cases, as described in Chapter 2, to determine the potential impact of acceleration and topography on the chemical development of the coma. The acceleration should reduce the two-body chemical reaction rates, and the topography

should enhance them.

- Comparison of results from trials with different production rates to determine to what level different chemical phenomena should be considered when studying chemistry in high-activity comets.

For the trials conducted here, the nucleus will be placed at a heliocentric distance of 1 A.U. The nuclei will have gas production rates of either 5×10^{29} molecules s^{-1} for comet Halley or 10^{31} molecules s^{-1} for comet Hale-Bopp, unless indicated otherwise. For comet Hale-Bopp, attenuation of the ultraviolet radiation is incorporated into the program to regulate the photodissociation processes of H_2O. The attenuation is described in Appendix C. All trials incorporate gas-phase chemistry; none of these trials contain dust (aside from its effect on the acceleration, which cannot be easily extracted). The constant temperature, constant velocity profile is referred to as Case 1, the variable temperature and velocity profile of gas from a spherical nucleus is Case 2, and the variable temperature and velocity profile of gas coming from a concavity is Case 3. All cases use the same nuclear composition (See Table 3.1), with chosen abundances that are representative for comets.

3.2 Outflow Behavior

Because the numerical studies of Crifo & Rodionov (1997) were performed for a much lower level of activity[1] than comets Halley and Hale-Bopp, the trials to examine the effects of outflow behavior in all three cases use a production rate of

[1]The Crifo & Rodionov (1997) numerical studies were designed to study comet Wirtanen, the original target for the European Space Agency's *Rosetta* mission.

Table 3.1. Abundances of Molecules Released from Nucleus

Molecular Species	Relative Abundance*
H_2O	100
CO	5
CO_2	5
CH_3OH	2
H_2CO	1
HCOOH	0.5

*Values are given as % by number relative to H_2O.

10^{28} s^{-1}. Case 1 uses a gas temperature of 30 K and an outflow velocity of 0.8 km s^{-1}.

3.2.1 Species Comparison

Figure 3.1 shows the relative abundances of all species ([Species]/[H_2O]) released from the nucleus in Case 1[2]. The profiles of CO and CO_2 turn upward at large distances. For CO_2, this is the result of the depleted H_2O concentration. For CO, this is the result of a combination of H_2O depletion as well as CO formation in the coma. The other species all have downward turning profiles due to their depletion by photodissociation. H_2CO has a "shoulder" beyond 10,000 km, due to the contribution of CH_3OH photodissociation to the H_2CO abundance. Changing the outflow behavior had no visible impact on the relative abundances of these species, including CO, over the region of the coma examined in these simulations.

[2]In all plots showing relative abundances in Chapters 3 and 4, the profiles are *not* adjusted for photodissociation lifetime differences in the species.

Figure 3.2 shows the relative abundances of all neutral-charge species formed in the coma in Case 1. In general, the relative abundances increase throughout the entire portion of the coma examined in the simulations. However, HCO, $O(^1D)$, and O_2 level off or decrease at thousands of kilometers. HCO comes from parents with short photodissociation lifetimes, and is itself short-lived, thus its abundance tapers off quickly upon depletion of its parent species. $O(^1D)$ tapers off as the level lifetime of $O(^1D)$ is reached as it travels away from the nucleus, as well as collisional de-excitation, chemical reactions, and the slow depletion of its parent species (most notably H_2O). However, at the outer edge of the region covered by the simulations, the $O(^1D)$ abundance does not become depleted in like manner as HCO since the photodissociation of OH becomes an increasingly important contributor to the $O(^1D)$ abundance. The O_2 abundance is tied to the $O(^1D)$ abundance since it is made through a reaction with $O(^1D)$ in these studies. Therefore, its curve looks somewhat similar to the $O(^1D)$ curve.

Among the neutral-charge daughter species, there are some differences in the relative abundances of HCO, $O(^1D)$, O_2, and H^* across the three outflow cases. These differences are highlighted in Figure 3.3. The results demonstrated modest inner coma enhancements in the relative abundance of HCO, as well as inner coma depletions of $O(^1D)$ and H^* for Case 3. In the outer regions of the simulated comae, there is an enhancement in O_2 in Case 3. If indeed O_2 is only formed through chemical reactions, and is ever definitively observed in comets, the results here suggest that topography may be a factor in its abundance.

Among the profiles shown here, it is possible to compare the $O(^1D)$ profiles with observations. For comparison, a profile of [O I] emission from the observation of comet Tuttle by Fink & Johnson (1984) was used. At the time of observation,

it had similar production rate and heliocentric distance to the conditions used in studying the three outflow cases. Figure 3.4 shows the O(^{1}D) profiles (not shown as n $\times$ r^2) for all three outflow cases. Their shapes follow the general trend of model predictions of [O I] emission for a comet of comparable production rate as calculated by Festou & Feldman (1981) and O(^{1}D) profiles calculated with the models of Bhardwaj & Haider (2002). However, the near-nucleus behavior of models with acceleration take on a slightly different shape than the case where the velocity remained constant. In Figure 3.5, the O(^{1}D) profiles are compared to the Tuttle observation. Because the nature of the 1-D models makes an exact brightness comparison difficult, the profiles were compared over the same region of the coma in order to analyze their power-law behaviors. In all three outflow cases, the dilution of O(^{1}D) concentration was steeper than observed, with the greatest deviation seen in Case 3. In order to examine the effect of chemical reactions on the O(^{1}D) profile, Case 1 was run again, using the same nuclear composition as shown in Table 3.1, but using photochemical processes only. The result is also shown in Figure 3.5b, along with the other cases. Although this result is approximately 4% flatter than Case 1 with all reactions, the consistently steep power-law behaviors exhibited by all three outflow cases suggest that greater near-nucleus acceleration is needed to match the Tuttle observation, and/or there is a slight overestimation of collisional de-excitation of O(^{1}D) by H_2O.

Figure 3.6 is a plot of the relative abundances of the ionic species. Just like the neutral-charge species, the relative abundances of all ionic species increase with distance as photochemical and two-body processes form them. The relative abundances of H_3O^+, $CH_3OH_2^+$, and H_3CO^+ level off with respect to the other ionic species as a result of the many reactions in which they take part. CO_2^+ in

particular, does not match observations, which peaks at the nucleus (Woods et al. 1986). Either there are one or more chemical reactions not included here that are necessary to better match this behavior, or there is a physical phenomenon in the near-nucleus environment not currently accounted for.

Figures 3.7 and 3.8 show differences in the relative abundances of many of the ions across the three outflow cases. In general, Case 3 exhibits moderate inner coma depletions of many ionic species, most likely due to the many recombination reactions with electrons, which have large collisional cross-sections. For species such as H_3CO^+ and $CH_3OH_2^+$, the cumulative effects of chemical reactions and outflow behavior are manifest in the results in the outer portion of the simulated comae, with relative abundances varying by as much as an order of magnitude across the three outflow cases. The results suggest that some ionic species may be sensitive to the behavior of the outflow.

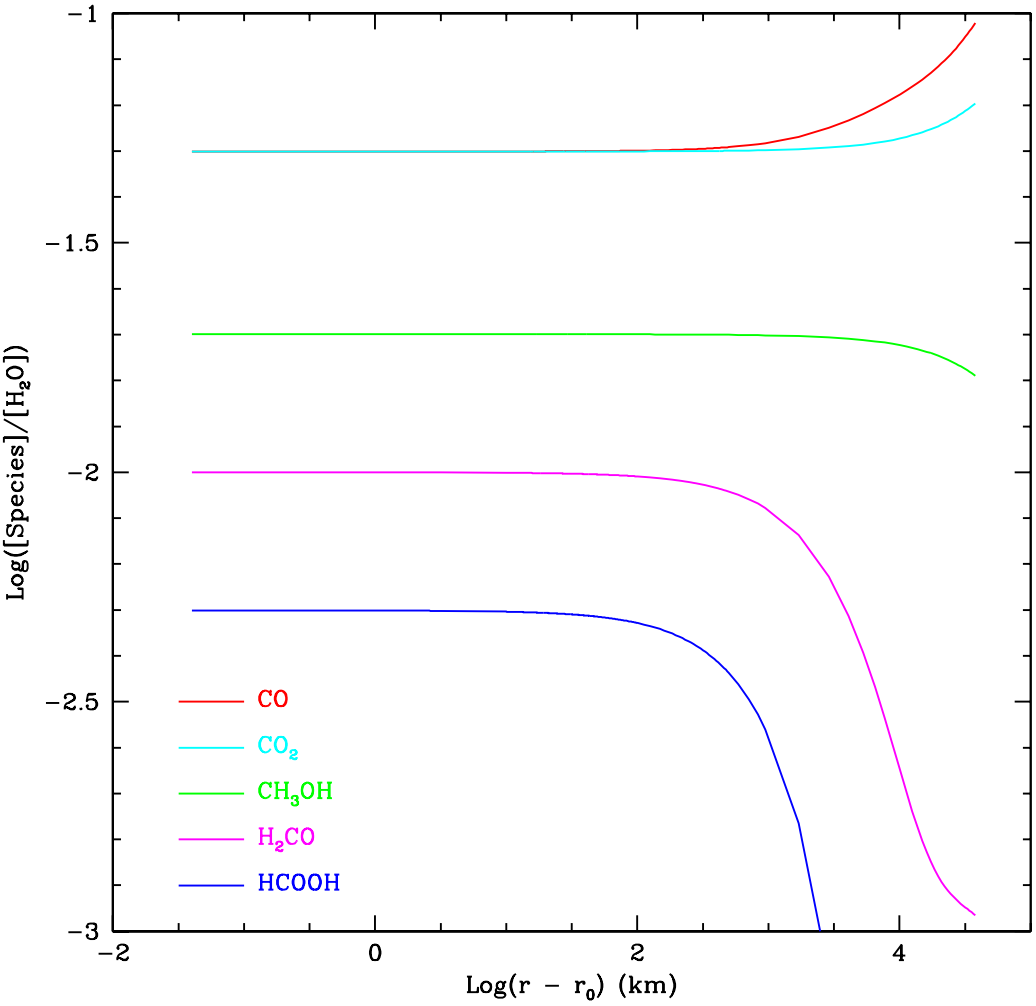

Figure 3.1 – Plot of the relative abundances of all species released from the nucleus in Case 1.

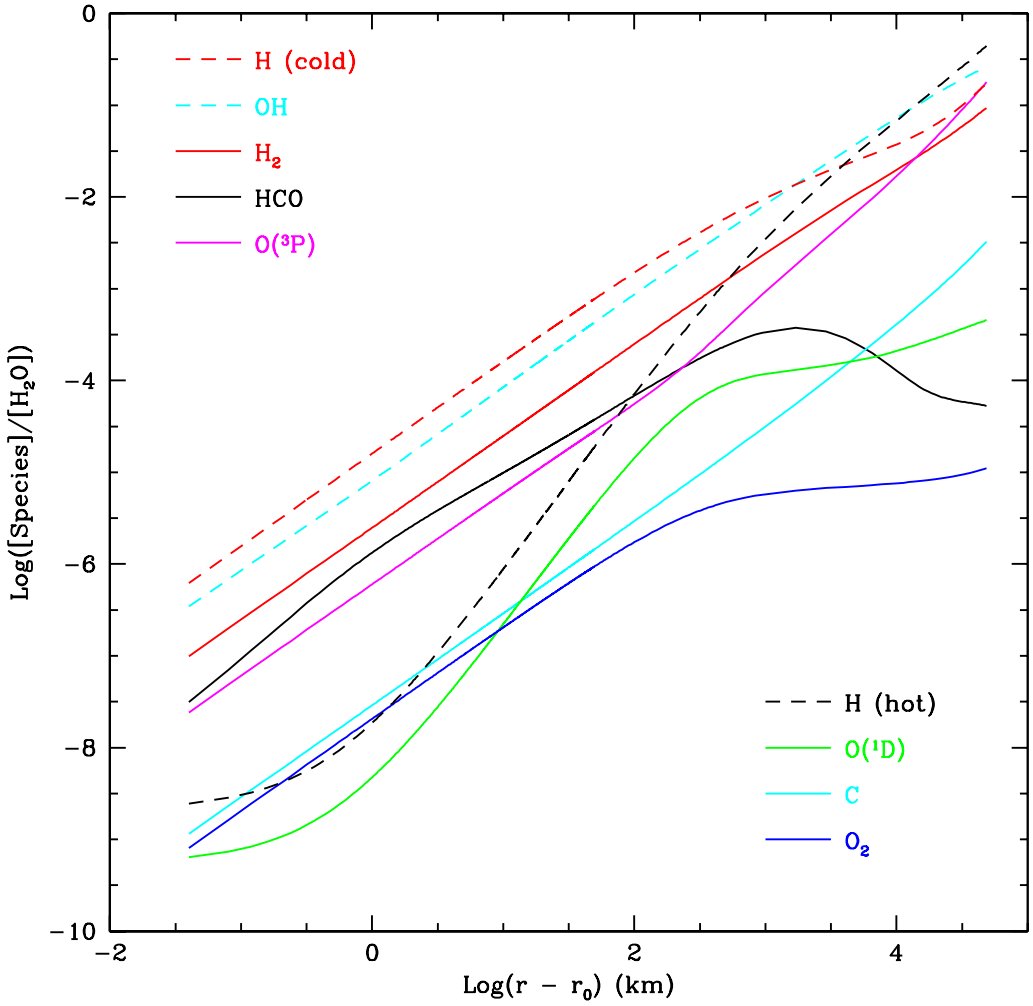

Figure 3.2 – Plot of the relative abundances of all neutral-charge species formed in the coma in Case 1.

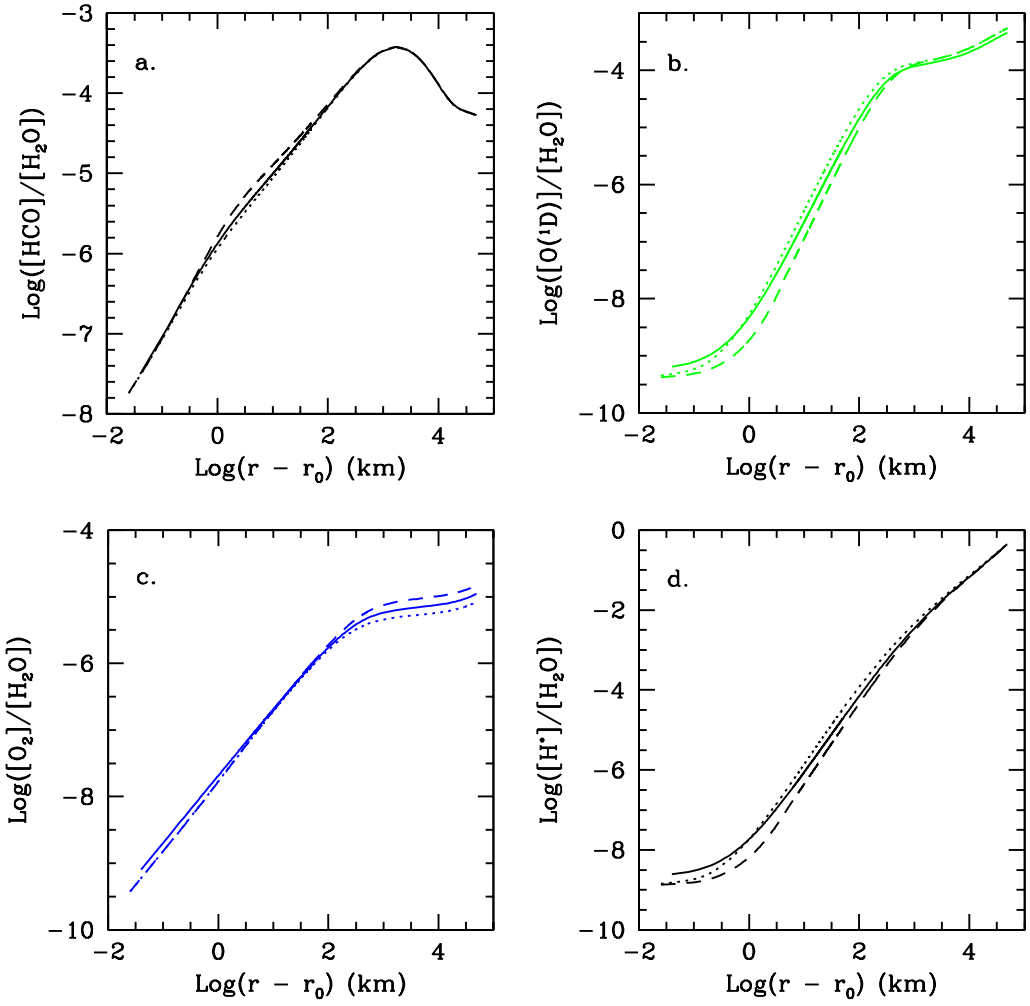

Figure 3.3 – Plot of the relative abundances of four neutral-charge species formed in the coma for all three outflow cases: a. HCO, b. $O(^1D)$, c. O_2, d. H^*. The colors of the lines are identical to the colors in Fig. 3.2. The solid line is Case 1, the dotted line is Case 2, and the dashed line is Case 3.

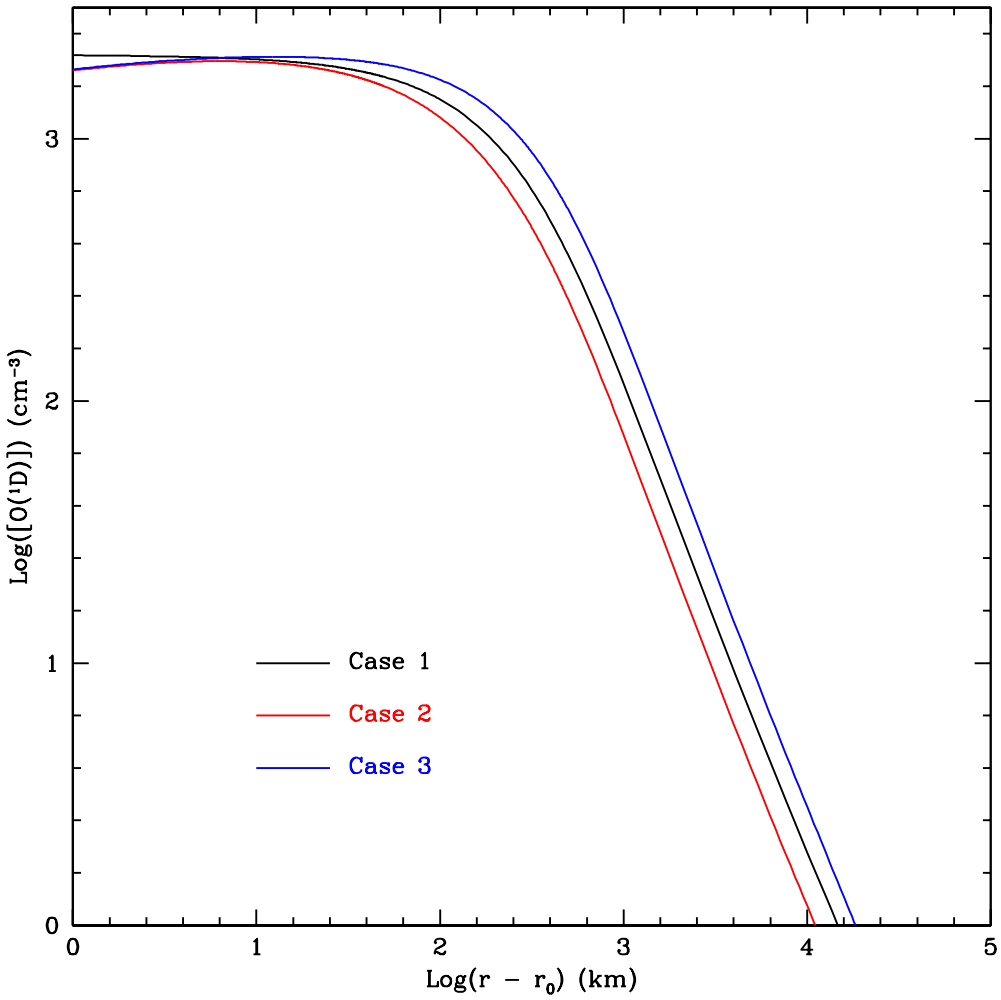

Figure 3.4 – Plot of O(^{1}D) profiles obtained from Cases 1-3.

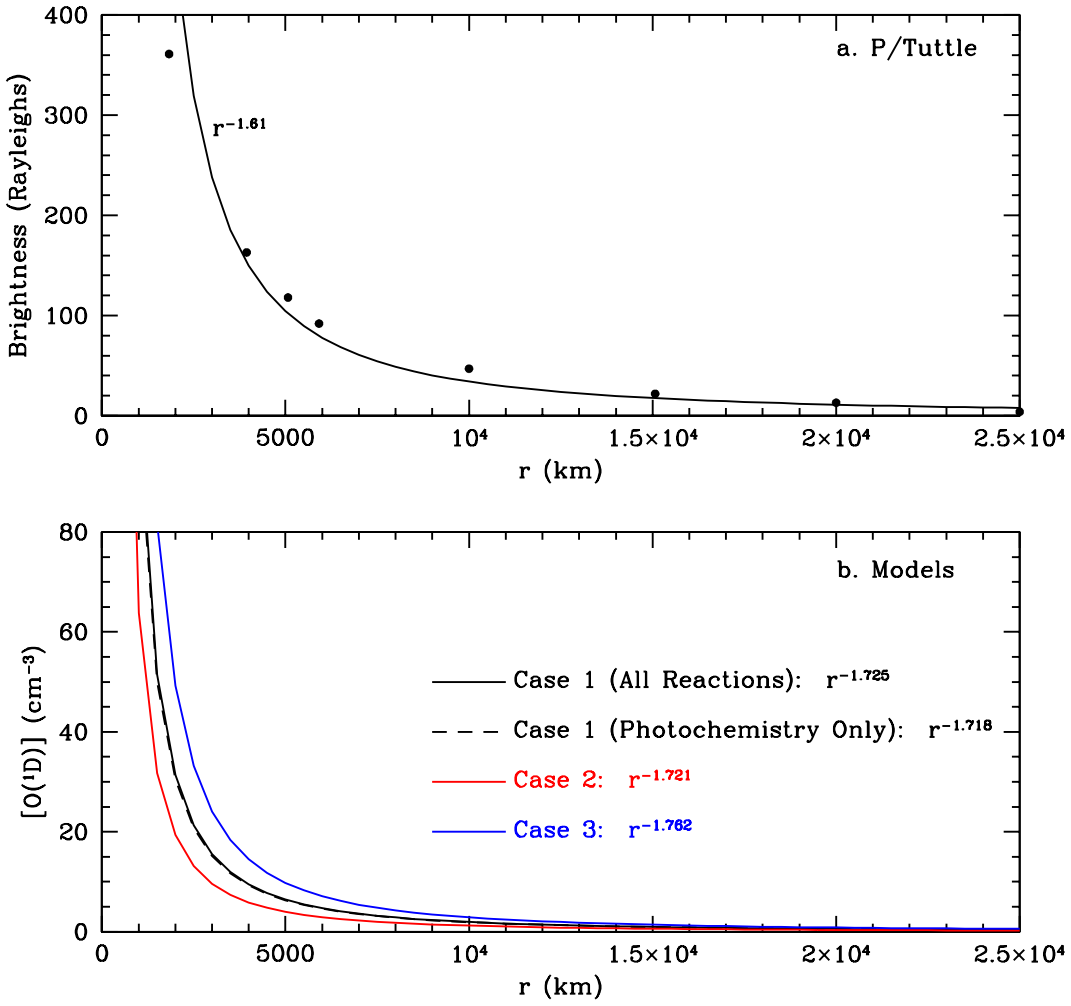

Figure 3.5 – a. Brightness of [O I] emission as a function of cometocentric distance for comet P/Tuttle, showing the observed profile (dots) and the power-law behavior of the data (solid line). Data points taken from Fig. 4 of Fink & Johnson (1984). b. O(^{1}D) profiles from Cases 1-3, indicating the power-law behavior of the profiles from all three outflow cases in the same region of the coma as the observations.

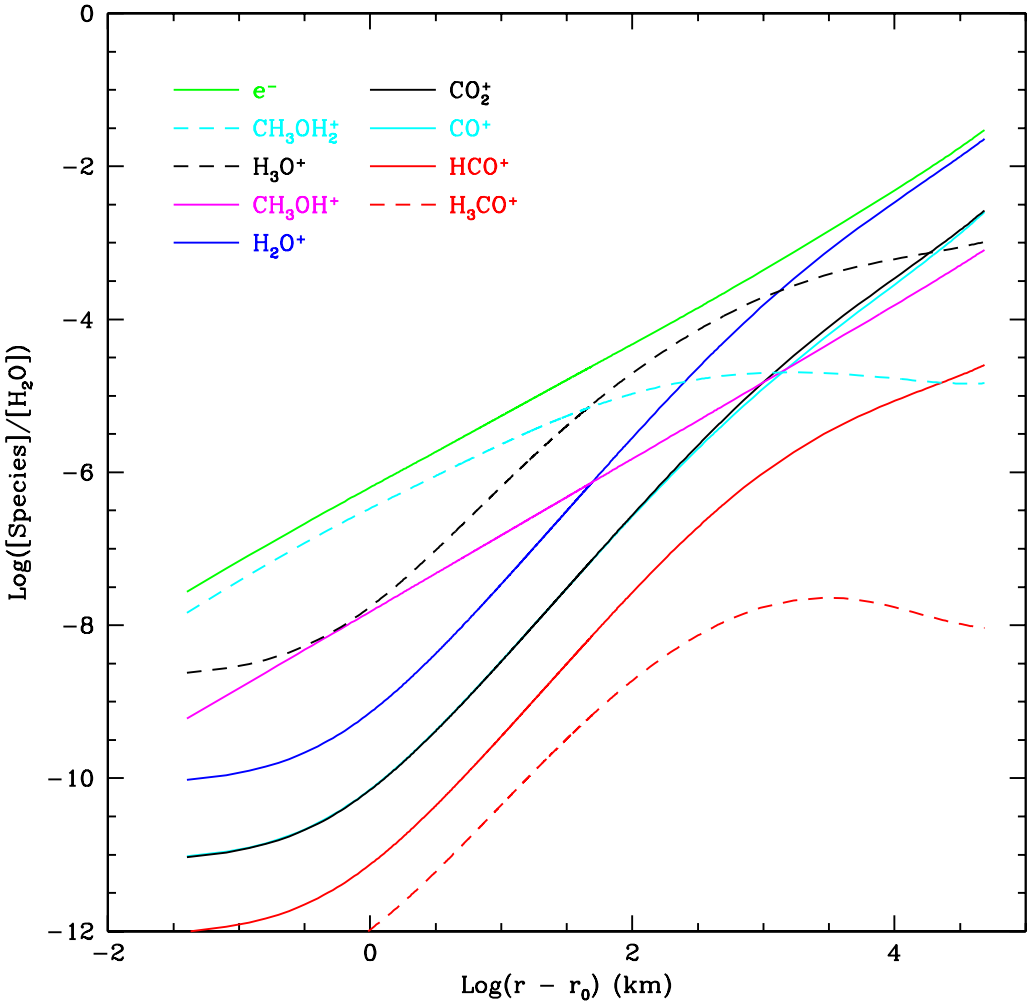

Figure 3.6 – Plot of the relative abundances of all ionic species formed in the coma in Case 1.

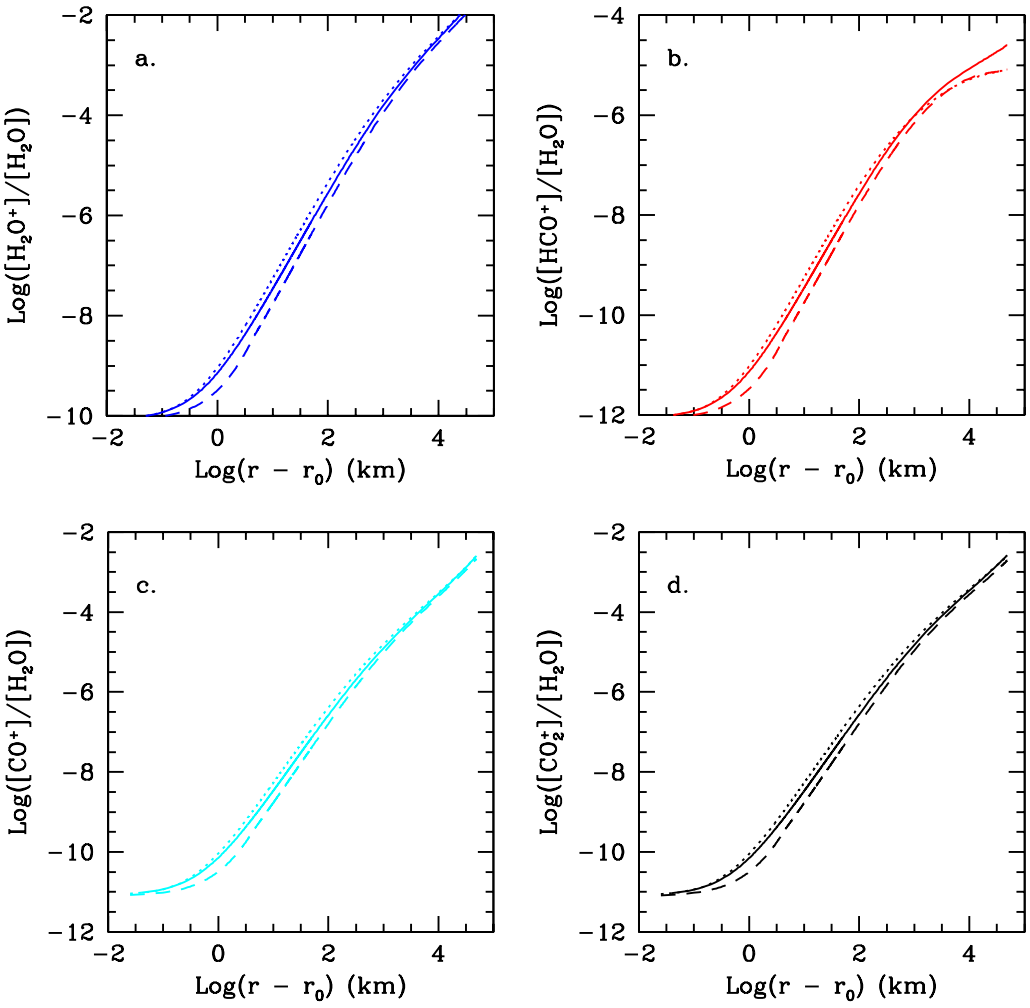

Figure 3.7 – Plots of the relative abundances of four ionic species for all three outflow cases: a. H_2O^+, b. HCO^+, c. CO^+, d. CO_2^+. The colors of the lines are identical to the colors in Fig. 3.6. The solid line is Case 1, the dotted line is Case 2, and the dashed line is Case 3.

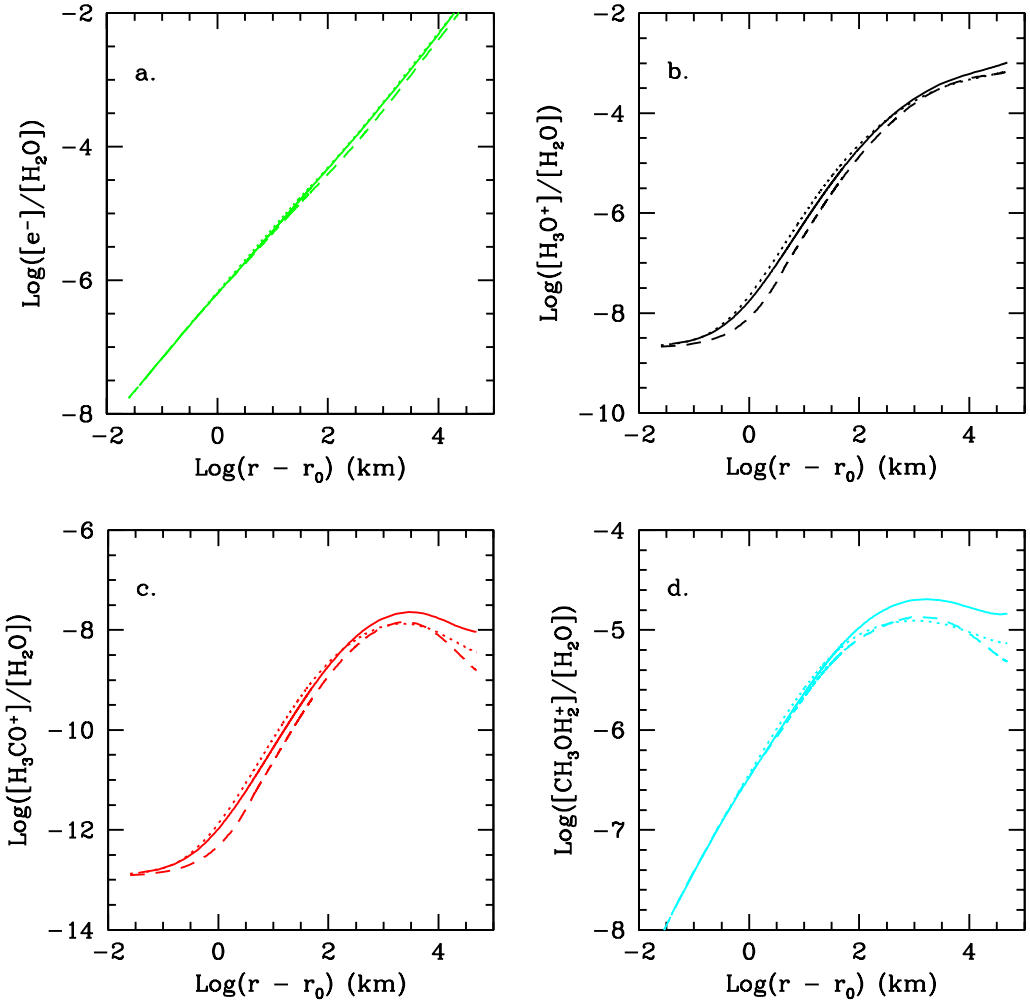

Figure 3.8 – Plots of the relative abundances of four ionic species for all three outflow cases: a. e^-, b. H_3O^+, c. H_3CO^+, d. $CH_3OH_2^+$. The colors of the lines are identical to the colors in Fig. 3.6. The solid line is Case 1, the dotted line is Case 2, and the dashed line is Case 3.

3.2.2 Comparison of CO Formation and Destruction Rates

Figure 3.9 shows the relative contribution of all CO formation mechanisms to the overall CO formation rate for Case 1. The dominant CO formation mechanisms were photodissociation processes. For low activity comets, this suggests that two-body reactions are not significant contributors to the CO abundance. To compare the result with Cases 2 and 3, Figure 3.10 shows the relative contribution of all CO formation processes to the overall CO formation rate for all three outflow cases. In all three cases, the dominant mechanisms of CO formation are the same, namely H_2CO and HCO photodissociation beyond a few thousand kilometers. Two-body chemical reactions have little importance in the cases examined here, but differences in outflow behavior did manifest themselves in these trials, even for the modest production rate used here. Case 2 exhibits the lowest relative contributions from chemical reactions over most of the coma since it has significant acceleration without the flatted density dilution present in the inner coma of Case 3. Overall, the greatest differences appear in the neutral-charge two-body reactions, especially the self reaction of HCO. Since there also appears to be a near-nucleus enhancement of HCO with topography, the results suggest that the inner coma abundance of HCO is sensitive to the outflow behavior of the gas from the nucleus.

Figure 3.11 shows the relative contribution of all CO destruction mechanisms for Case 1. The dominant loss mechanisms for CO were also photodissociation processes. For comparison, Figure 3.12 shows the relative contribution of all CO destruction mechanisms for all three cases. In all three cases, the dominant loss mechanisms were CO photodissociation and photoionization. As with the formation mechanisms, Case 3 exhibits greater fractional contribution from the

two-body destruction mechanisms over most of the coma. The chemical reaction with the greatest influence in the innermost coma is the reaction of CO + OH, which has been speculated by other researchers to be one of the more significant reactions that may take place in the inner comae of comets (Giguere & Huebner 1978; Glinski et al. 2004). Although some suggest that this may be the dominant CO loss mechanism in the inner coma, that is not demonstrated here, suggesting the result may depend on how many sources and sinks of OH are included in the chemical reaction network.

Figure 3.13 shows the total fractional contribution of two-body chemical reactions to the overall CO formation and destruction rates for all three outflow cases. Case 3 exhibits higher fractional contributions of two-body reactions to both CO formation and destruction, as demonstrated by examining the individual formation and destruction rates. The results suggest that outflow behavior does influence CO formation and destruction. However, with the exception of the region around 1 km from the surface, the overall contribution was well under 50% over the coma sampled in these trials.

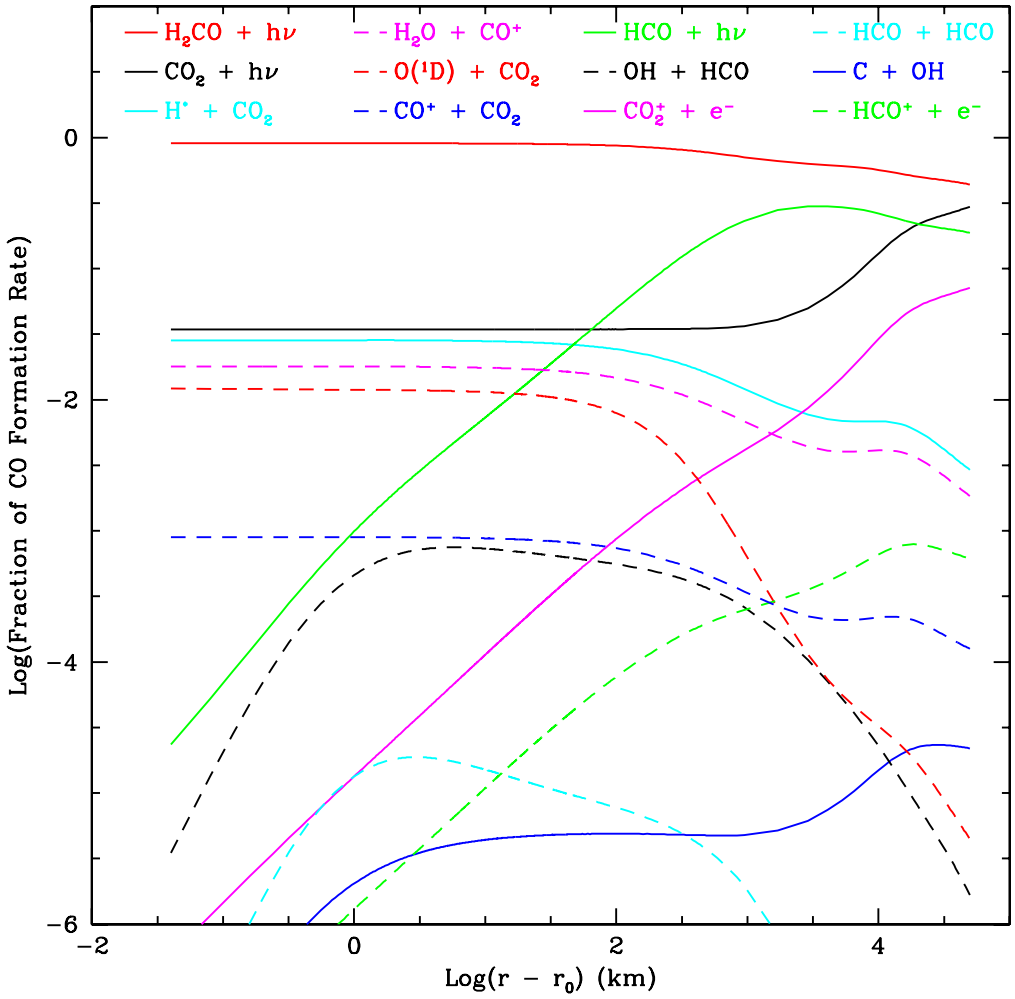

Figure 3.9 – CO formation rates (given as the log of their fractional contribution to the total CO formation rate) for Case 1.

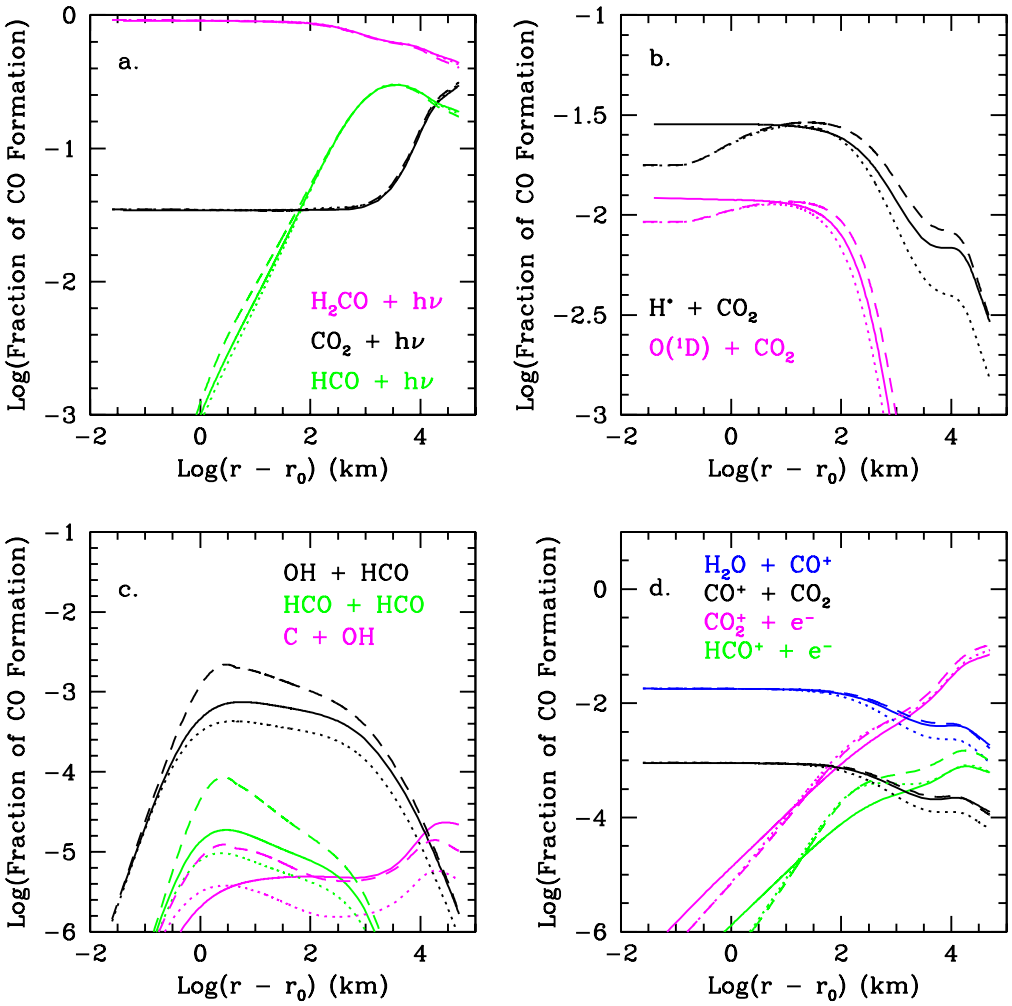

Figure 3.10 – Comparison of CO formation rates (given as the log of their fractional contribution to the total CO formation rate) from multiple processes for three outflow cases: a. photochemical processes, b. two-body reactions involving species in excited states, c. neutral-charge two-body reactions, d. ion reactions. The solid line is Case 1, the dotted line is Case 2, and the dashed line is Case 3.

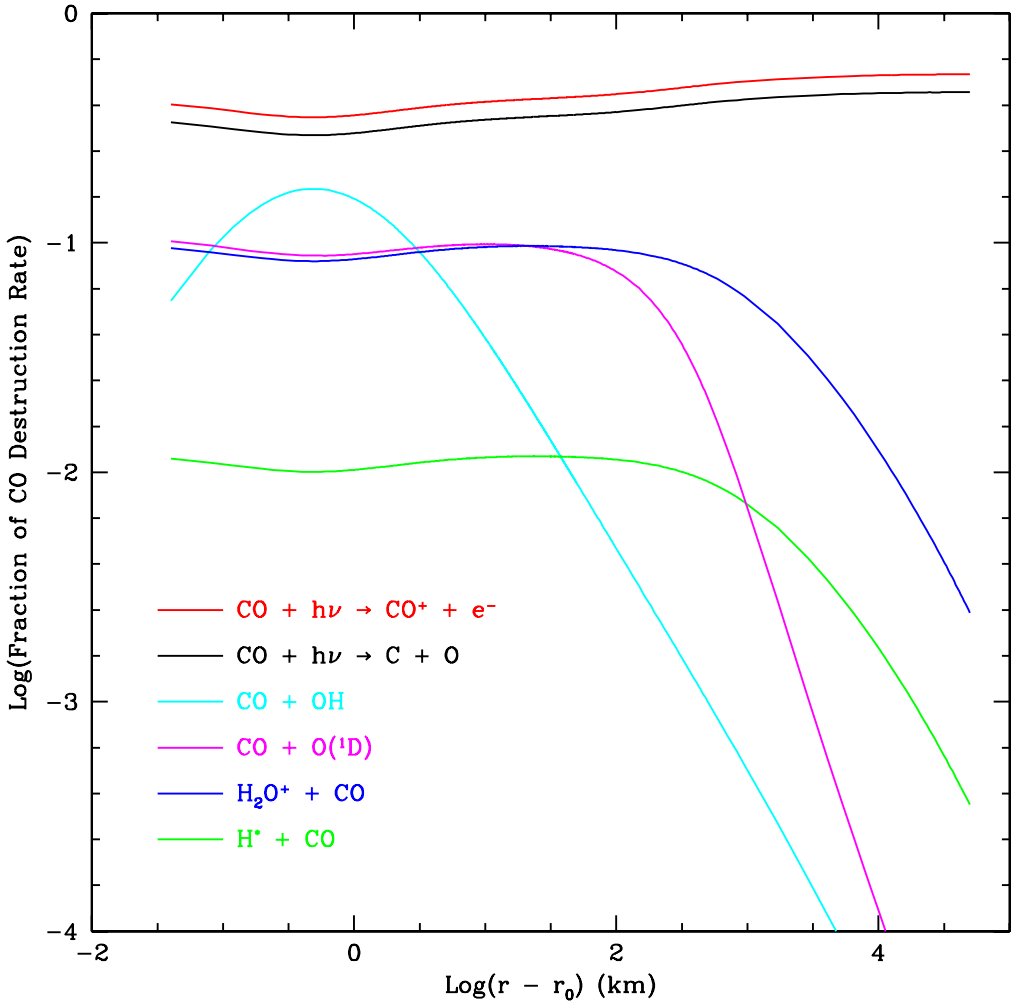

Figure 3.11 – CO destruction rates (given as the log of their fractional contribution to the total CO formation rate) for Case 1.

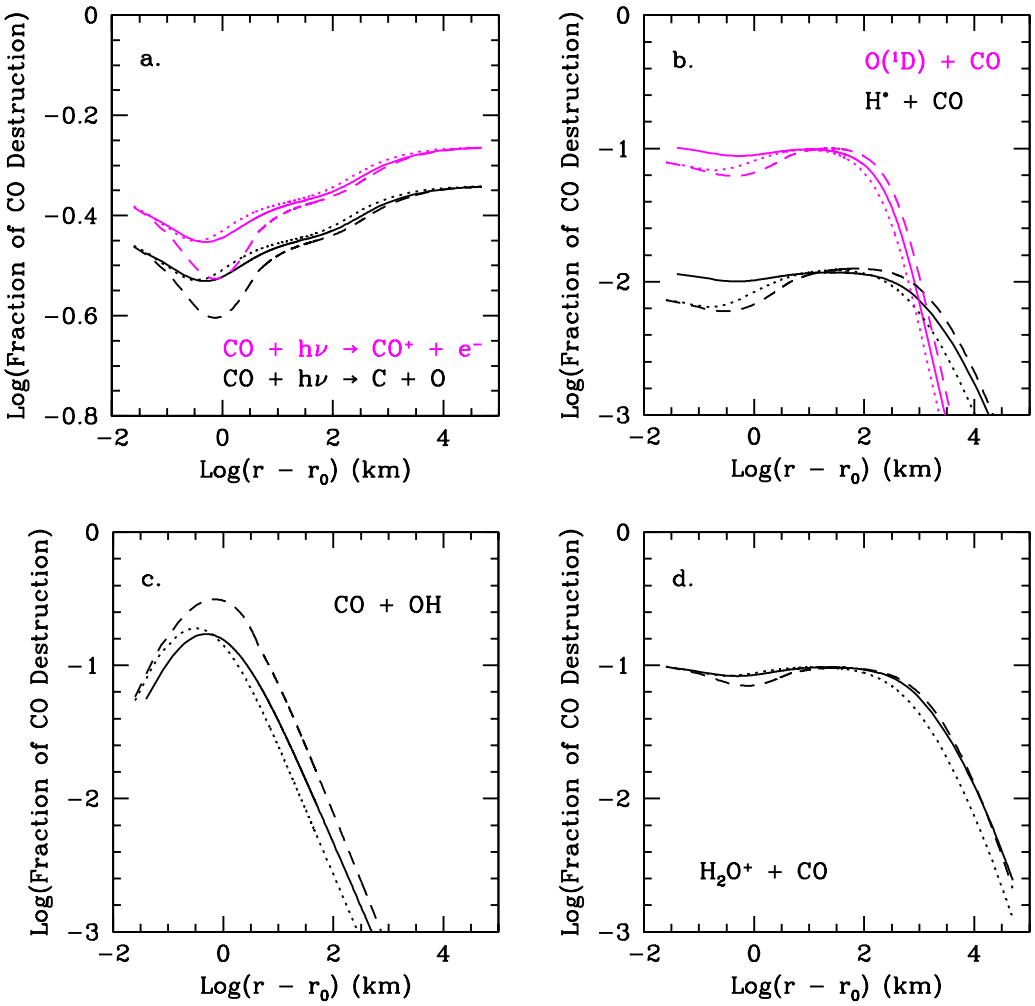

Figure 3.12 – Comparison of CO destruction rates (given as the log of their fractional contribution to the total CO formation rate) for three outflow cases: a. photochemical processes, b. two-body reactions involving species in excited states, c. neutral-charge two-body reactions, d. ion reactions. The solid line is Case 1, the dotted line is Case 2, and the dashed line is Case 3.

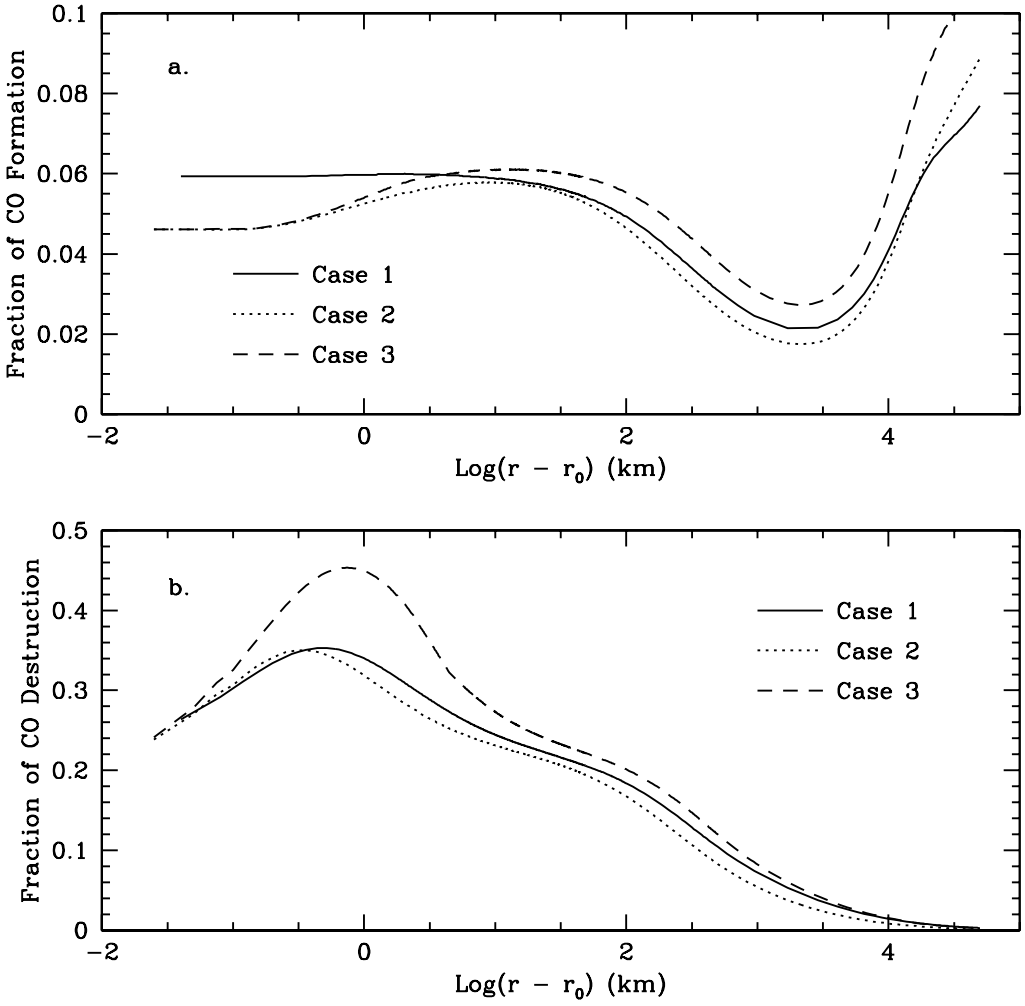

Figure 3.13 – Fraction of the total CO formation (a) and CO destruction (b) from all chemical reactions for the three cases of outflow behavior.

3.3 Production Rate

The production rate, the number of molecules released from the nucleus per unit time, should have an influence on chemical reaction rates. Therefore, the results of trials conducted at three different production rates are compared with each other to identify potential changes to the fractional contribution of chemical reactions to the overall CO formation rate, as well as the impact on the abundances of species in the coma. All three trials use the same chemical composition, as shown in Table 3.1, and they all use the same outflow behavior. For simplicity, the profile of constant temperature and velocity is used, with v = 0.8 km s^{-1} and T = 60 K for Q = 5×10^{29} s^{-1}, and v = 1.0 km s^{-1} and T = 100 K for Q = 10^{31} s^{-1}. For the case using Q = 10^{31} s^{-1}, ultraviolet attenuation of H_2O is added.

3.3.1 Comparison of Species

Figure 3.14 shows the relative abundances of CO and H_2CO for all three production rates. With increasing production rate, the chemical reaction network is capable of producing increased relative abundance of CO. As the corresponding curve for H_2CO shows, the increased relative abundance of CO is accompanied by a decreased relative abundance of H_2CO over most of the coma simulated here, the result of increased reaction rates of reactions in which it is involved.

Figure 3.15 highlights differences in the relative abundances of neutral-charge species formed in the coma for all three production rates. The abundances of many of these species are noticeably depleted in Q = 10^{31}, because they are related to the photochemistry of H_2O, which is attenuated in the inner coma. There is also evidence of increased abundance of HCO in the inner coma, similar to what was seen in the outflow behavior comparison except more pronounced,

further suggesting that chemical reactions may influence its inner coma abundance. Along similar lines, the abundance of O_2 appears greater for high-activity comets. O_2 has not been definitively identified in comets, but this result suggests that O_2 might be found in high-activity comets. It has no permanent dipole moment, but O_2 could photoionize to O_2^+, which would be visible in the outer coma. This result is consistent with the results of Glinski et al. (2004), which suggests that O_2 could be made in the coma by two-body chemical reactions.

A comparison between modeled and observed O(^{1}D) profiles was done again in order to see whether the models match observations. For this comparison the results from Q = 5×10^{29} s^{-1} were compared to an O(^{1}D) observation taken by Magee-Sauer et al. (1988). The results are shown in Fig. 3.16. As with the examination of outflow behavior, the power-law behavior of O(^{1}D) over the relevant region of the coma is again steeper than what is observed. The profile compared with the observation contains no acceleration, thus making the power-law behavior of the modeled profile too steep.

Figures 3.17 and 3.18 highlight the differences in relative abundances of several ionic species formed in the coma. The results overall are similar to what was seen in the outflow behavior comparison, namely that cases where chemical reactions are likely to be more important exhibit relatively depleted abundances of many ionic species. However, across the large difference in production rates, the effects are more pronounced. While some of these differences are attributed to ultraviolet attenuation in the highest-activity trial, the results suggest that two-body reactions have a significant effect on ion chemistry in active comets.

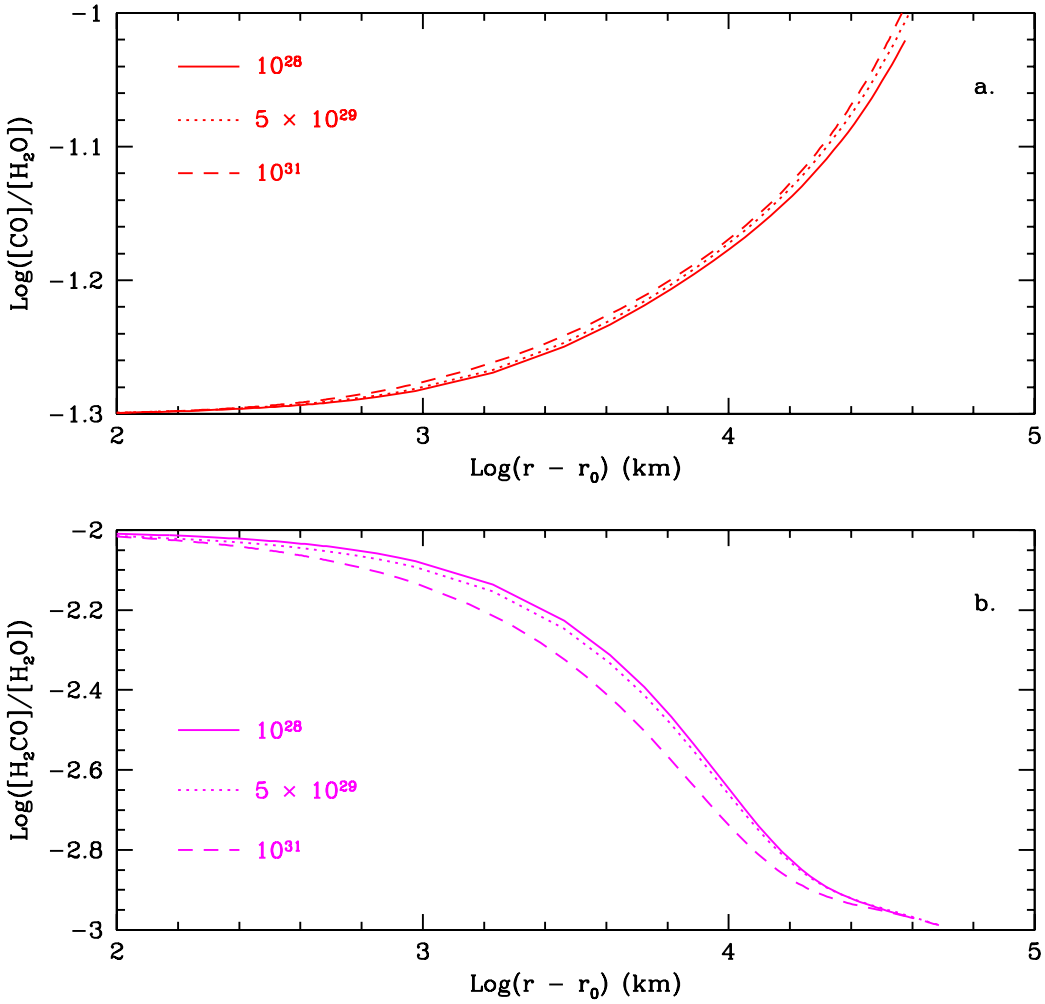

Figure 3.14 – Comparison of species released from the nucleus for three different production rates: a. CO, b. H_2CO. The solid line is Q = 10^{28} s^{-1}, the dotted line is Q = 5×10^{29} s^{-1}, and the dashed line is Q = 10^{31} s^{-1}. The colors match those used in Fig. 3.1.

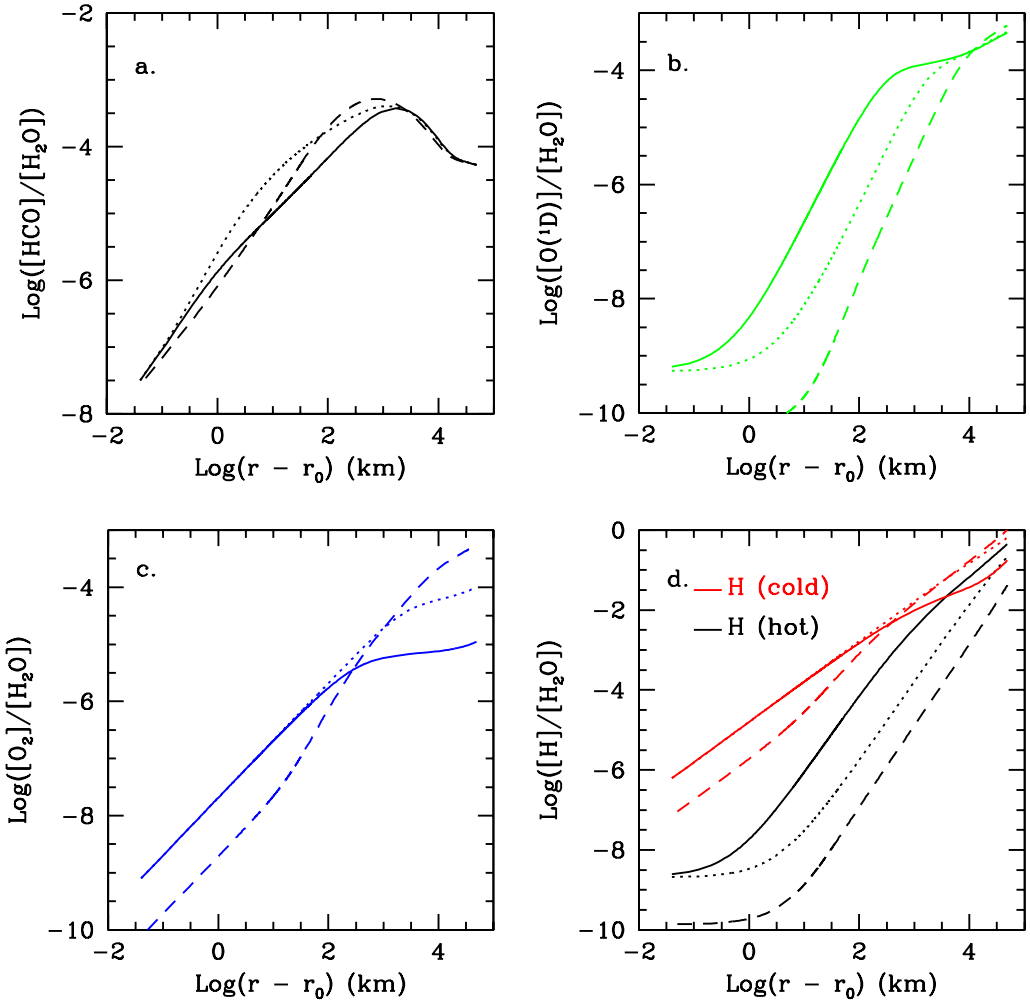

Figure 3.15 – Comparison of several neutral-charge species formed in the coma for three different production rates: a. HCO, b. $O(^1D)$, c. O_2, d. H (hot and cold). The solid line is Q = 10^{28} s^{-1}, the dotted line is Q = 5 × 10^{29} s^{-1}, and the dashed line is Q = 10^{31} s^{-1}. The colors match those used in Fig. 3.2.

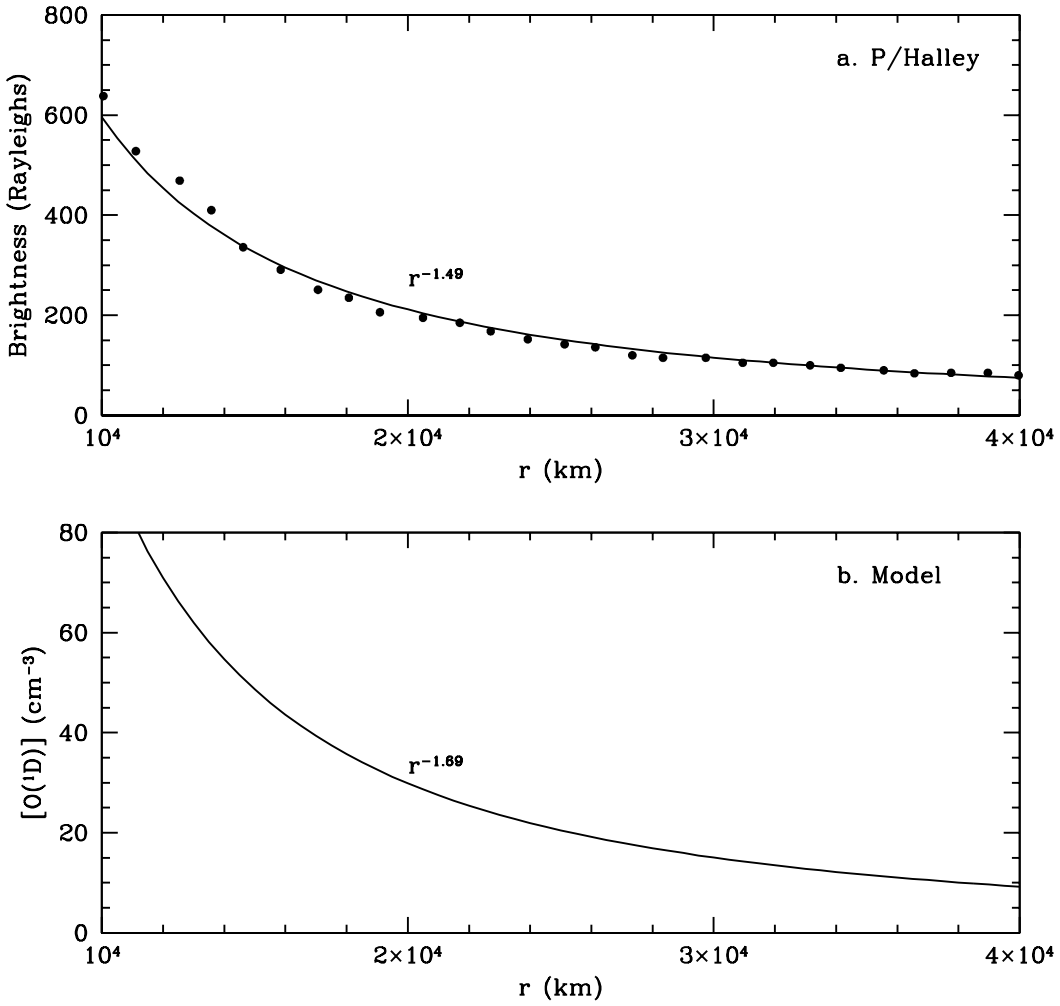

Figure 3.16 – a. Brightness of [O I] emission as a function of cometocentric distance for comet P/Halley, showing the data (dots), and the power-law behavior of the profile (solid line). Data derived from Fig. 2a of (Magee-Sauer et al. 1988). b. O(^{1}D) profile from Q = 5 × 10^{29} s^{-1}, showing power-law behavior over the same region of the coma as the Halley observation.

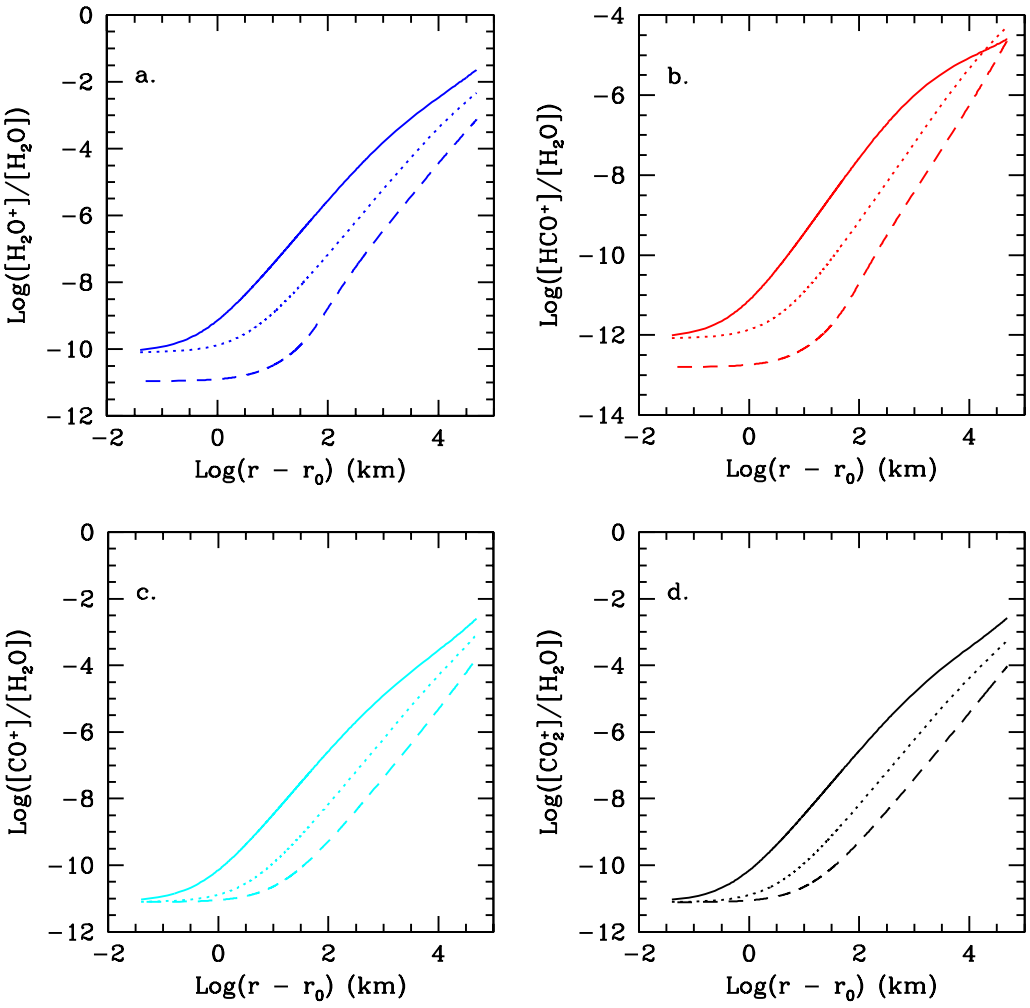

Figure 3.17 – Comparison of several ionic species formed in the coma for three different production rates: a. H_2O^+, b. HCO^+, c. CO^+, d. $CO_2{}^+$. The solid line is Q = 10^{28} s^{-1}, the dotted line is Q = 5 × 10^{29} s^{-1}, and the dashed line is Q = 10^{31} s^{-1}. The colors match those used in Fig. 3.6.

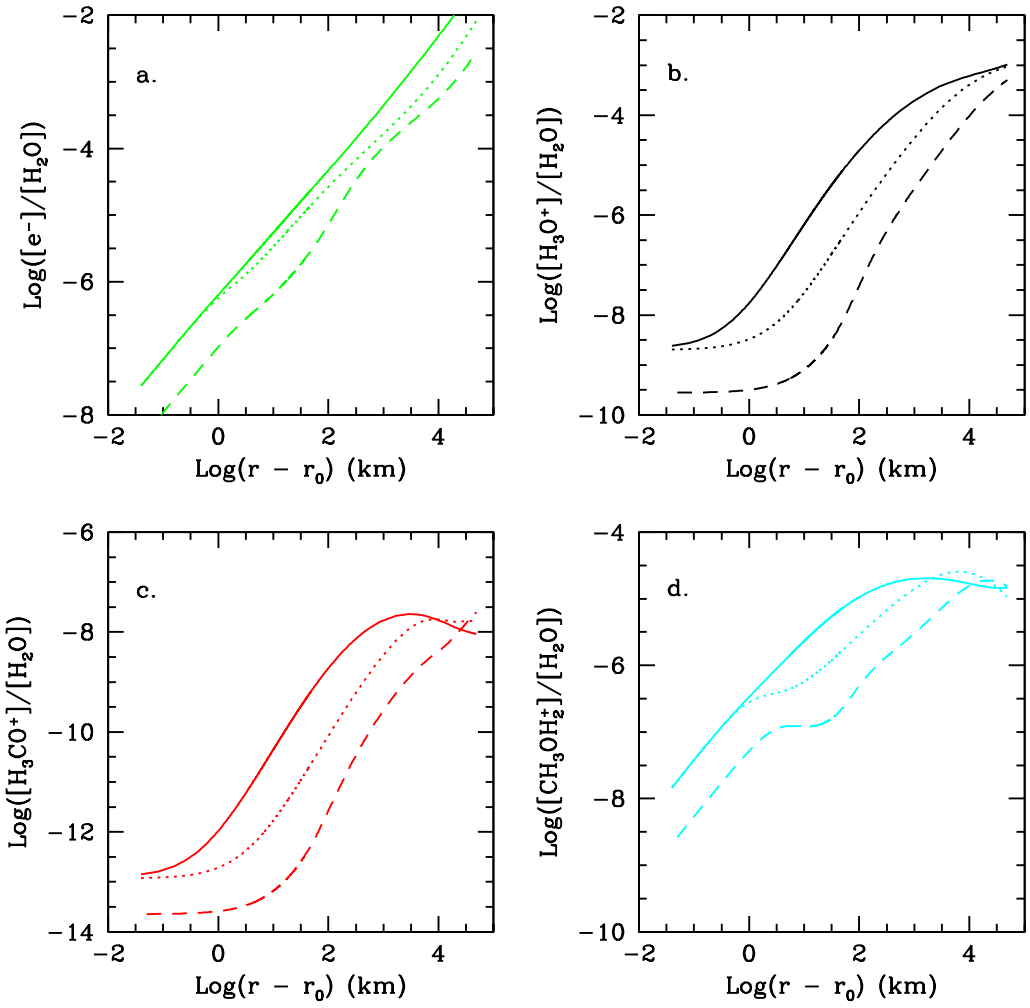

Figure 3.18 – Comparison of several ionic species formed in the coma for three different production rates: a. e^-, b. H_3O^+, c. H_3CO^+, d. $CH_3OH_2^+$. The solid line is Q = 10^{28} s^{-1}, the dotted line is Q = 5 × 10^{29} s^{-1}, and the dashed line is Q = 10^{31} s^{-1}. The colors match those used in Fig. 3.6.

3.3.2 Reaction Rate Comparison

Figure 3.19 shows the fractional contributions of CO formation rates for all three production rates. With increased production rate, chemical reactions generally contribute a larger fraction of the total CO formation in the coma. Reactions that were inconsequential in the original case ($Q = 10^{28}$ s^{-1}), such as C + OH, jump dramatically in relative importance for high activity comets. The dramatic increase in reaction rates involving OH suggests that OH plays a far greater role in coma chemistry than merely being a source of hydrogen and $O(^1D)$. The reactions involving $O(^1D)$ and H^* are modest contributors in all three cases, but their relative contribution to the total CO formation rate also increases noticeably with the production rate, with the fractional contribution from the H^* + CO_2 reaction rivaling the photodissociation of CO_2 beyond 1,000 km and HCO beyond 10,000 km for the highest production rate. As a result, the fractional contribution of photochemistry to the total CO formation rate generally decreases with production rate, as seen in Fig. 3.19a. The exception is HCO in the inner coma, which is made by chemical reactions as well as photochemistry, and the larger HCO formation rate contributes to its larger photochemical contribution in the inner coma.

Figure 3.20 shows the CO destruction rates from multiple processes in the coma. In the innermost coma, the contribution of photochemistry to the total CO destruction rate goes down as production rate increases, so long as ultraviolet attenuation of H_2O is not factored into coma processes. When attenuation is considered, it decreases the amount of several key reactants in the CO destruction process, thus making photochemical destruction relatively more important. However, beyond a few hundred kilometers, chemical reactions become larger

fractional contributors to the overall CO destruction rate. Yet in all three cases, the dominant loss mechanisms overall are the photochemical processes, outside of a few hundred kilometers in the inner coma, where CO + OH is most likely to occur. As mentioned previously, CO + OH has been speculated by others as an important chemical reaction to consider in coma chemistry, and the results for large production rates also suggest this.

Figure 3.21 shows the total fractional contribution of chemical reactions to the formation and destruction of CO. For large production rates, the fractional contribution of chemical reactions to the CO formation rate can reach 30% at distances of a few hundred kilometers from the nucleus, and the fractional contribution of chemical reactions to the destruction rate can be as high as 50%, suggesting that chemical reactions cannot be completely ignored for comets with large production rates.

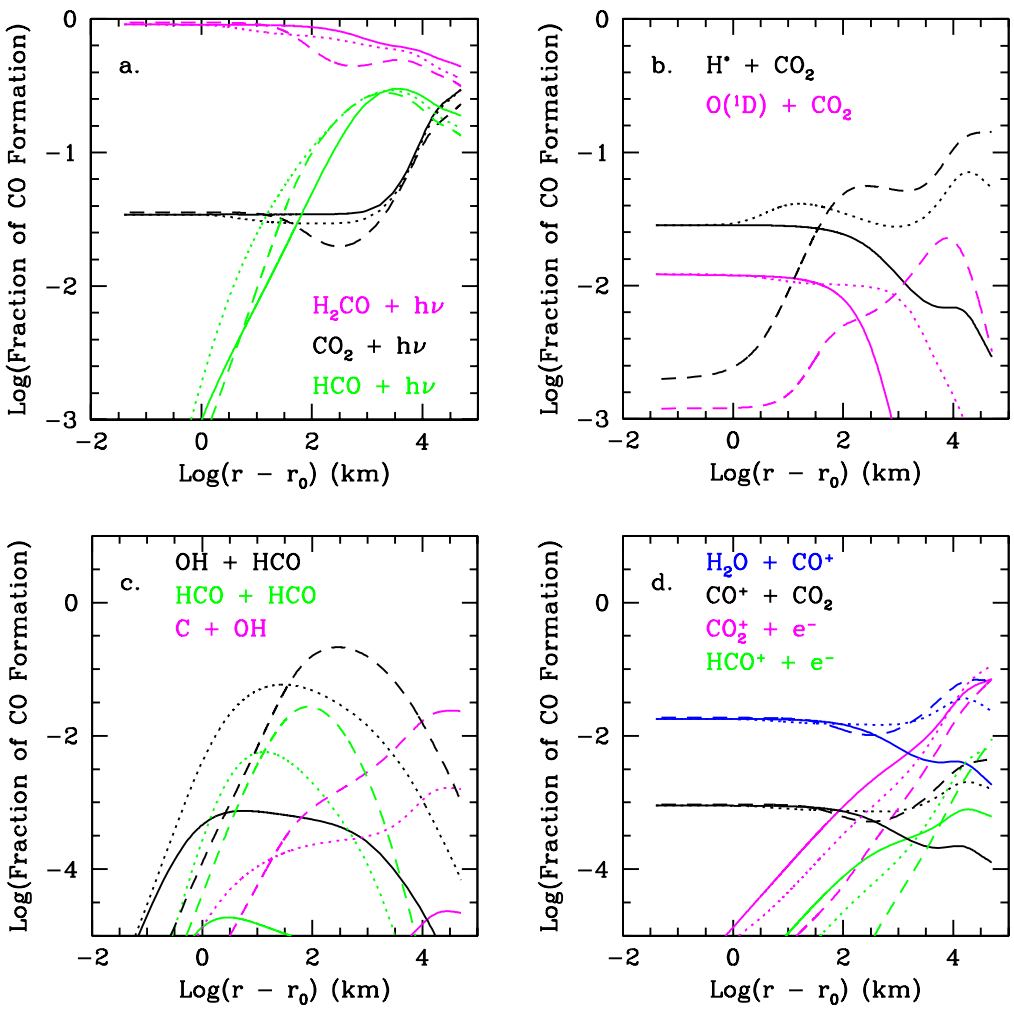

Figure 3.19 – Comparison of CO formation rates (given as the log of their fractional contribution to the total CO formation rate) from multiple processes for three different production rates: a. photochemical processes, b. two-body reactions involving species in excited states, c. neutral-charge two-body reactions, d. ion reactions. The solid line is Q = 10^{28} s^{-1}, the dotted line is Q = 5 × 10^{29} s^{-1}, and the dashed line is Q = 10^{31} s^{-1}.

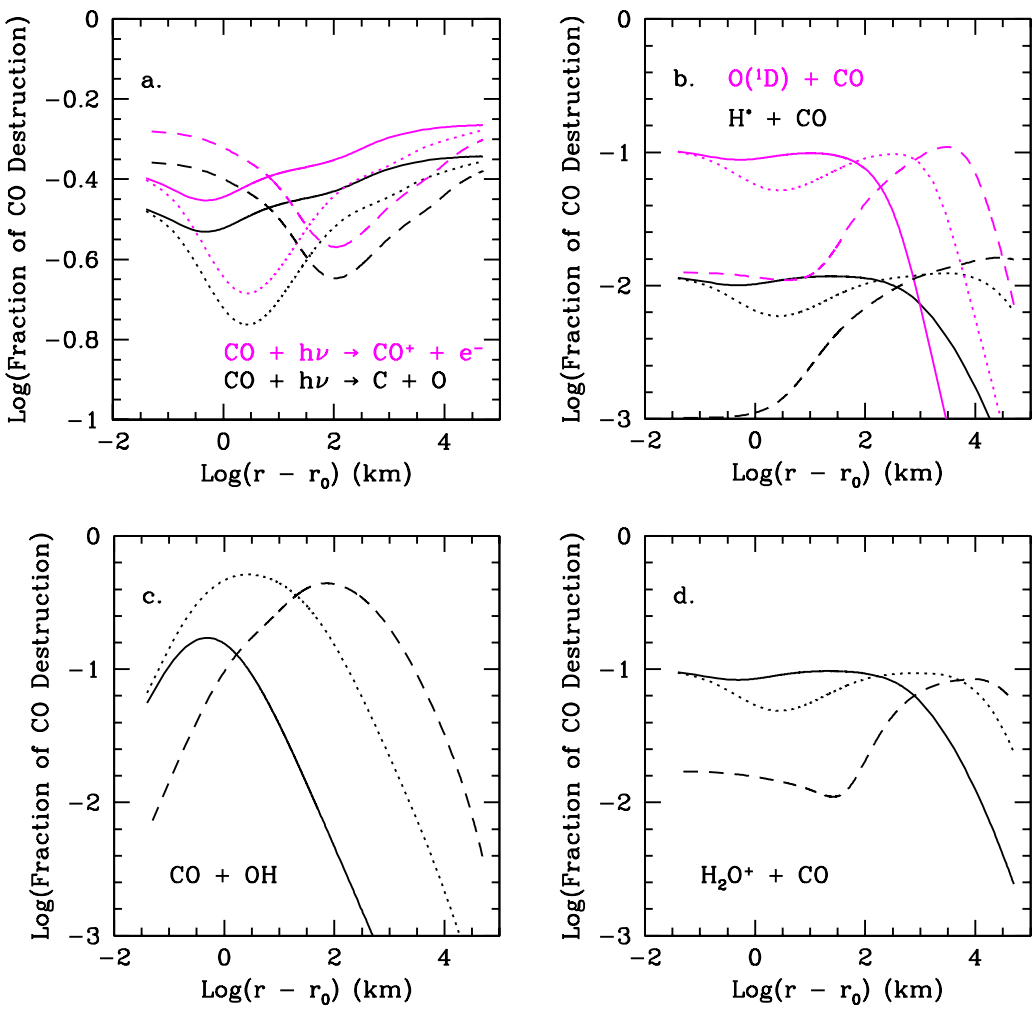

Figure 3.20 – Comparison of CO destruction rates (given as the log of their fractional contribution to the total CO formation rate) for three different production rates: a. photochemical processes, b. two-body reactions involving species in excited states, c. neutral-charge two-body reactions, d. ion reactions. The solid line is Q = 10^{28} s^{-1}, the dotted line is Q = 5 × 10^{29} s^{-1}, and the dashed line is Q = 10^{31} s^{-1}.

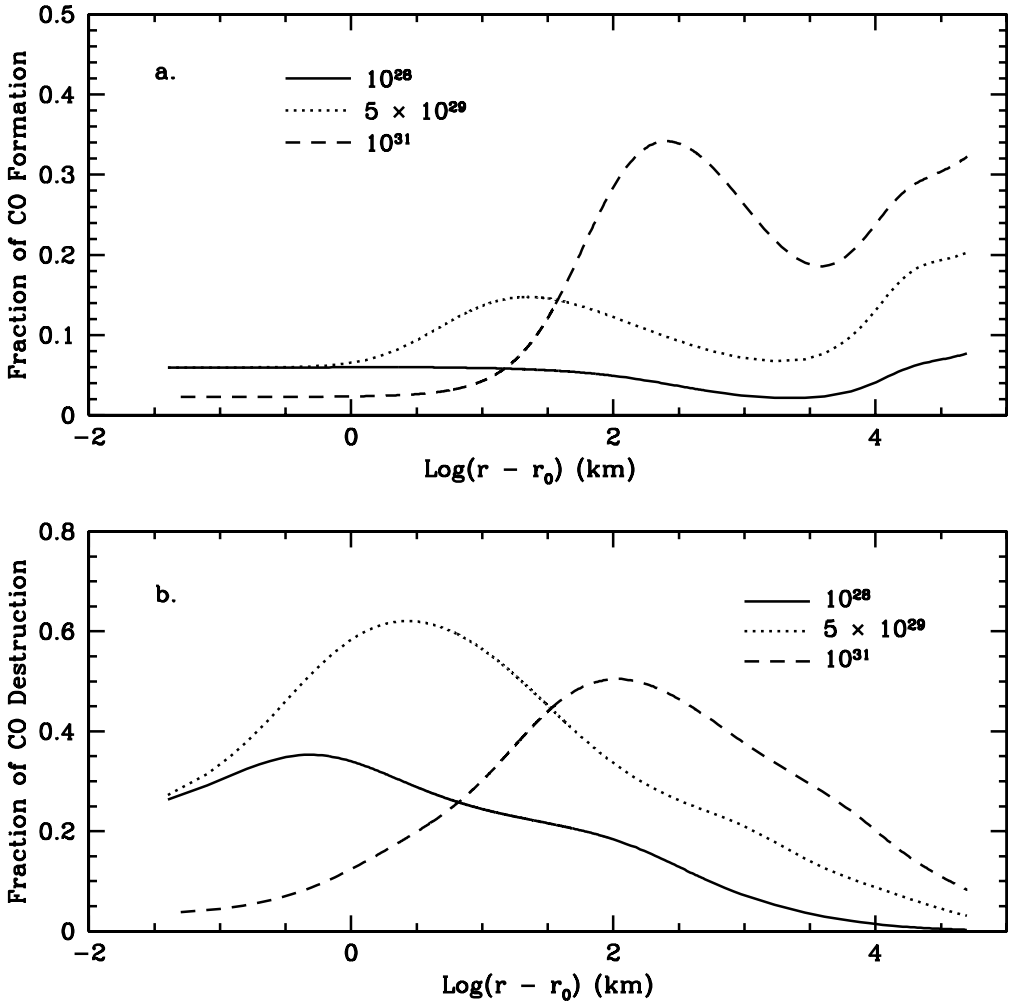

Figure 3.21 – Fraction of the total CO formation (a) and CO destruction (b) from all chemical reactions for three different production rates.

3.4 Conclusions

The influence of outflow behavior did not impact the relative abundance of CO. However, the behavior of the outflow did impact several neutral-charge and ionic species formed in the coma, suggesting that the abundances of some species, especially some ionic species, may be sensitive to acceleration and topography. Including the potential impact of large-scale negative-relief topography, as indicated by the simulation results of Crifo & Rodionov, in the chemical studies increased the relative contribution of two-body chemical reactions to both the formation and destruction of CO. For any comets found to exhibit such surface features, topographic effects may need to be considered when attempting to explain abundances of some daughter species, and perhaps some coma asymmetries.

Changing the production rate had a much greater effect on chemical reaction rates in the coma. Overall, chemical reactions contributed as much as 30% of the CO formation rate, and 50% of the CO destruction rate in the case using the highest production rate, suggesting that chemical reactions should be considered as part of coma phenomena in comets with large production rates. Of particular interest is the dramatic increase in the relative importance of neutral-charge two-body reactions with production rate. Of the body of chemical reactions that have been considered here, as well as by other researchers, the two-body reactions involving ionic species have been more readily accepted as being important players in the formation of some coma species due to their large collisional cross sections. The results here suggest that in comets with large production rates, neutral-charge two-body reactions should also be added to the body of chemical phenomena in the coma.

Chapter 4

The Impact of Gas-Phase Chemistry on Extended CO

4.1 Introduction

Solving the chemical puzzle in cometary comae includes identifying the processes responsible for extended sources of chemical species. As mentioned in Section 1.2.2, there is strong evidence for an extended source of CO in comet Halley. Other observations of Halley revealed that H_2CO and CN most likely have extended sources as well (Meier et al. 1992; Eberhardt 1999; Klavetter & A'Hearn 1994). Multiple observations of Hale-Bopp (C/1995 O1) also showed evidence for extended sources of these species in the coma (DiSanti et al. 2001; Lederer 2000; Woodney 2000). Given the relatively high production rates of these comets, it is highly probable that more phenomena than solely photochemistry occurred in their comae (Combi 2002).

The generally-accepted explanation for the extended CO is release from grains. CHON particles, particles composed of Carbon, Hydrogen, Oxygen, and Nitrogen, discovered in mass spectra during the *Giotto* flyby of comet Halley (Kissel et

al. 1986), could be releasing CO or a precursor to CO, into the coma. However, other studies have indicated that grains may be only partially responsible for the vast amounts of CO produced in the coma (Greenberg & Li 1998). This could be a result of incomplete information about the size distribution, composition, and porosity of dust, as well as the influence of anisotropic outgassing and jet-like structures in the coma (Samarasinha & Belton 1994). The reported detection of CO jets in IRAM observations of comet Hale-Bopp (Henry et al. 2002) lend credence to the suggestion that observations suggesting a CO extended source could be caused by CO-enhanced regions in the coma. Other IRAM observations of comet Hale-Bopp also suggest that most of the CO comes from the nucleus (Biver et al. 1999).

Assuming the extended CO sources are real and the additional CO ultimately comes from grains, one CO precursor could be formaldehyde polymers, or polyoxymethylene (POM) (Eberhardt et al. 1987; Boehnhardt et al. 1990; Cottin et al. 2001), which Huebner (1987) claims are responsible for several peaks observed in the *Giotto* ion data. Given the substantial heating to which the cometary surface is subjected, it would be easy for H_2CO polymers to thermally dissociate into monomer form and subsequently photodissociate (Hanner 1985; Boehnhardt et al. 1990; Moore & Tanabe 1990; Cottin et al. 2001). However, the identification of POMs has been challenged by Mitchell et al. (1989), saying that a mixture of compounds, such as NH, CH_2, O, or N, connected to complex hydrocarbons could also produce the observations. Furthermore, Cottin et al. (2001) point out that POMs only explain the CO source in Halley; they are not likely to be responsible for all of the extended CO source in comet Hale-Bopp, if it exists, due to the low observed abundance of H_2CO.

Another CO parent that could be released from a grain is carbon suboxide (C_3O_2), which can photodissociate by a two-step process, such that $C_3O_2 \rightarrow C_2O$ + CO and $C_2O \rightarrow C$ + CO (Huntress et al. 1991). In order to reproduce the CO extended source in Halley, C_3O_2 would have to be present in an abundance of ~3-4% relative to H_2O. C_3O_2 is a highly symmetric molecule, which can be difficult to detect at infrared wavelengths, but it does have a fairly strong C-O antisymmetric stretch at 4.43 μm, which Crovisier et al. (1991) suggest may be the source of a band seen at approximately that wavelength in spectra from the IKS infrared spectrometer on the *Vega 1* spacecraft which flew by comet Halley. If the identification is correct, the derived abundance of C_3O_2 relative to H_2O was determined to be 0.11%. However, Allen (1991) point out that the calculation was based on C_3O_2 being released from the nucleus, not an extended source as was originally proposed, thus C_3O_2 could still be present in the coma in substantial quantities. Laboratory experiments conducted by Gerakines & Moore (2001) have shown that in water-dominated ices, it is difficult to form C_3O_2, but suggest it could still form and polymerize in cometary nuclei if CO is released from H_2O as the surface layers of the nucleus are heated.

Here, the potential for known cometary species to reproduce the extended sources of CO through gas-phase chemical phenomena is examined. Trials incorporating the observed abundances of species are compared to the CO abundances derived from observations. Furthermore, the efficiency of the CO formation process is examined to determine whether photochemistry and chemical reactions serve as efficient mechanisms for CO formation over the scale where CO needs to be formed to explain observations.

4.2 Effects of the Initial Gas Composition

Because all of the reaction rates, both photochemical and two-body, depend on the concentration of reactants, the potential impact of nuclear composition on the formation and destruction of CO in the coma should be examined. Through these trials, the effect of two-body reactions on the CO abundance can be quantified, and the crucial species necessary for significant CO formation can be identified. All of these trials were performed using the constant T, constant v profile, and a production rate of 5×10^{29} s^{-1} (See initial description of the physical parameters in Section 3.3). The nuclear compositions for all trials are listed in Table 4.1. The range of abundances were chosen to reflect the general range of cometary abundances of these species. Furthermore, each case was performed twice: once with the entire chemical reaction network, and once with photochemistry only.

Table 4.1. Nuclear Compositional Cases

Species	1[1]	2	3	4	5	6	7	8	9	10
H_2O	100	100	100	100	100	100	100	100	100	100
CO	5	5	5	5	5	0	10	20	5	5
CO_2	5	5	5	5	5	5	5	5	0	10
CH_3OH	2	2	2	0	0	2	2	2	2	2
H_2CO	1	0	2	1	0	1	1	1	1	1
HCOOH	0.5	0.5	0.5	0.5	0.5	0.5	0.5	0.5	0.5	0.5

[1]Identical to the compositional case used in Chapter 3 (See Table 3.1).

4.2.1 The Nuclear H_2CO Abundance

H_2CO has been detected in several comets at levels from a fraction of a percent to a few percent relative to H_2O. Although it remains unclear whether H_2CO in comets exists in the nucleus in significant quantities or is released through one or more processes in the coma, it is possible for it to be released to monomer form fairly quickly upon release of a polymer source from the nucleus (Boehnhardt et al. 1990). Therefore, the impact of different levels of H_2CO are examined as if the H_2CO comes from the nucleus. The nuclear compositions for these cases are shown in Table 4.1, listed under Cases 1 - 3.

Figure 4.1 shows the CO abundance generated from these cases. Raising the initial abundance of H_2CO by 1% relative to H_2O has far greater impact than adding chemical reactions on top of photochemistry in the chemical reaction network. Furthermore, two-body chemical reactions matter more when there is less H_2CO in the near-nucleus environment, but even then, the full chemistry only increases the CO abundance by a few percent over pure photochemistry at distances greater than 45,000 km. The photodissociation of H_2CO to form CO is efficient, and nearly every H_2CO released from the nucleus ultimately generates one CO molecule. It is clear from these results that the presence of H_2CO in the coma is far more crucial in generating the CO abundance than the presence of two-body chemical reactions. This is also consistent with the results of Chapter 3, in which it was shown that the dominant CO formation mechanism was H_2CO photodissociation. This result is also consistent with other work showing the importance of H_2CO in CO formation Eberhardt (1999); Meier et al. (1992); Cottin et al. (2001).

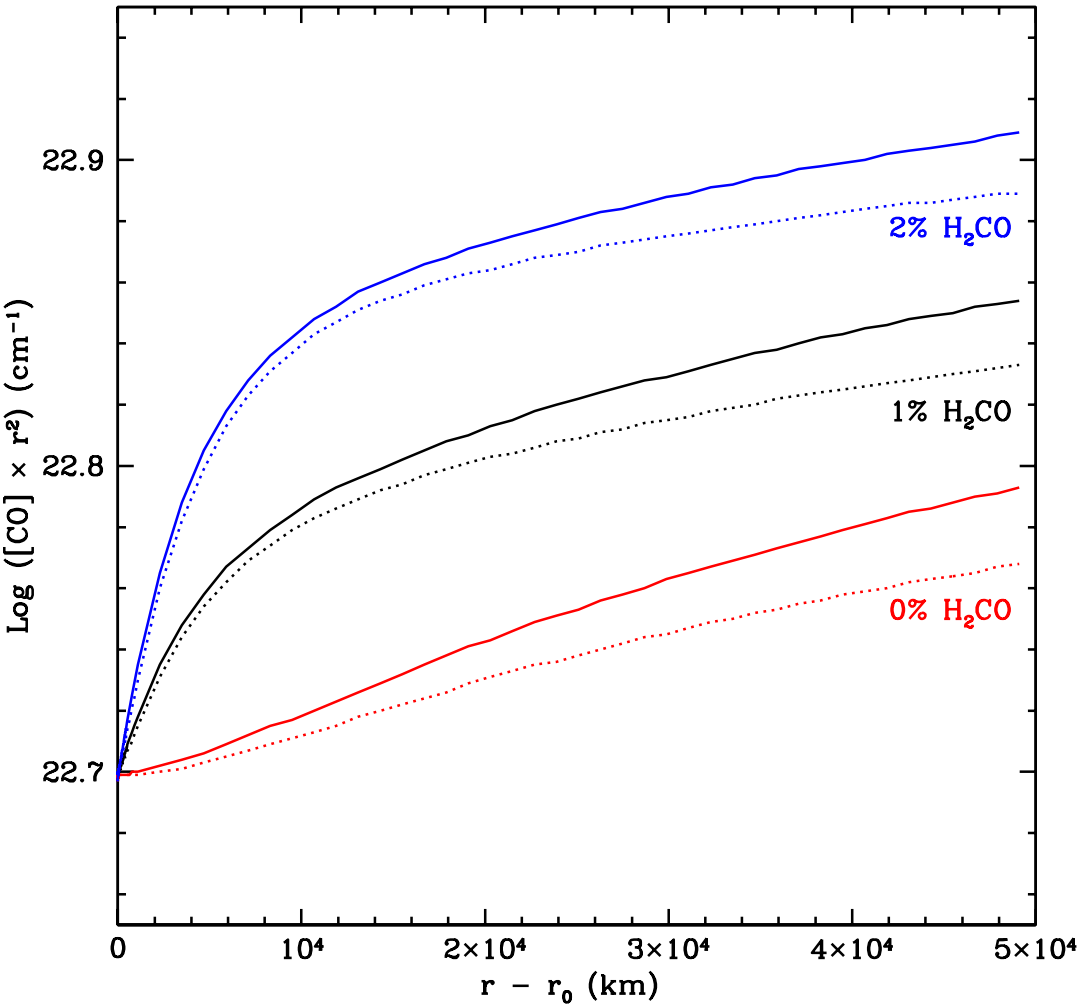

Figure 4.1 – Profiles of [CO] × r^2 for trials containing different nuclear abundances of H_2CO (Cases 1 (1%) Case 2 (0%) and Case 3 (2%)). Solid lines indicate trials using the entire chemical reaction network. Dotted lines indicate the corresponding trials using only photochemistry.

4.2.2 The Nuclear CH_3OH Abundance

A parent species of H_2CO, CH_3OH has been detected at comparable levels in several comets, with a relative abundance as much as 4% with respect to H_2O, as seen in comet Austin (Hoban et al. 1991). It has the potential to produce CO in the coma because its photodissociation products ultimately yield CO through multiple processes. Therefore, it is necessary to examine the impact of CH_3OH on the CO abundance in the coma. Effects of the CH_3OH abundance were examined with Cases 1, 2, 4, and 5 as given in 4.1.

Figure 4.2 shows the results for the four compositional cases. Similar to the H_2CO cases, varying the CH_3OH abundance by 2% relative to H_2O had greater impact than incorporating two-body chemical reactions into the chemical network. As mentioned previously, one of the CH_3OH photochemical products is H_2CO, and once the H_2CO is produced, the CO will promptly follow. This is illustrated nicely in Fig. 4.2, where Case 4 (0% CH_3OH and 1% H_2CO) overlaps with Case 2 (2% CH_3OH and 0% H_2CO) beyond 35,000 km. The results demonstrate that CH_3OH has an impact on the CO abundance when it is present in the nucleus, and it is possible for nuclei of two different chemical compositions to produce a similar result far from the nucleus. However, the shape of the curve suggests that the production of CO from CH_3OH peaks too far from the nucleus for it to be the primary contributor to extended CO on the distance scales as seen in comet Halley (10,000-15,000 km) and comet Hale-Bopp (5,000 km).

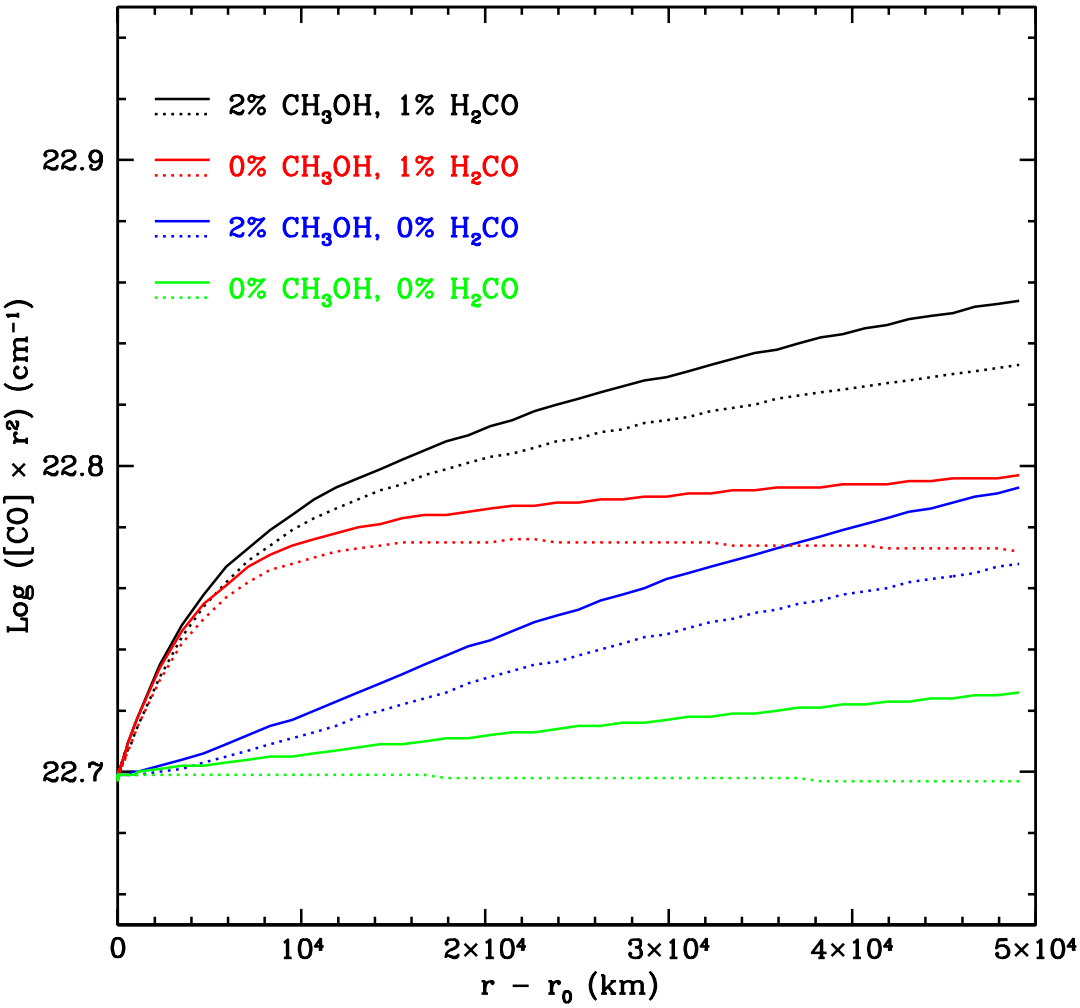

Figure 4.2 – Profiles of [CO] × r^2 for trials containing different nuclear abundances of CH_3OH for two different levels of H_2CO (Cases 1, 2, 4, and 5). Solid lines indicate trials using the entire chemical reaction network, and the dotted lines indicate the corresponding trials using only photochemistry.

4.2.3 The Nuclear CO_2 Abundance

CO_2 is generally regarded as one of the more abundant species in comets after H_2O. It is capable of producing CO through photodissociation, resulting in Cameron band emission from CO at 2000 Å, allowing CO_2 abundances to be gauged when the bands are detected (Weaver et al. 1994), as CO_2 does not possess a permanent dipole moment. However, its photodissociation lifetime is long, thus it has historically been less favored as the source of extended CO (Eberhardt et al. 1987; Meier et al. 1992; Eberhardt 1999). However, it can undergo chemical reactions, and the reaction with H^* would produce CO on shorter timescales than CO_2 photodissociation. This may in turn serve as a significant loss mechanism for CO_2, as speculated by Herbst & Talbi (1998) and Rodgers & Charnley (2005). In order to examine the impact of the nuclear CO_2 abundance on CO, three compositional cases were examined, with initial CO_2 abundances ranging from 0% to 10% relative to H_2O. These are listed as Cases 1, 9, and 10 in Table 4.1.

Figure 4.3 shows the CO results for all three cases. As the nuclear CO_2 abundance is increased, the difference in CO abundance between trials using the entire reaction network and the photochemical network increase, with differences approaching 10% at 50,000 km. As Fig. 4.3 demonstrates, when chemical reactions are considered, it is possible for a nucleus with 5% CO_2 to actually produce more CO than a nucleus with 10% CO_2 using only photochemistry, primarily the result of including the reaction between CO_2 and H^*. Overall, the CO_2 abundance does not have a great impact on CO in the inner coma. However, it may impact the CO and CO^+ abundances in the outer coma, and may impact large-aperture observations of CO, such as the observation of Comet West (Feldman 1978).

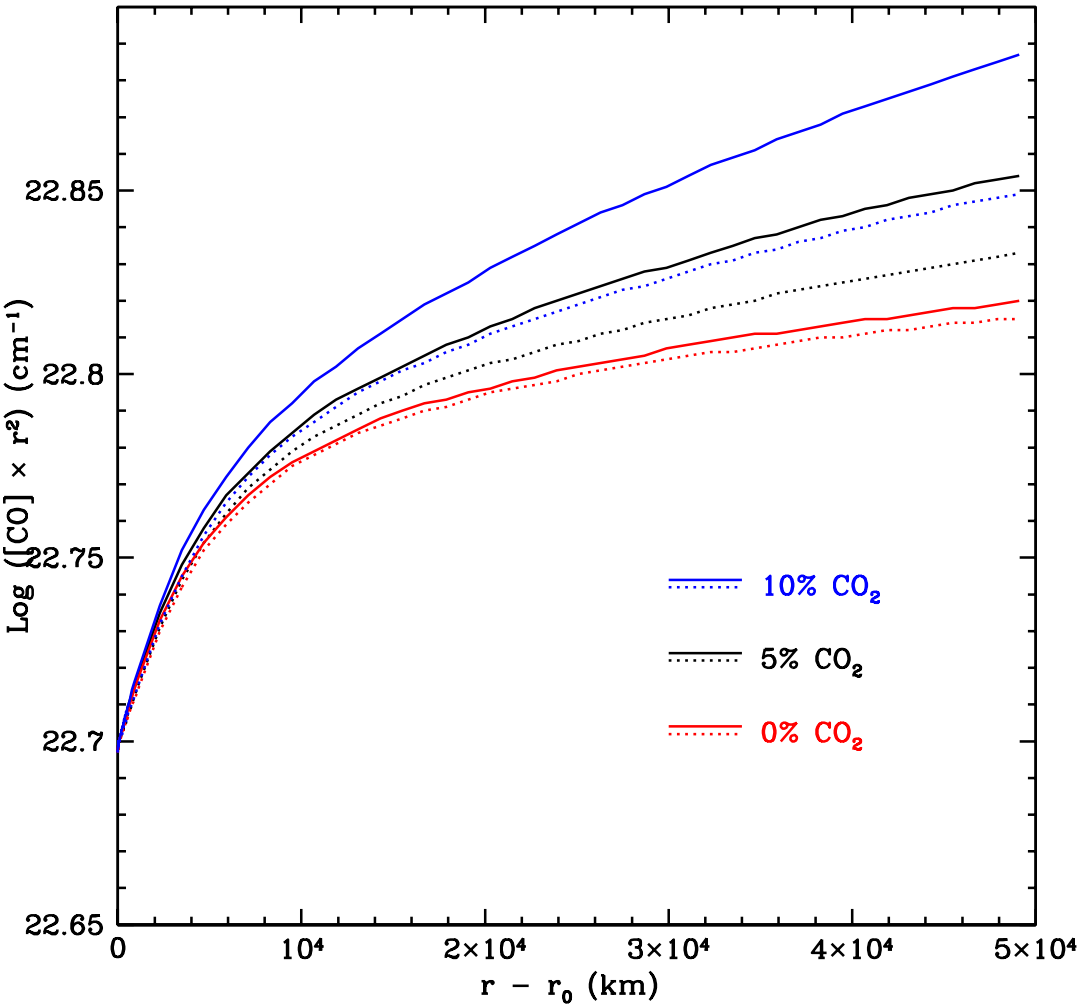

Figure 4.3 – Profiles of [CO] × r^2 for trials containing different nuclear abundances of CO_2 (Cases 1 (5%), 9 (0%), and 10 (10%)). Solid lines indicate trials using the entire chemical reaction network, and the dotted lines indicate the corresponding trials using only photochemistry.

4.2.4 The Nuclear CO Abundance

As demonstrated by the results of the three outflow cases examined in Chapter 3, the presence of chemical reactions in the inner coma can rival photochemical destruction of CO. Therefore, trials incorporating different levels of initial CO were performed to examine its effects on the efficiency of CO formation in the coma. These trials are listed as Cases 1, 6, 7, and 8 in Table 4.1, with abundances ranging from 1 - 20% relative to H_2O in order to cover the range over which CO has been observed in comets.

The CO profiles for these cases are shown in Fig. 4.4. The more CO-abundant cases have flatter profiles, indicating that all of the combined CO formation processes are insufficient to generate significant changes in the CO abundance in the coma. Furthermore, the differences in the results between pure photochemistry and chemical reactions decrease with increasing CO abundance, and essentially disappear at the highest initial abundance. This is not only the result of low CO yield with respect to the abundances already present – it also suggests that the efficiency of CO production by chemical reactions is diminished with increasing nuclear CO.

The latter idea can be examined by looking at the CO formation and destruction rates for the four compositional cases presented in Fig. 4.4. In Fig. 4.5a, the total CO formation and destruction rates are shown for Case 1 with all reactions. Over the entire region sampled in the simulation, the total CO formation rate is greater than the total CO destruction rate, indicating that the net effect is CO formation. The net CO formation rate is also shown in Fig. 4.5a. The net formation rate closely follows the total formation rate, which is consistent with the total formation rate being much higher than the total destruction rate. In

Fig. 4.5b, the ratio of net CO formation to total CO formation is shown over the region of the coma sampled in the simulation. This ratio is greater than 0.9 in the first 10,000 kilometers, indicating that formation dominates over destruction in this region and is consistent with Fig. 4.5a.

Fig. 4.6 shows the ratio of net CO formation to total CO formation as a function of distance in the coma for all the compositional cases shown in Fig. 4.4. As the nuclear abundance is increased, formation efficiency goes down in all cases, but sees greater reduction with the presence of two-body reactions. The photochemical cases drop off more sharply with distance because the primary photochemical contributors have short lifetimes, and the photochemical processes that destroy CO increase with distance. The shallower curves of the chemical reactions are the result of multiple two-body reactions that continue to engage in small levels of CO formation beyond 10,000 km. In the innermost coma, however, two-body reactions significantly reduce CO formation efficiency. While CO formation efficiency is always reduced with increasing CO abundance, the presence of chemical reactions takes a greater toll on CO formation in the innermost coma. These results suggest that the formation of the extended CO source must come from either an overwhelming photochemical process and/or gradually introduced to the coma through some other phenomenon not included here.

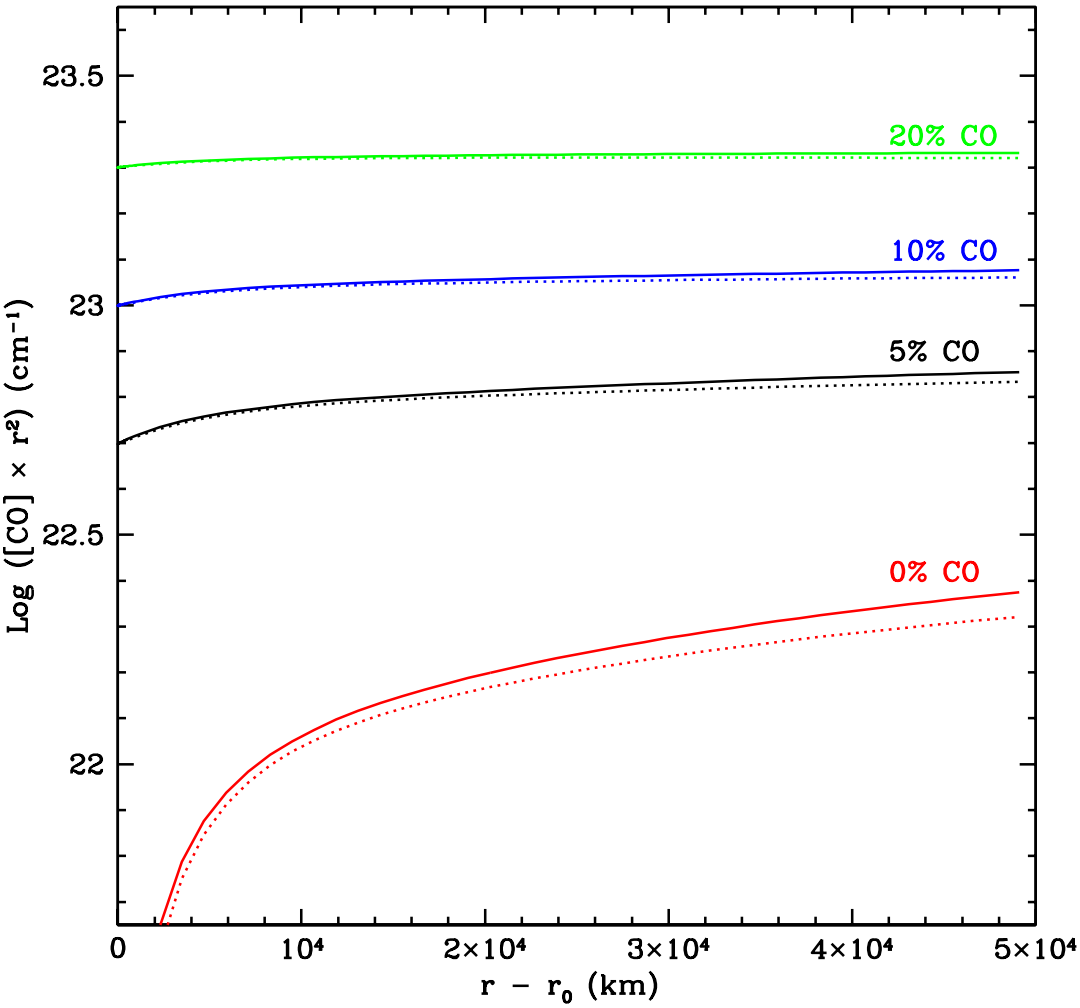

Figure 4.4 – Profiles of [CO] × r^2 for trials containing different nuclear abundances of CO (Case 1 (5%), Case 6 (0%), Case 7 (10%), and Case 8 (20 %)). Solid lines indicate trials using the entire chemical reaction network. Dotted lines indicate the corresponding trials using only photochemistry.

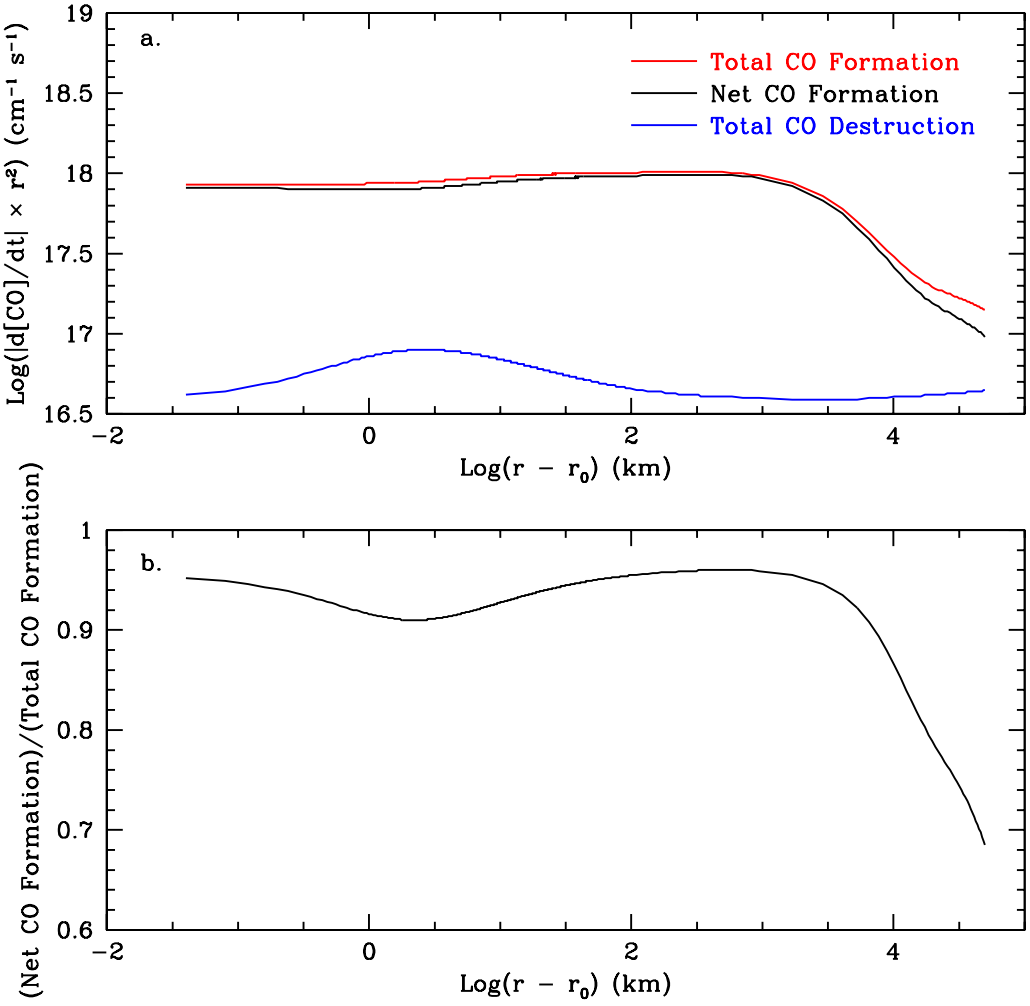

Figure 4.5 – a. Plot of d[CO]/dt × r^2 as a function of distance for Case 1 with all reactions, showing the total CO formation rate from all processes (red), the total CO destruction rate from all processes (blue) and the resulting net CO formation rate (black). b. The ratio of net CO formation to total CO formation throughout the region of the coma sampled in the simulation.

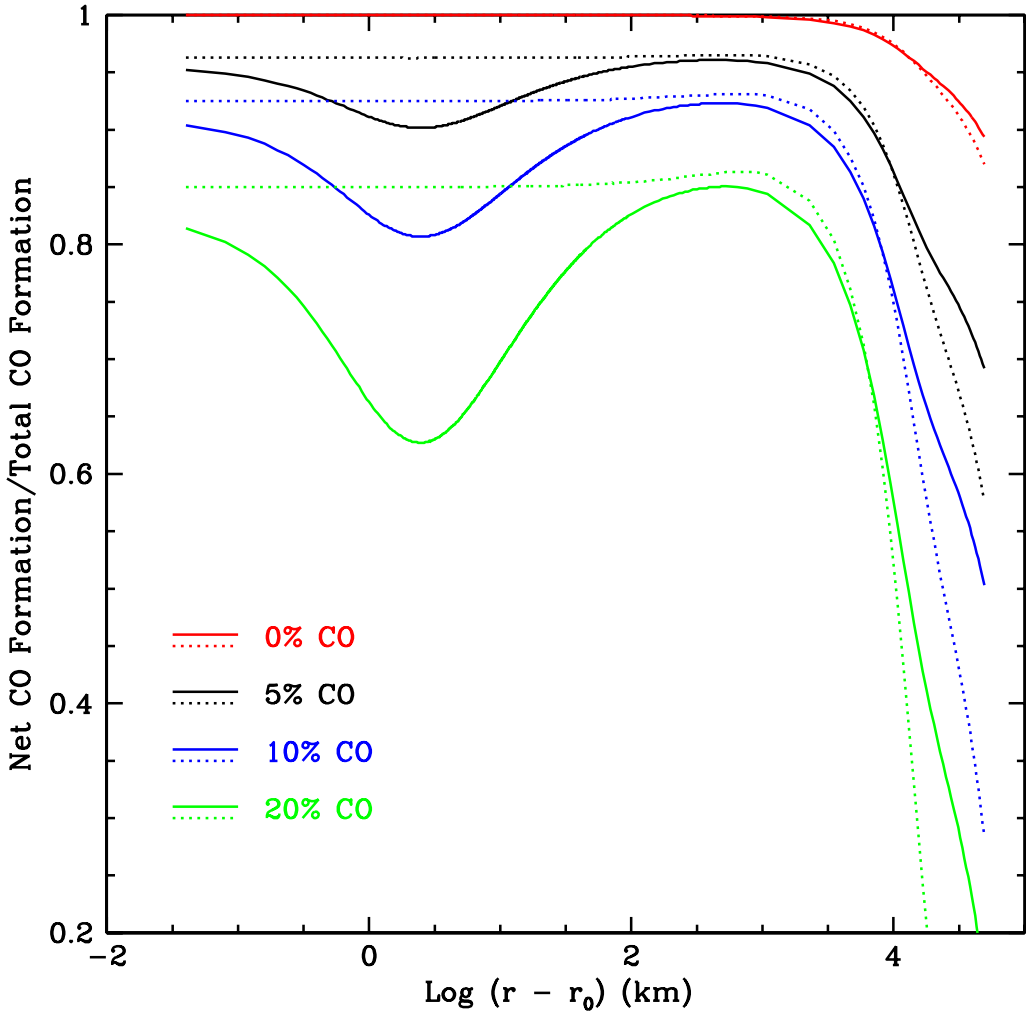

Figure 4.6 – Ratio of the net CO formation rate to the total CO formation rate as a function of cometocentric distance for the four cases shown in Fig. 4.4. Solid lines indicate trials using the entire chemical reaction network. Dotted lines indicate the corresponding trials using only photochemistry.

4.3 Unknown – HCO Photodissociation Lifetime

As mentioned in Chapter 2 (Section 2.3), the photodissociation lifetime of HCO is not known. Given the uncertainty in the estimated lifetime (owing to the potential unreliability of the detection of HCO in comet IRAS-Araki-Alcock), and its importance as a CO formation mechanism as seen in Chapter 3, it is necessary to examine the impact of HCO photodissociation lifetime on the overall CO result. Therefore, several trials were examined using three different photodissociation lifetimes of HCO: 80 s, 800 s, and 8000 s (an order of magnitude less than and greater than the derived lifetime, respectively). These trials were all performed using abundances listed under Case 1 in Table 4.1.

Figure 4.7 shows the impact of HCO photodissociation lifetime on the CO abundance. The 800 s lifetime (shown in black) is the value used in all other cases examined in Chapters 3 and 4. Although a significantly longer lifetime does lower the CO abundance in the inner coma, it does so only by an amount that would be difficult to measure. Beyond 30,000 km, the results are essentially indistinguishable. However, the dissociation energy of HCO is significantly less than the dissociation energy of H_2CO (Okabe 1978), which has a photodissociation lifetime of 8600 s, thus the 80 s and 800 s lifetimes for HCO are favored as more reasonable estimations of the HCO lifetime. Overall, the uncertainty in HCO lifetime does not significantly impact the CO result, as the CO results shown in Section 4.2 would still exhibit the same relative placement with respect to each other.

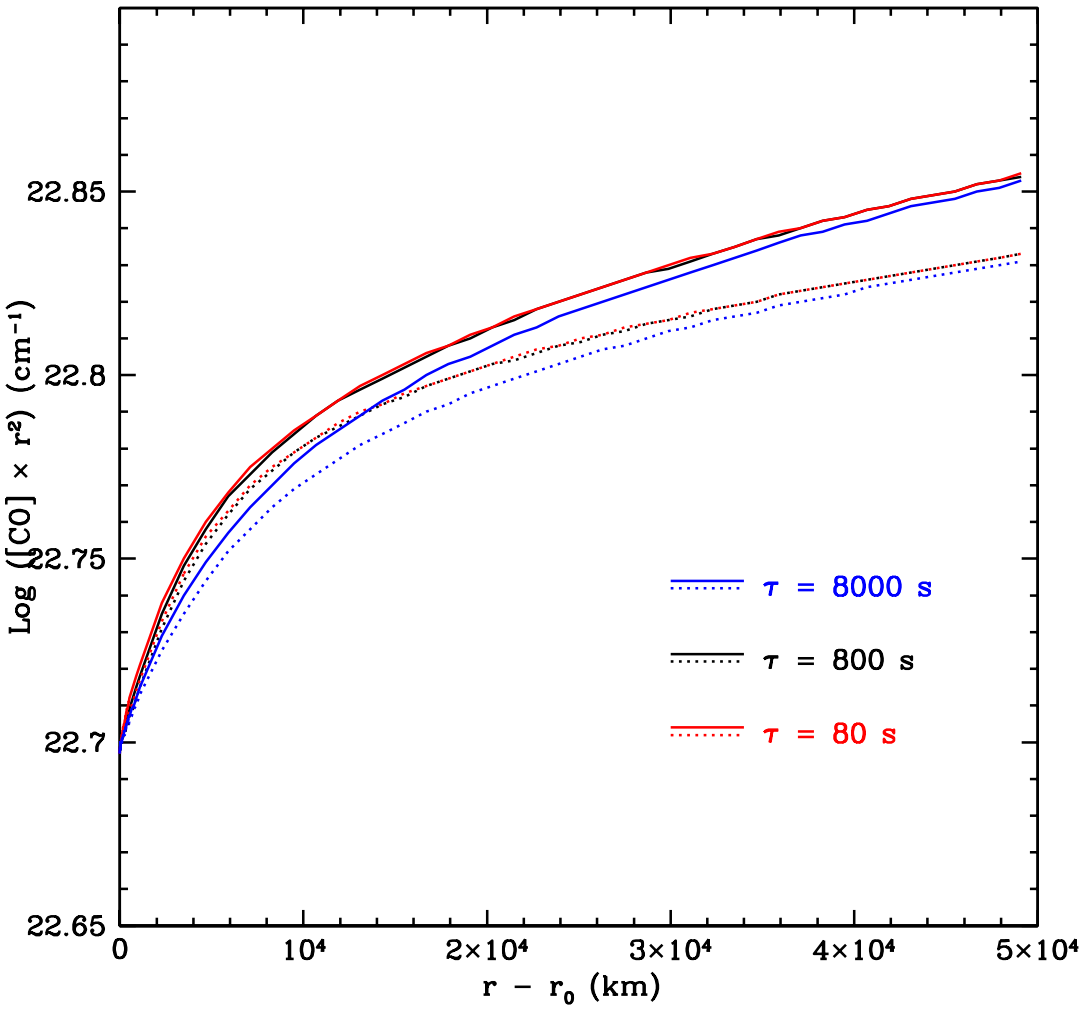

Figure 4.7 – Profiles of [CO] $\times$ r^2 for trials using three different photodissociation lifetimes for HCO (The 800 s lifetime derived for this study from the reported detection by Cosmovici & Ortolani (1984) is shown in black). Solid lines indicate trials using the entire chemical reaction network. Dotted lines indicate the corresponding trials using only photochemistry.

4.4 Simulating Extended CO in Comets Halley and Hale-Bopp

The results of Section 4.3 are useful for quantifying the effect of the addition of chemical reactions to the chemical network in the coma and for determining which species are crucial to understanding CO extended sources. In this section, the extended sources of CO in comets Halley and Hale-Bopp are examined in light of these results. The chemical model was tested using a constant temperature, constant velocity profile and production rates of 10^{30} s^{-1} for comet Halley, and 10^{31} for comet Hale-Bopp (See Section 3.3 for the original description of the physical parameters of these cases.). Ultraviolet attenuation of H_2O chemistry is included in the Hale-Bopp case. The abundances of the species released from the nucleus are listed in Table 4.2, using values derived from several observations (c.f. (Bockelée-Morvan et al. 2004) and references therein, (Eberhardt 1999)).

Table 4.2. Nuclear Abundances of Comets Halley and Hale-Bopp

Molecular Species	Halley	Hale-Bopp
H_2O	100	100
CO	3.5	12
CO_2	3.5	6
CH_3OH	1.8	2.4
H_2CO[1]	7.5	1.1
HCOOH	0.0	0.009

[1]Total abundance from nuclear and extended sources. Halley abundance from Eberhardt (1999).

Figure 4.8 shows the result for comet Halley. Plotted are values of [CO] $\times$ r^2 for the model results and data from the *Giotto* NMS (Eberhardt et al. 1987). The curves reproduce the observed abundance beyond 10,000 km. However, the model fails to reproduce the shape of the curve inside 10,000 km. This suggests that the H_2CO abundance is sufficient to explain CO observations far from the nucleus, but is not released into the gas at or close to the nucleus. It is more likely that the H_2CO is released into the gas coma gradually. However, the abundance of H_2CO derived from observations covers distances well beyond the peak of the extended source, and the results of Biver et al. (1999) suggest that the distance over which the H_2CO is produced could be larger than the distance over which the H_2CO produces CO. As a result, it is possible that not all of the CO sources are fully accounted for. Yet given the information available, these results are consistent with other studies which conclude that H_2CO is responsible for most of the CO formation in the coma of comet Halley (Meier et al. 1992; Eberhardt 1999; Cottin et al. 2001).

Figure 4.9 shows the result for CO in Hale-Bopp. The gas-phase chemistry is clearly insufficient to generate the CO abundance observed by (DiSanti et al. 2001), where the derived abundances indicate that $\sim$50% of the CO is nuclear, and 50% is extended. The numerical prediction is even worse when the result of Brooke et al. (2003) is considered, in which the derived abundance is 37-41% with respect to H_2O, and the observations indicate that the breakdown in CO is 10% nuclear and 90% extended. However, the result does confirm DiSanti et al.'s statement that the H_2CO abundance in Hale-Bopp is insufficient to account for the extended CO abundance. Although preliminary, a recent re-analysis of the data recently performed by (Bockelée-Morvan et al. 2005), in which additional

temperature and infrared opacity effects are considered, suggests that all of the CO is nuclear. However, many of these effects were also included in the analysis of Brooke et al., which yielded a stronger extended source than the DiSanti et al. result. Until the relevant physics for analysis of Hale-Bopp data are identified, it is clear that the interpretation of CO having an extended source requires one or more additional chemical processes that are not currently included in coma chemical modeling.

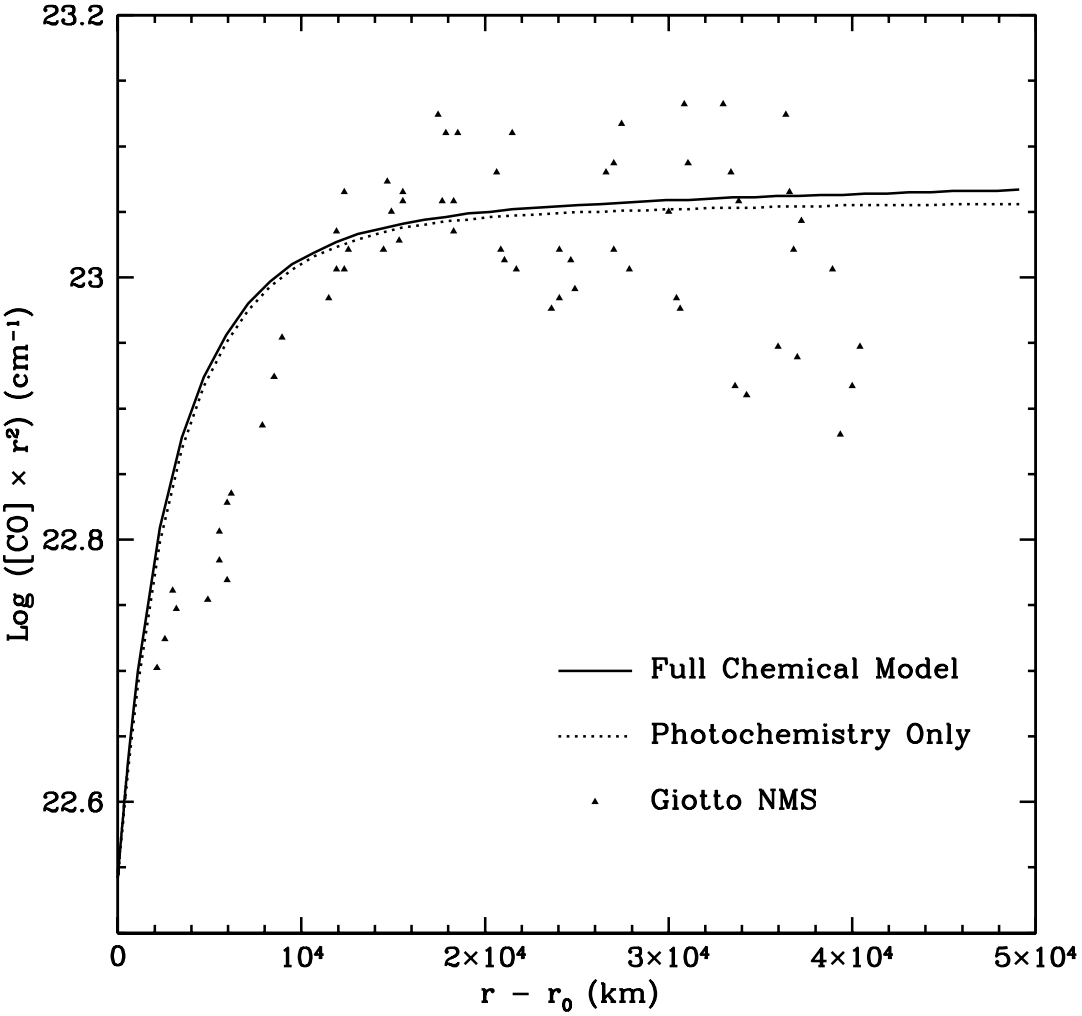

Figure 4.8 – Comparison of the numerical results for cases with the full chemical model (solid line) and the photochemical model (dotted line) with *Giotto* NMS data from comet Halley.

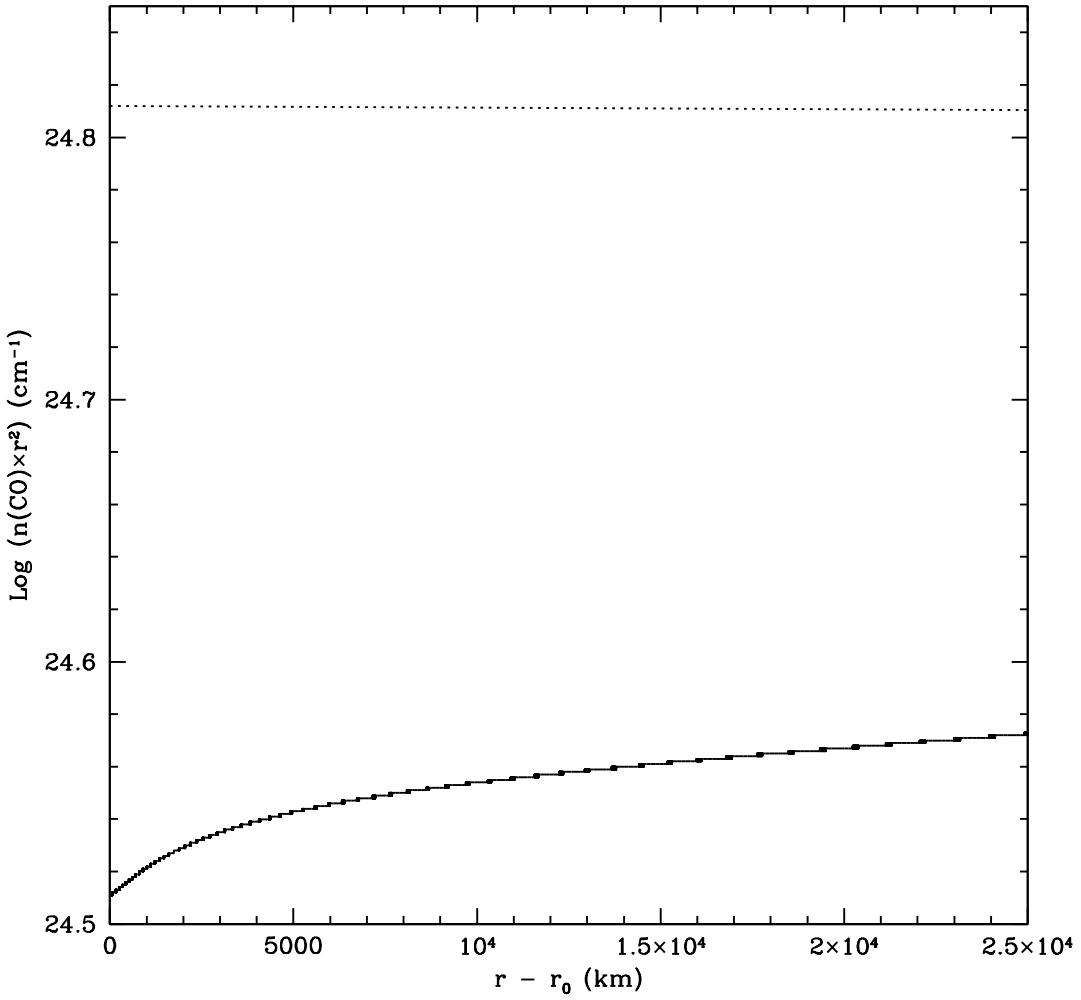

Figure 4.9 – Comparison of the numerical results with observations of CO in comet Hale-Bopp. The solid line is the numerical result, and the dotted line represents the level of observed CO (native and extended) from the observations of (DiSanti et al. 2001).

4.5 Other Potential Sources of CO

Given the recent discoveries of several organic species in comets, it is likely that these species contribute to CO abundances in the coma. One new discovery, ethylene glycol ($HOCH_2CH_2OH$) was found in the coma of comet Hale-Bopp (Crovisier et al. 2004b). In the solar radiation field, ethylene glycol would most likely lose an H atom, yielding the $HOCH_2CH_2O$ radical, which could in turn lose an H atom and produce glycolaldehyde (CH_2OHCHO). Isomerization may also occur, yielding acetic acid (CH_3COOH) or methyl formate ($HCOOCH_3$)[1]. (Rodgers, private communication). The small abundance of ethylene glycol is itself insufficient to contribute much CO to the coma because its abundance was determined to be $\sim$0.5% relative to H_2O. On the other hand, if other similarly large organic species are present in comets, their combined influence could yield abundances of CO at levels of a few percent, particularly if they can yield more than one CO per molecule.

A high CO-yield per molecule makes C_3O_2 an intriguing possibility worth revisiting. Its photodestruction could yield two CO molecules each, so it need only be present at levels of a few percent relative to H_2O to produce substantial quantities of CO. As mentioned in Section 4.1, C_3O_2 may have been detected at 4.43 μm in Halley. However, the resolution of those spectra was low, and the band could also be from isocyanic acid (HNCO), which has been detected in comets[2] and its NCO antisymmetric stretch occurs at that wavelength (Shimanouchi 2005). Furthermore, if C_3O_2 comes from an extended source, the distribution could render

[1] $HCOOCH_3$ has been reported to be in comet Hale-Bopp (Bockelée-Morvan et al. 2000)

[2] HNCO was detected in comet Hyakutake at 0.07% (Lis et al. 1997) and in comet Hale-Bopp at 0.1% (Bockelée-Morvan et al. 2000).

an ample supply extremely difficult to detect. On the other hand, one of the photodissociation products of C_3O_2, C_2O, has a transition at 5.08 μm from its C-O stretch. C_2H_2 has a competing transition near that wavelength, but it is Raman active (Shimanouchi 2005) and should not contribute serious contamination. CO has an extremely strong transition at 4.7 μm, but high-resolution spectroscopy would easily distinguish the two bands.

Could it also be possible that chemical reactions are taking place on the grain surfaces? This process is generally thought to occur in cold regions of the ISM to form H_2 (Gould & Salpeter 1963). Almost no published data on grain surface chemistry in comets exists, but if it does happen, it would most likely occur the very innermost coma. Furthermore, reaction rate data do not exist, but if they did, they would still be highly uncertain without better knowledge of the level of defects on the grain surfaces (Huebner, private communication). For the case of H_2CO, grain surface chemistry as a mechanism for formation is thought to be unlikely (Huebner 1970). More work has instead focused on the presence of POMs in the nucleus (Hanner 1985; Boehnhardt et al. 1990; Moore & Tanabe 1990).

4.6 Conclusions

From these results, the contribution of chemical reactions to the source of extended CO on the spatial scales seen in comets Halley and Hale-Bopp is minimal. Although the chemical reactions do take place, the photodissociation of H_2CO, even when present at 1% relative to H_2O, is far more important. This is consistent with the results of Chapter 3, in which H_2CO photodissociation was the dominant CO formation mechanism. Furthermore, the photodissociation of CH_3OH

was more important than chemical reactions. One of its photodissociation paths yields H_2CO, and from there, the CO is quickly produced. For chemical reactions to be the principal CO formation mechanism, the nuclear abundance of H_2CO and CH_3OH would have to be near zero. Even then, they couldn't produce enough CO in the coma to account for the abundances of CO observed in the comae of high-activity comets, where chemical reactions would have the highest chance of occurring.

It is also clear that the CO extended source is tied to H_2CO, which itself has an extended source. It is therefore likely that the extended sources of CO and H_2CO are linked. The abundance of H_2CO in comet Halley may be sufficient to explain observations if it is released gradually from something else that is released from the nucleus. However, the H_2CO abundance in comet Hale-Bopp is insufficient to explain the abundance of extended CO, thus another source of CO is required. Given the increasingly large organic molecules now being found in comets, particularly comet Hale-Bopp, it is possible that other large organic species may contribute to the extended CO abundance in some way which currently remains elusive.

Chapter 5

Conclusions

5.1 Two-Body Chemical Reactions

Photochemical processes are already known to be important for understanding observed abundances of species in cometary comae. By modeling potentially important chemical reactions under various conditions in the coma, it is possible to gauge the level of importance of two-body chemical reactions on the abundances of these species as well. Although prior studies suggest ways to form several observed cometary species with chemical reactions, the impact of two-body reactions on the abundance of such major cometary species as CO or CO_2 has been less clear.

The results of the numerical studies presented here demonstrate that the contribution of two-body chemical reactions to chemical processes in the near-nucleus coma cannot be immediately dismissed for high-activity comets. In some parts of the coma, the contribution of two-body chemical reactions to the CO formation rate was greater than 30% . While this did not have an impact on the CO abundance greater than a few percent above the yield from pure photochemistry,

it did significantly impact the abundances of some species that are exclusively formed in the coma.

While the contribution of ion-molecule reactions in the coma is more readily accepted than neutral-charge two-body reactions, there are some neutral-charge reactions which had significant formation rates in the near-nucleus coma. These reactions typically include abundant species engaging in reactions with large rate constants. Other neutral-charge reactions involving excited species such as H^* and $O(^1D)$ were relatively modest contributors in some cases, but relatively more important in others. Because the abundances of these species in the near-nucleus coma depend on collisional de-excitation, models incorporating near-nucleus acceleration and/or topographic effects could yield different results for the relative contributions of some chemical processes to the formation and destruction of species in the coma.

5.2 The CO Extended Source

In these studies, the contribution of two-body chemical reactions to the source of extended CO observed in some comets shows that while these reactions contribute to CO formation at some level, their contribution is small compared to the photodissociation of H_2CO. Given that H_2CO has a relatively short photodissociation lifetime and multiple photodissociation paths which ultimately yield CO, it is crucial to consider the abundance of H_2CO in the coma when interpreting the CO abundance. Along these lines, the presence of CH_3OH in the coma can yield H_2CO, suggesting that the abundance of CH_3OH must also be considered, particularly when analyzing CO observations made with a wide field of view.

However, it is not entirely clear whether monomeric H_2CO exists in significant quantities in the nucleus. If H_2CO is released from the nucleus in polymer form, the multiple photodissociations required for the polymers to release CO would explain why it takes thousands of kilometers to form CO, and in comet Halley, why the extended source scale length is so much longer than the scale length of monomeric H_2CO. On the other hand, the scale length for CO formation in comet Hale-Bopp was shorter than the scale length for H_2CO, suggesting further that another source in addition to H_2CO is required for this comet. This also suggests that there may not be one answer to the extended CO problem – the answer may be comet dependent.

5.3 Future Work

Additional modeling of coma chemistry, adding new species as they are discovered, will further contribute to the understanding of the chemical development of the coma as a whole. So far, the modeling of the formation and destruction of CO in the coma has shown that the presence of two-body chemical reactions does not significantly alter the abundance of CO in the coma, but it may be significant for daughter species formed exclusively in the coma. In order to determine the full contribution of two-body reactions to these species, chemical reaction networks specifically tailored to examine all potential formation and destruction mechanisms of these species will be required to assess whether these processes will promote their net formation or destruction. These networks will be substantially larger than the one examined here. Additionally, the consideration of the energy states of species may also need to be considered for some chemical reactions, as emphasized here with $O(^1D)$ and H^*. Another species for which

excitation should be examined is atomic carbon and the impact of $C(^1D)$ versus $C(^1S)$ reaction rates.

It is also known from observations that the outflowing material from comets comes from only a fraction of the surface. Additional modeling to incorporate the effects of outgassing from discrete volatile-rich patches on the surface of the nucleus could also influence chemical reaction rates because the production rate would be concentrated in these regions rather than being evenly dispersed over the surface area of the nucleus, which is typically done in chemical modeling and was done in the numerical studies here. Furthermore, such studies would allow the effects of nuclear heterogeneity on the composition of the coma to be examined, as different surface patches could contain different abundances of molecules.

Future generations of chemical models may also consider the role of grains alongside two-body reactions in the coma. Grains have the potential to release vast amounts of additional species to the coma, which could also be an additional source of reactants for chemical reactions. Furthermore, collisions of grains can collimate the jets, which would set up significant flattening of the dilution from r^{-2} on scales several orders of magnitude larger than what is likely for pure gas jets. Coupled with the high density, this could make chemical reactions more important than demonstrated in the cases studied in Chapter 3. The potential for gas models to incorporate grains remains hampered by the lack of knowledge of grain structure and potential release mechanisms for the chemical species of interest. However, the recently-returned cometary and interstellar grain samples from the *Stardust* mission will begin to supply the relevant information necessary to perform this type of modeling.

The recent and upcoming missions to comets, such as *Deep Impact* and *Rosetta*, will yield more clues to the chemical composition of cometary nuclei. These results, coupled with ongoing laboratory studies of the processing of ices by the heating mechanisms to which the nuclei may be subject during dynamical storage and repeated apparitions in the inner Solar System will provide a better picture of the chemical composition of the outer layers of nuclei. From these results, more realistic starting conditions for chemical modeling can be devised in order to better understand how to relate the chemistry of the coma back to the nucleus, and thus place comets in the proper context of Solar System formation.

Appendix A

Collisional Cooling of Hot Hydrogen

Upon photodissociation of the H_2O molecule by solar ultraviolet radiation, extra translational energy is imparted to the H and OH products. Given that H has 1/17th the mass of the OH counterpart, the H-atom product exhibits a high level of translational energy. In the inner coma, this energy is lost to repeated collisions with other species, most notably H_2O. When examining the role of H^* in two-body chemical reactions in the inner coma, the collisional cooling of H^* must be considered as a significant loss mechanism for this reactant.

The following is a more detailed discussion of the equations describing the collisional cooling of H^* which were mentioned briefly in Section 2.5.1. This discussion follows the same treatment of particle collisions as described by Huxley & Crompton (1962).

To begin, consider a particle of mass m_1 with velocity $\mathbf{v}_1$ encountering a particle of mass m_2 and velocity $\mathbf{v}_2$, as shown in Figure A.1. The velocities of m_1 before and after collision are

$$\mathbf{v}_1 = \mathbf{V} + \mathbf{u}_1; \quad \mathbf{v'}_1 = \mathbf{V} + \mathbf{u'}_1 , \tag{A.1}$$

where $\mathbf{V}$ is the velocity of the centroid of the system, designated by X, and $\mathbf{u}_1$

and $\mathbf{u'}_1$ are the internal velocities of m_1 before and after encounter, respectively. The magnitudes of these velocities are represented by

$$v_1^2 \;=\; V^2 \;+\; u_1^2 \;+\; 2\mathbf{V}\cdot\mathbf{u}_1; \quad v_1'^2 \;=\; V^2 \;+\; u_1'^{\,2} \;+\; 2\mathbf{V}\cdot\mathbf{u}'_1\,. \tag{A.2}$$

Let $\mathbf{u}$ be allowed to assume all possible directions, then its mean value is $\alpha\mathbf{u}$, where $\alpha = \overline{\cos\theta}$. The mean value of $\mathrm{v_1}^2$ - $\mathrm{v_1'}^2 = 2(1 - \alpha)\mathbf{V}\cdot\mathbf{u}$, where $\mathbf{V}\cdot\mathbf{u}$ is given by

$$\mathbf{V}\cdot\mathbf{u} \;=\; \frac{m_1\mathbf{v}_1 \;+\; m_2\mathbf{v}_2}{m_1 \;+\; m_2}\,\frac{m_2}{m_1 \;+\; m_2}\,(\mathbf{v}_1 \;-\; \mathbf{v}_2)\,. \tag{A.3}$$

Substituting this equation, assuming $\alpha = 0$ for an average over all possible scattering directions and simplifying, we get

$$\mathbf{v}_1^2 \;-\; \mathbf{v}_1'^2 = \frac{2\,m_2}{(m_1 \;+\; m_2)^2}\,[\,m_1 v_1^2 \;-\; m_2 v_2^2 \;+\; (m_2 - m_1)\mathbf{v}_1\cdot\mathbf{v}_2\,]\,. \tag{A.4}$$

The term $\mathbf{v}_1\cdot\mathbf{v}_2$ vanishes in the mean, since values of $\mathbf{v}_2$ are distributed isotropically. Therefore, the mean loss of energy of mass m_1 upon collision with mass m_2 is

$$\Delta E_1 \;=\; -\,\frac{2\,m_1\,m_2}{(m_1 \;+\; m_2)^2}\,(E_1 \;-\; E_2)\,. \tag{A.5}$$

where$E_1 = \frac{1}{2}\; m_1 {v_1}^2$ and $E_2 = \frac{1}{2}\; m_2 {v_2}^2$.

Upon substituting E_1 and E_2 and re-arranging terms,

$$\frac{\Delta v_1^2}{v_1^2} \;=\; -\,\frac{2\,m_2}{(m_1 \;+\; m_2)^2}\left[m_1 \;-\; m_2\left(\frac{v_2}{v_1}\right)^2\right]\,. \tag{A.6}$$

If v_1 is the velocity of m_1 before collision, and v_1' is the velocity of m_1 after collision, then the left-hand side of A.6 can be rewritten in the following way:

$$\frac{\Delta v_1^2}{v_1^2} \;=\; \frac{v_1^2 \;-\; v_1'^2}{v_1^2} \;=\; \frac{(v_1 \;+\; v_1')\,(v_1 \;-\; v_1')}{v_1^2} \;=\; \frac{(v_1 \;+\; v_1')\,\Delta v_1}{v_1^2}\,. \tag{A.7}$$

If v_1 - v_1' is small, then $v_1 + v_1' \approx 2v_1$ and

$$\frac{(v_1 \;+\; v_1')\,\Delta v_1}{v_1^2} \;=\; \frac{2\,\Delta v_1}{v_1}\,. \tag{A.8}$$

If the right-hand side of A.8 is substituted into the left-hand side of A.6, then the equation to determine the width of the velocity bins becomes

$$\frac{\Delta v_1}{v_1} = -\frac{m_2}{(m_1 + m_2)^2}\left[m_1 - m_2\left(\frac{v_2}{v_1}\right)^2\right] . \tag{A.9}$$

For the case of a collision between H and H_2O, $m_1 = m_H$, and $m_2 = m_{H_2O}$. By substituting these masses for m_1 and m_2, and substituting the velocities accordingly, we arrive at Equation 2.39, which provides the velocity width of the hot hydrogen bins:

$$\frac{\Delta v_H}{v_H} = -\frac{m_{H_2O}}{(m_H + m_{H_2O})^2}\left[m_H - m_{H_2O}\left(\frac{v_{H_2O}}{v_H}\right)^2\right] . \tag{A.10}$$

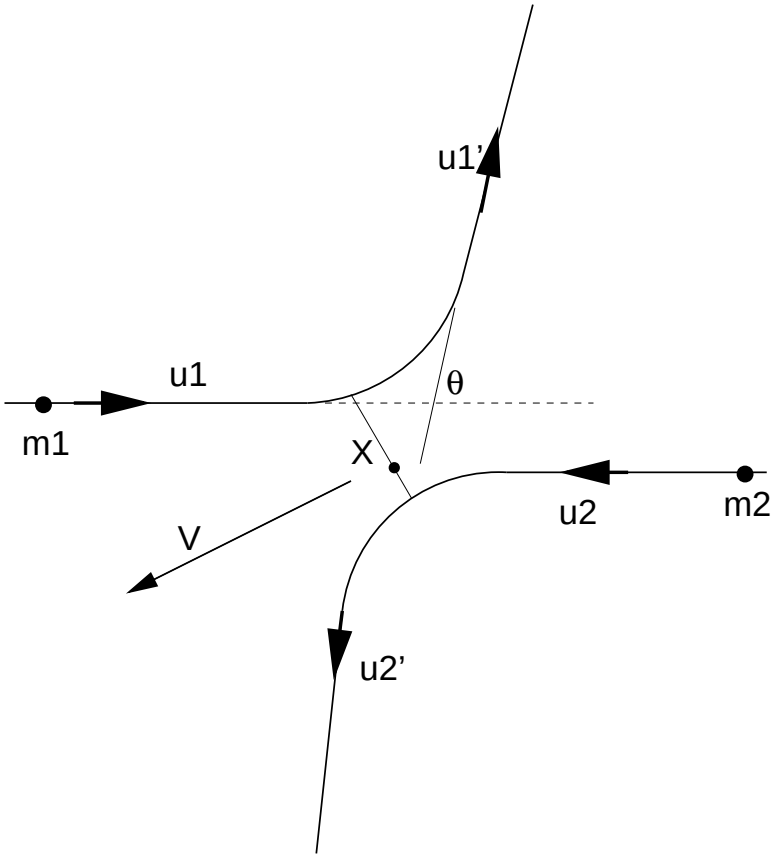

Figure A.1 – Encounter geometry of particles m_1 and m_2. The center of mass of the system is designated by X, with the velocity of the centroid designated by V. The angle through which m_1 is deflected is represented by θ.

Appendix B

Numerical Integration Technique

One of the more robust techniques for solving sets of ordinary differential equations (ODE) is the Bulirsch-Stoer routine (Stoer & Bulirsch 1980; Press et al. 1992). This method provides a combination of high accuracy with little computational effort. It uses the integration principle of *Richardson's deferred approach to the limit*, whereby the final answer to the numerical calculation is treated as if it is an analytic function of some adjustable parameter (usually the stepsize). This analytic function is found by performing the calculation for a particular stepsize (which does not necessarily have to be small enough to meet the accuracy requirements), and fitting a polynomial to the solution. The polynomial is then evaluated at zero stepsize. If the final solution meets the desired accuracy requirements, the final value is returned, or else the process is repeated again using a smaller stepsize.

In order to arrive at a solution, the routine uses the *modified midpoint method*, which advances the dependent variable from point x to point $x + H$ by a sequence of n steps of size h, where $h = H/n$. The calculations are first tried with $n = 2$. If the solution meets the accuracy requirements, the routine proceeds to point

$x + H$. Otherwise, the calculation is attempted again for $n = 4$. The routine proceeds with even numbers of n as needed to perform the calculation. However, the modified midpoint method must be modified for use here because the system of equations describing the behavior of the chemical species represents a common problem encountered when solving multiple equations simultaneously – finding a suitable stepsize to maintain the stability of the entire system.

The differential equations describing the changes of chemical species concentrations are coupled to one another since their creation and destruction involve reactions which depend on the other species. Because these species can have several sources and sinks, the changes in species concentrations could be subject to concentrations which vary over multiple spatial scales. Equations such as these are referred to as *stiff equations*. In principle, one must follow the variations in the solutions on the shortest length scales in order to avoid catastrophic stability loss.

For example, consider the following equation as a simple version of a chemical rate equation

$$\dot{y} \;=\; -\,c\,y \tag{B.1}$$

where y represents some species and the constant $c > 0$ is the rate constant for the reaction. If one wanted to solve this equation numerically, the general method for solving this is to use an explicit scheme (i.e. Euler Method) of evaluating y at the new location in terms of y at the old location

$$y_{n+1} \;=\; y_n \;+\; h\,\dot{y}_n \;=\; (1 \;-\; c\,h)\,y_n \;. \tag{B.2}$$

This method is unstable if the stepsize $h > 2/c$, because $|y_n| \to \infty$ as $n \to \infty$.

One way to overcome this problem without resorting to extremely small stepsizes necessary to accommodate the most dynamic terms is to solve the equation

implicitly by finding the value of the right-hand side of the previous equation at the new y location. Therefore, we have

$$y_{n+1} \;=\; y_n \;+\; h\,\dot{y}_{n+1}\;. \tag{B.3}$$

If we evaluate Equation B.1 for y_{n+1}, we get

$$\dot{y}_{n+1} \;=\; -\,c\,y_{n+1}\;. \tag{B.4}$$

Substituting this into the right-hand side of Equation B.3 yields

$$y_{n+1} \;=\; y_n \;-\; c\,h\,y_{n+1}\;, \tag{B.5}$$

which, when rewritten, is

$$y_{n+1} \;=\; \frac{y_n}{(1 \;+\; c\,h)}\;. \tag{B.6}$$

This now makes y_{n+1} stable over all h since $c > 0$ and $h > 0$.

Now, if we extrapolate these results to a system of equations represented by the vectors $\mathbf{y}$ and $\dot{\mathbf{y}}$

$$\mathbf{f}(\mathbf{y}) \;=\; \dot{\mathbf{y}} \tag{B.7}$$

will be evaluated using the implicit scheme such that

$$\mathbf{y}_{n+1} \;=\; \mathbf{y}_n \;+\; h\,\mathbf{f}(\mathbf{y}_{n+1})\;. \tag{B.8}$$

This gets extremely difficult to solve for an entire system of equations. However, upon linearization of this equation using Newton's method, we get

$$\mathbf{y}_{n+1} \;=\; \mathbf{y}_n \;+\; h\left[\mathbf{f}(\mathbf{y}_n) \;+\; \left.\frac{\partial \mathbf{f}}{\partial \mathbf{y}}\right|_{\mathbf{y}_n} \cdot\; (\mathbf{y}_{n+1} \;-\; \mathbf{y}_n)\right]\;, \tag{B.9}$$

where $\partial\mathbf{f}/\partial\mathbf{y}$ is a matrix of partial derivatives of all of the equations involved. This equation can then be rewritten in the form

$$\mathbf{y}_{n+1} \;=\; \mathbf{y}_n \;+\; h\left[\mathbf{1} \;-\; h\,\frac{\partial \mathbf{f}}{\partial \mathbf{y}}\right]^{-1} \mathbf{f}(\mathbf{y}_n)\;. \tag{B.10}$$

This becomes the semi-implicit method of solving the system of equations.

Because the modified midpoint method is explicit, variations on the above equations are used to make the method work for semi-implicit schemes. Here, a technique developed by Bader & Deuflhard (1983) is used. The result is known as the *semi-implicit midpoint rule*:

$$\left[\mathbf{1} - h\frac{\partial \mathbf{f}}{\partial \mathbf{y}}\right]\mathbf{y}_{n+1} = \left[\mathbf{1} + h\frac{\partial \mathbf{f}}{\partial \mathbf{y}}\right]\mathbf{y}_{n-1} + 2h\left[\mathbf{f}(\mathbf{y}_n) - \frac{\partial \mathbf{f}}{\partial \mathbf{y}}\mathbf{y}_n\right] \qquad \text{(B.11)}$$

The matrix in brackets on the left-hand side of the equation is inverted using LU decomposition and backsubstitution, where the matrix is converted into two matrices, (one upper triangular, the other lower triangular), the product of which is the original matrix.

Figure B.1 is a flowchart showing the essential features of the program. The subroutines from Press et al. (1992) are used to perform the Bulirsch-Stoer routine in the program. The following are brief descriptions of these routines, in the general order in which they are encountered in the program:

- **odeint** – The driver routine for solving ODEs. It evaluates the scaling with which to monitor accuracy, stores any intermediate steps, and returns the final values to the main program to be written to file when the integration is complete.

- **derivs** – Solves the righthand side of the ODEs for all chemical species, adding up all formation and destruction mechanisms.

- **stifbs** – The routine which tells the program to do the numerical integration according to the Bulirsch-Stoer routine, modified for the semi-implicit integration scheme.

- **jacobn** – Evaluate the Jacobian matrix ($\partial \mathbf{f}/\partial \mathbf{y}$ in the description above).
- **simpr** – Performs the semi-implicit midpoint rule.
- **ludcmp** – Performs the LU decomposition of the matrix.
- **lubksb** – Performs the LU backsubstitution.
- **pzextr** – Fits a polynomial to the solution provided by **simpr** and evaluates it at zero stepsize.

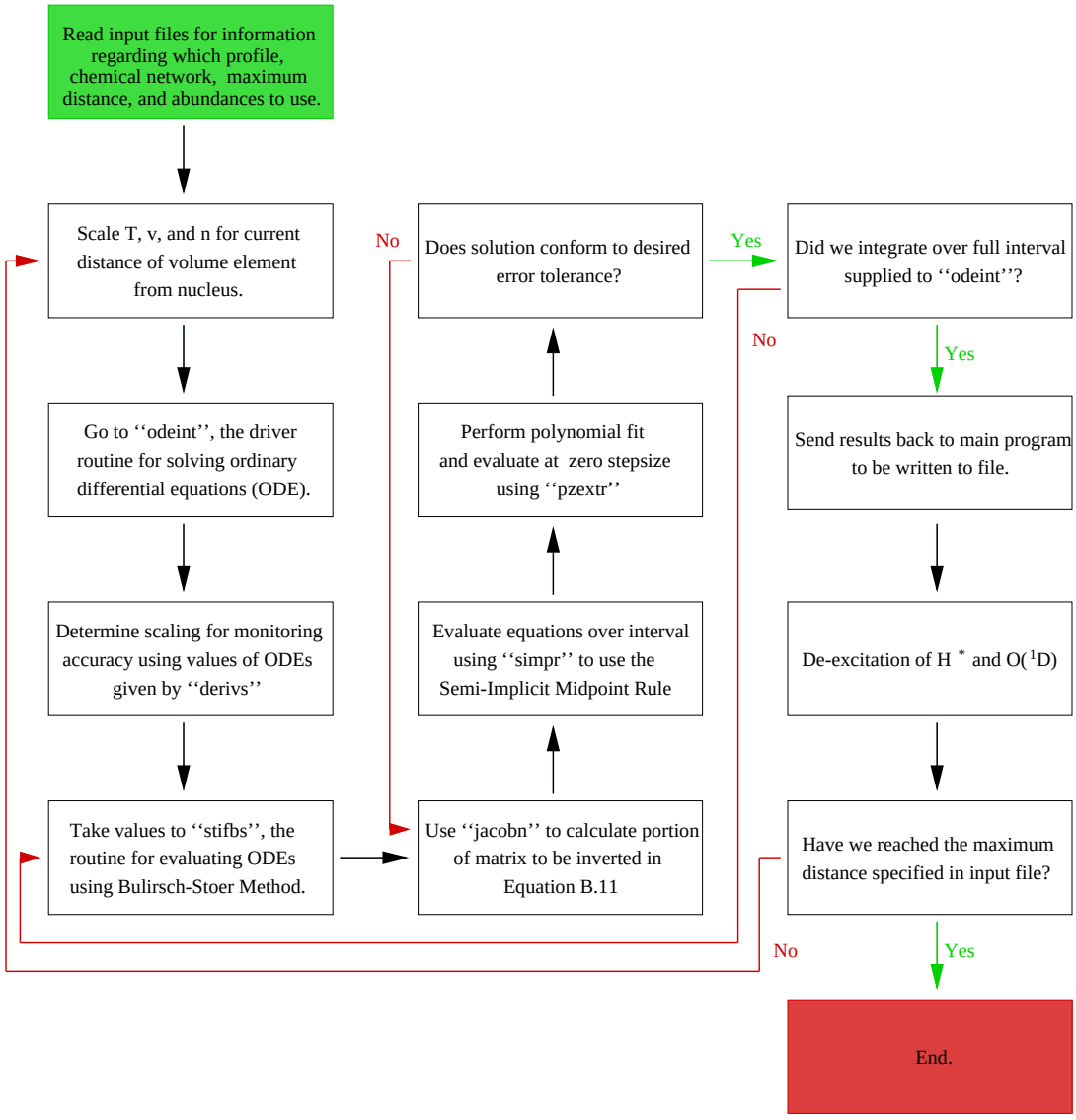

Figure B.1 – A flowchart illustrating the main features of the numerical integration process.

Appendix C

Attenuation of Ultraviolet Radiation

In a gas-rich cometary coma, ultraviolet radiation is attenuated by photochemistry. Since H_2O is by far the dominant coma species, it is the primary molecule responsible for the attenuation of ultraviolet radiation. The following is a description of the attenuation process as it occurs in the model. This treatment was originally used in the models of Marconi & Mendis (1982), but has also been used in models developed by others.

The three photochemical processes associated with H_2O, with their relevant wavelength regimes, are:

- $H_2O \rightarrow H^* + OH \quad \lambda \leq 1860$ Å
- $H_2O \rightarrow H_2 + O \quad \lambda \leq 1450$ Å
- $H_2O \rightarrow H_2O^+ + e^- \quad \lambda \leq 984$ Å

The ultraviolet spectrum over which the photochemical processes are important is divided into three wavelength regimes. Let J_1 be the solar UV flux in the wavelength range 1450 - 1860 Å, J_2 be the flux in the range 984 - 1450 Å, and J_3 be the flux in the range 0 - 984 Å. For each J_i, the rate of change in the coma is

represented by

$$\frac{dJ_i}{dr} = \sum_{j=1}^{3} \overline{\sigma}_{ji}\, n_{H_2O}\, J_i \tag{C.1}$$

where $\overline{\sigma}_{ji}$ is the average photodestruction cross section of H_2O for process j in wavelength range i and n_{H_2O} is the number density of H_2O. Therefore, for a given distance, r, in the coma, the flux is given by

$$J_i(r) = J_i(\infty)\, exp(-\tau_i(r)), \tag{C.2}$$

where $J_i(\infty)$ is the unattenuated solar flux in wavelength range i at 1 A.U., and τ_i is given by

$$\tau_i(r) = \sum_{j=1}^{3} \overline{\sigma}_{ji} \int_r^{\infty} n_{H_2O}\, dr. \tag{C.3}$$

The values for J_i (in $cm^{-2}\ s^{-1}$) are $J_1 = 3.5 \times 10^{12}$, $J_2 = 4.2 \times 10^{11}$, and $J_3 = 4.5 \times 10^{10}$. Values for $\overline{\sigma}_{ji}$ are given in Table C.1.

In similar spirit to the derivation of the attenuated UV flux, the photochemical rates in the attenuated UV field become

$$k_{ji}(r) = k_{ji}(\infty)\, exp(-\tau_i(r)) \tag{C.4}$$

where k_{ji} is the rate constant (in s^{-1}) for photochemical process j in wavelength range i, and $k_{ji}(\infty)$ is the rate constant for unattenuated radiation (see Table 2.1).

The attenuation in this model is only applied to the H_2O chemistry, because its photochemical products are important in the two-body chemical reactions. The photodissociation of HCOOH, HCO, and H_2CO occur at visible wavelengths, which aren't severely attenuated. The photodissociation of CH_3OH is not attenuated because its photochemistry is not significant to CO formation or destruction in the inner coma where the attenuation is high. By similar reasoning, the attenuation of CO and CO_2 are also not included.

Table C.1. Photodestruction Cross Sections for H_2O

Wavelength Range i	$\overline{\sigma}_{1i}$ (cm^2)	$\overline{\sigma}_{2i}$ (cm^2)	$\overline{\sigma}_{3i}$ (cm^2)
1	2.6×10^{-18}	0.0	0.0
2	2.9×10^{-18}	2.4×10^{-18}	0.0
3	2.9×10^{-18}	1.0×10^{-18}	8.4×10^{-18}

In order to calculate τ_i, the number density profile of H_2O must be known over the entire coma. Therefore, an unattenuated case will be calculated first to get n_{H_2O} throughout the coma.

BIBLIOGRAPHY

A'Hearn, M. F. 2005. Deep Impact: The experiment. *Bull. Am. Astron. Soc.* **37**, 35.02.

A'Hearn, M. F., C. Arpigny, P. D. Feldman, W. M. Jackson, R. Meier, H. A. Weaver, D. D. Wellnitz, and L. M. Woodney 2000. Formation of S_2 in comets. *Bull. Am. Astron. Soc.* **32**, 44.01.

A'Hearn, M. F., and Feldman, P. D. 1980. Carbon in comet Bradfield (1979l). *Astrophys. J. Lett.* **242**, 187-190.

Allen, M. 1991. Carbon suboxide in Halley. *Nature* **354**, 272.

Bader, G., and P. Deuflhard 1983. *Numerische Mathematik*, **41**, 373-398. (As referenced in Press et al., 1992).

Bar-Nun, A., and Kleinfeld, I. 1989. On the temperature and gas composition in the region of comet formation. *Icarus* **80**, 243-253.

Bhardwaj, A. and S. A. Haider 2002. Chemistry of O(^{1}D) atoms in the coma: Implications for cometary missions. *Adv. Space Res.* **29**, 745-750.

Biermann K. 1968. *JILA Rep.* 93.

Biermann, L, and E. Trefftz 1964. Über die Mechanismen der Ionisation und der Anregung in Kometenatmosphären. *Z. Astrophys.* **59**, 1-28.

Biver, N., D. Bockelée-Morvan, J. Crovisier, J. K. Davies, H. E. Matthews, J. E. Wink, H. Rauer, P. Colom, W. R. F. Dent, D. Despois, R. Moreno, G. Paubert, D. Jewitt, and M. Senay. 1999. Spectroscopic monitoring of comet C/1996 B2 (Hyakutake) with the JCMT and IRAM radio telescopes. *Astron. J.* **118**, 1850-1872.

Bockelée-Morvan, D., J. Boissier, J. Crovisier, F. Henry, and H. A. Weaver 2005. The carbon monoxide extended source in comet Hale-Bopp revisited. *Bull. Am. Astron. Soc.* **37**, 11.07.

Bockelée-Morvan, D., and J. Crovisier 1987. The role of water in the thermal balance of the coma. In *On the Diversity and Similarity of Comets ESA SP-278*, 235-240.

Bockelée-Morvan D., J. Crovisier, M. J. Mumma, and H. A. Weaver 2004. The composition of cometary volatiles. In *Comets II* (M. C. Festou, H. U. Keller, and H. A. Weaver, eds.), The University of Arizona Press, Tucson, Arizona.

Bockeleée-Morvan, D. D. C. Lis, J. E. Wink, D. Despois, J. Crovisier, R. Bachiller, D. J. Benford, N. Biver, P. Colom, J. K. Davies, E. Gérard, B. Germain, M. Houde, D. Mehringer, R. Moreno, G. Paubert, T. G. Phillips, and H. Rauer 2000. New molecules found in comet C/1995 O1 (Hale-Bopp). Investigating the link between cometary and interstellar material. *Astron. Astrophys.* **353**, 1101-1114.

Boehnhardt, H., H. Fechtig, and V. Vanysek 1990. The possible role of organic polymers in the structure and fragmentation of dust in the coma of comet P/Halley. *Astron. Astrophys.* **231**, 543-547.

Boice, D. C., L. A. Soderblom, D. T. Britt, R. H. Brown, B. R. Sandel, R. V. Yelle, B. J. Buratti, Hicks, Nelson, Rayman, J. Oberst, and N. Thomas 2002. The Deep Space 1 encounter with comet 19P/Borrelly. *Earth, Moon, Planets* **89**, 301-324.

Brooke, T. Y., H. A. Weaver, G. Chin, D. Bockelée-Morvan, S. J. Kim, and L.-H. Xu 2003. Spectroscopy of comet Hale-Bopp in the infrared. *Icarus* **166**, 167-187.

Brown, M. E., and H. Spinrad 1993. The velocity distribution of cometary hydrogen: Evidence for high velocities? *Icarus* **104**, 197-205.

Carruthers, G. R., C. B. Opal, T. L. Page, R. R. Meier, and D. K. Prinz 1974. Lyman-α imagery of comet Kohoutek. *Icarus.* **23**, 526-537.

Chang, S., T. Scattergood, S. Aronowitz, and J. Flores 1979. Organic chemistry on Titan. *Rev. Geophys. and Space Phys.* **17**, 1923-1933.

Charnley, S. B., and T. J. Millar 1994. The chemistry of phosphorus in hot molecular cores. *Mon. Not. R. Astron. Soc.* **270**, 570-574.

Cochran, A. L. 1985. A re-evaluation of the Haser model scale lengths for comets. *Astron. J. 90*, 2609-2514.

Cochran, A. L., and W. D. Cochran 2001. Observations of O(^{1}S) and O(^{1}D) in spectra of C/1999 S4 (LINEAR). *Icarus* **154**, 381-390.

Code, A. D., T. E. Houck, and C. F. Lillie 1972. Scientific results from the Orbiting Astronomical Observatory (OAO-2). *NASA-SP*, A. D. Code, ed. **310**, 109.

Colwell, J. E., and B. M. Jakosky 1987. The evolution of topography on a comet. *Icarus* **72**, 128-134.

Colwell, J. E., B. M. Jakosky, B. J. Sandor, and S. A. Stern 1990. Evolution of topography on comets. II. Icy Craters and Trenches. *Icarus* **85**, 205-215.

Combes, M., V. I. Moroz, J.-F. Crifo, J. M. Lamarre, J. Charra, N. F. Sanko, A. Soufflot, J. P. Bibring, S. Cazes, N. Coron, J. Crovisier, C. Emerich, T. Encrenaz, R. Gispert, A. V. Grigoryev, G. Guyot, V. A. Krasnopolsky, Nikolsky, V. Yu, and F. Rocard 1986. Infrared sounding of comet Halley from Vega 1. *Nature* **321**, 266-268.

Combi, M. R. 1987. Sources of cometary radicals and their jets - Gases or grains. *Icarus* **71**, 178-191.

Combi, M. R. 1989. The outflow speed of the coma of Halley's comet. *Icarus* **81**, 41-50.

Combi, M. R. 2002. Hale-Bopp: What makes a big comet different? Coma Dynamics: Observations and theory. *Earth Moon Planets* **89**, 73-90.

Combi, M. R., and A. H. Delsemme 1980. Neutral cometary atmospheres. I. Average random walk model for dissociation in comets. *Astrophys. J.* **237**, 663-641.

Combi, M. R., and W. H. Smyth 1988. Monte Carlo particle-trajectory models for neutral cometary gases. II. The spatial morphology of the Lyman-Alpha coma. *Astrophys. J.* **327**, 1026-1059.

Combi, M. R., B. J. Bos, and W. H. Smyth 1993. The OH distribution in cometary atmospheres: A collisional monte carlo model for heavy species. *Astrophys. J.* **408**, 668-677.

Combi, M. R., M. E. Brown, P. D. Feldman, H. U. Keller, R. R. Meier, and W. H. Smyth 1998. Hubble Space Telescope ultraviolet imaging and high-resolution spectroscopy of water photodissociation products in comet Hyakutake (C/1996 B2). *Astrophys. J.* **494**, 816-821.

Combi, M. R., W. M. Harris, and W. H. Smyth 2004. Gas dynamics and kinetics in the cometary coma: Theory and observations. In *Comets II* (M. C. Festou, H. U. Keller, and H. A. Weaver, eds.), The University of Arizona Press, Tucson, Arizona.

Cosmovici, C. B., and S. Ortolani 1984. Detection of new molecules in the visible spectrum of comet IRAS-Araki-Alcock (1983 d). *Nature* **310**, 122-124.

Cottin, H., M. C. Gazeau, Y. Benilan, and F. Raulin 2001. Polyoxymethylene as parent molecule for the formaldehyde extended source in comet Halley. *Astrophys. J. Lett.* **556**, 417-420.

Crifo, J. F., and A. V. Rodionov 1997. The dependence of the circumnuclear coma structure on the properties of the nucleus. II. First investigation of the coma surrounding an homogeneous, aspherical nucleus. *Icarus* **129**, 72-93.

Crifo, J. F., and A. V. Rodionov 1999. Modeling the circumnuclear coma of comets: objectives, methods, and recent results. *Planet. Space Sci.* **47**, 797-826.

Crovisier, J. 1999. Infrared observations of volatile molecules in comet Hale-Bopp. *Earth, Moon, Planets* **79**, 125-143.

Crovisier, J., D. Bockelée-Morvan, N. Biver, P. Colom, P. Despois, and D. C. Lis 2004. Ethylene glycol in comet C/1995 O1 (Hale-Bopp). *Astron. Astrophys. Lett.* **418**, 35-38.

Crovisier, J., D. Bockelée-Morvan, N. Biver, P. Colom, P. Despois, D. C. Lis, and others 2004. The composition of ices in comet C/1995 O1 (Hale-Bopp) from radio spectroscopy. Further results and upper limits on undetected species. *Astron. Astrophys.* **418**, 1141-1157.

Crovisier, J., T. Encrenaz, and M. Combes 1991. Carbon suboxide in comet Halley. *Nature* **353**, 610.

DiSanti, M. A., M. J. Mumma, N. Dello Russo, and K. Magee-Sauer 2001. Carbon monoxide production and excitation in comet C/1995 O1 (Hale-Bopp): Isolation of native and distributed CO sources. *Icarus* **153**, 361-390.

Eberhardt, P. 1999. Comet Halley's gas composition and extended sources: Results from the neutral mass spectrometer on *Giotto*. *Space Science Reviews* **90**, 45-52.

Eberhardt, P., D. Krankowsky, W. Schulte, U. Dolder, P. Lämmerzahl, J. J. Berthelier, J. Woweries, U. Stubbemann, R. R. Hodges, J. H. Hoffman, and J. M. Illiano 1987. The CO and N_2 abundance in comet P/Halley. *Astron. Astrophys.* **187**, 481-484.

Eddington, A. S. 1910. The envelopes of c 1908 (Morehouse). *Mon. Not. Royal Astron. Soc.* **70**, 442-458.

Feldman, P. D., and W. H. Brune 1976. Carbon production in comet West 1975n. *Astrophys. J. Lett.* **209**, 45-48.

Feldman, P. D. 1978. A model of carbon production in a cometary coma. *Astron. Astrophys.* **70**, 547-553.

Festou, M. C. 1981. The density distribution of neutral compounds in cometary atmospheres. *Astron. Astrophys.* **95**, 69-79.

Festou, M. C., and P. D. Feldman 1981. The forbidden oxygen lines in comets. *Astron. Astrophys.* **103**, 154-159.

Festou, M. C., and P. D. Feldman 1987. Comets. In *Exploring the Universe with the IUE Satellite.* (Y. Kondo, ed.), Astrophysics and Space Science Library **129**, 101-118, D. Reidel, Dordrecht, Holland.

Fink, U., and M. D. Hicks 1996. A survey of 39 comets using CCD spectroscopy. *Astrophys. J.* **459**, 729-743.

Fink, U., and J. R. Johnson 1984. Luminosity and spatial distribution of the [O I] 6300-Å emission in comets. *Astronomical J.* **89**, 1665-1672.

Flynn, G. W. 1989. Chemical cartography: Finding the keys to the kinetic labyrinth. *Science* **246**, 1009-1015.

Francis, P. J. 2005. The demographics of long-period comets. *Astrophys. J.* **635**, 1348-1361.

Gerakines, P. A., and M. H. Moore 2001. Carbon suboxide in astrophysical ice analogs. *Icarus* **154**, 372.

Gibb, E. L., M. J. Mumma, N. Dello Russo, M. A. DiSanti, and K. Magee-Sauer 2003. Methane in Oort cloud comets. *Icarus*, **165**, 391-406.

Giguere, P. T., and W. F. Huebner 1978. A model of comet comae. I. Gas-phase chemistry in one dimension. *Astrophys. J.* **223**, 638-654.

Gladman, B. 2005. The Kuiper belt and the solar system's comet disk. *Science* **307**, 71-75.

Glinski, R. J., B. J. Ford, W. M. Harris, C. M. Anderson, and J. P. Morgenthaler 2004. Oxygen/Hydrogen chemistry in the inner comae of active comets. *Astrophys. J.* **608**, 601-609.

Goldfield, E. M., S. K. Gray, and L. B. Harding 1993. Quantum dynamics of Renner-Teller vibronic coupling: The predissociation of HCO. *J. Chem. Phys.* **99**, 5812-5827.

Gombosi, T. I., T. E. Cravens, and A. F. Nagy 1985. A time-dependent dusty gasdynamical flow near cometary nuclei. *Astrophys. J.* **293**, 328-341.

Gomes, R., H. F. Levison, K. Tsiganis, and A. Morbidelli 2005. Origin of the cataclysmic Late Heavy Bombardment period of the terrestrial planets. *Nature* **435**, 466-469.

Gould, R. J., and E. E. Salpeter 1963. The interstellar abundance of the hydrogen molecule: I. Basic processes. *Astrophys. J.* **138**, 393-407.

Greenberg, J. M., and A. Li 1998. From interstellar dust to comets: The extended CO source in comet Halley. *Astron. Astrophys.* **332**, 374-384.

Gutiérrez, P. J., J. L. Oritz, R. Rodrigo, and J. J. López-Moreno 2000. A study of water production and temperature of rotating irregularly shaped cometary nuclei. *Astron. Astrophys.* **355**, 809-817.

Gutiérrez, P. J., J. L. Oritz, R. Rodrigo, and J. J. López-Moreno 2001. Effects of irregular shape and topography in thermophysical models of heterogeneous cometary nuclei. *Astron. Astrophys.* **374**, 326-336.

Hanner, M. S. 1985. A preliminary look at the dust in comet Halley. *Adv. Space Res.* **5**, 325-334.

Haser, L. 1957. Distribution d'intensité dans la tête d'une cométe. *Bull. Acad. Roy. Belgique*, Classes des Sciences, Ser. 5, **43**, 740-750.

Heidner, R. F., III, D. Husain, and J. R. Weisenfeld 1973. Kinetic investigation of electronically excited oxygen atoms, $O(2^1D_2)$, by time-resolved attenuation of atomic resonance radiation in the vacuum ultraviolet. Part 2. Collisional quenching by the atmospheric gases N_2, O_2, CO, CO_2, H_2O, and O_3. *J. Chem. Soc. Faraday Trans. 2* **69**, 927-938.

Henry, F., D. Bockelée-Morvan, J. Crovisier, and J. Wink 2002. Observations of rotating jets of carbon monoxide in comet Hale-Bopp with the IRAM interferometer. *Earth, Moon, Planets*, **90** 57-60.

Herbst, E., and D. Talbi 1998. The rate of the reaction between H and DCN. *Astron. Astrophys.* **338**, 1080-1083.

Herzberg, G. 1950. *Molecular Spectra and Molecular Structure: I. Spectra of Diatomic Molecules*, D. Van Nostrand Company, Princeton, New Jersey.

Herzberg, G., and E. Teller 1933. *Z. Phys. Chemie* **B21**, 410. (As referenced in Herzberg 1950.)

Hoban, S. M., Mumma, D. C. Reuter, M. DiSanti, R. R. Joyce, and A. Storrs 1991. A tentative identification of methanol as the progenitor of the 3.52-micron emission feature in several comets. *Icaurs* **93**, 122-134.

Hodges, R. R. 1990. Monte Simulation of nonadiabatic expansion in cometary atmospheres – Halley. *Icarus* **83**, 410-433.

Huebner, W. F. 1970. Einige Mikrowellenübergränge für en Kometen und im interstellaren Raum vermutete Moleküle. *Astron. Astrophys.* **7**, 359-366. (As referenced by Oppenheimer, 1975, p. 257.)

Huebner, W. F. 1987. First polymer in space identified in comet Halley *Science* **237**, 628-630.

Huebner, W. F., and P. T. Giguere, 1980. A model of comet comae. II Effects of solar photodissociative ionization. *Astrophys. J.* **238**, 753-762.

Huebner, W. F. J. J. Keady, D. C. Boice, H. U. Schmidt, and R. Wegmann 1987. Chemico-physical models of cometary atmospheres. In *Astrochemistry: IAU Symposium 120*, (M. S. Vardya and S. P. Tarafdar, eds.), D. Reidel, Dordrecht, Holland.

Huebner, W. F., J. J. Keady, and S. P. Lyon 1992. Solar photo rates for planetary atmospheres and atmospheric pollutants. *Astron. Astrophys. Suppl.* **195**, 102-104.

Huntress, W. T., M. Allen, and M. Delitsky 1991. Carbon suboxide in comet Halley? *Nature* **352**, 316-318.

Huxley, L. G. H., and Crompton, R. W. 1962. The motions of slow electrons in gases. *Atomic and Molecular Processes*, Academic Press, New York.

Ip, W.-H. 1989. Photochemical heating of cometary comae. III – The radial variation of the expansion velocity of CN shells in Comet Halley. *Astrophys. J.* **346**, 475-480.

Johnson, R. E. 1991. Irradiation effects in a comet's outer layer. *J. Geophys. Res.*, **96**, 17553-17557.

Kawakita, H., and J. Watanabe 2002. Unidentified bands in comet Ikeya-Zhang (C/2002 C1): The correlation between unidentified bands and H_2O^+. *Astrophys. J. Lett.* **574**, 183-185.

Keller, H. U. 1971. Wasserstoff als Dissoziationsprodukt in Kometen. *Mitt. Astron. Ges.* **30**, 143-147.

Keller, H. U. 1976. The interpretations of ultraviolet observations of comets. *Space Science Reviews.* **18**, 641-684.

Keller, H. U., and G. E. Thomas 1975. A cometary hydrogen model - Comparison with OGO-5 measurements of comet Bennett (1970 II). *Astron. Astrophys.* **39**, 7-19.

Keller, H. U., W. A. Delamere, W. F. Huebner, H. J. Reitsema, H. U. Schmidt, F. L. Whipple, K. Wilhelm, W. Curdt, R. Kramm, N. Thomas, C. Arpigny, C. Barbieri, R. M. Bonnet, S. Cazes, M. Coradini, C. B. Cosmovici, D. W. Hughes, C. Jamar, D. Malaise, K. Schmidt, W. K. H. Schmidt, and P. Seige 1987. Comet P/Halley's nucleus and its activity. *Astron. Astrophys.* **187**, 807-823.

Kissel, J., D. E. Brownlee, K. Buchler, B. C. Clark, H. Fechtig, E. Grün, K. Hornung, E. B. Igenbergs, E. K. Jessberger, F. R. Krueger, H. Kuczera, J. A. M. McDonnell, G. M. Morfill, J. Rahe, G. H. Schwehm, Z. Sekanina, N. G. Utterback, H. J. Volk, and H. A. Zook 1986. Composition of comet Halley dust particles from Giotto observations. *Nature* **321**, 336-337.

Klavetter, J. J., and M. F. A'Hearn 1994. An extended source for CN jets in comet P/Halley. *Icarus* **107**, 322-334.

Krankowsky, D., P. Lämmerzahl, I. Herrwerth, J. Woweries, P. Eberhardt, U. Dolder, U. Herrmann, W. Schulte, J. J. Berthelier, J. M. Illiano, R. R. Hodges, and J. H. Hoffmann 1986. In situ gas and ion measurements at comet Halley. *Nature* **321**, 326-330.

Lederer, S. M. 2000. *An Analysis of OH, C_2, and CN Jets in Comet Hale-Bopp (C/1995 O1)*, Ph.D. Thesis, University of Florida.

Le Teuff, Y. H., T. J. Millar, and A. J. Markwick 2000. The UMIST database for astrochemistry 1999. *Astron. Astrophys.* **146**, 157-168.

Lifshitz, A., and J. V. Michael 1991. Rate constants for the reaction, $O + H_2O \rightarrow OH + OH$, over the temperature range, 1500-2400 K, by the flash-photolysis technique: A further consideration of the back reaction. *Symp. Int. Combust. Proc.* **23**, 59-67.

Lis, D. C., J. Keene, K. Young, T. G. Phillips, D. Bockelée-Morvan, J. Crovisier, P. Schilke, P. F. Goldsmith, and E. Bergin 1997. Spectroscopic observations of comet C/1996 B2 (Hyakutake) with the Caltech Submillimeter Observatory. *Icarus*, **130**, 355-372.

Lovell, A. J., F. P. Schloerb, E. A. Bergin, J. E. Dickens, C. H. DeVries, M. C. Senay, and W. M. Irvine 1999. HCO^+ in the coma of comet Hale-Bopp. *Earth, Moon, Planets* **77**, 253-258.

Magee-Sauer, K., F. L. Roesler, F. Scherb, J. Harlander, R. J. Oliversen 1988. Spatial distribution of $O(^1D)$ from comet Halley. *Icarus* **76**, 89-99.

Magnani, L., and M. F. A'Hearn 1986. CO^+ fluorescence in comets. *Astrophys. J.* **302**, 477-487.

Marconi, M. L., and D. A. Mendis 1982. The photochemical heating of the cometary atmosphere. *Astrophys. J.* **260**, 386-394.

Marconi, M. L., and D. A. Mendis 1983. The atmosphere of a dirty-clathrate cometary nucleus – two-phase, multifluid model. *Astrophys. J.* **273**, 381-396.

Marconi, M. L., and D. A. Mendis 1984. The effects of the diffuse radiation fields due to multiple scattering and thermal radiation by dust on the dynamics and thermodynamics of a dusty cometary atmosphere. *Astrophys. J.* **287**, 445-454.

Marshall, M. D., B. V. Pond, and M. I. Lester 2003. Intermolecular vibrations of the hydrogen bonded OH-CO reactant complex. *J. Chem. Phys.* **118**, 1196-1205.

McGlynn, T. A., and R. D. Chapman 1989. On the nondetection of extrasolar comets. *Astrophys. J. Lett.* **346**, 105-108.

Meier, R. R., C. B. Opal, H. U. Keller, T. L. Page, and G. R. Carruthers 1976. Hydrogen production rates from Lyman-α images of comet Kohoutek (1973 XII). *Astron. Astrophys.* **52**, 283-290.

Meier, R., P. Eberhardt, D. Krankowsky, and R. R. Hodges 1992. The extended formaldehyde source in comet P/Halley. *Astron. Astrophys.* **277**, 677-690.

Milam, S. N., C. Savage, L. M. Ziurys, and S. Wyckoff 2004. HCO^+ observations toward comet Hale-Bopp (C/1995 O1): Ion-molecule chemistry and evidence for a volatile secondary source. *Astrophys. J.* **615**, 1054-1062.

Mitchell, D. L., R. P. Lin, K. A. Anderson, C. W. Carlson, D. W. Curtis, A. Korth, H. Reme, J. A. Sauvaud, C. D'Uston, and D. A. Mendis 1989. Complex organic ions in the atmosphere of comet Halley. *Adv. Space Res.* **9**, 35-39.

Mitchell, G. F., S. S. Prasad, and W. T. Huntress 1981. Chemical model calculations of C_2, C_3, CH, CN, OH, and NH_2 abundances in cometary comae. *Astrophys. J.* **244**, 1087-1093.

Moore, M. H. 1981. *Studies of Proton-Irradiated Cometary-Type Ice Mixtures.* Ph.D. Thesis, University of Maryland.

Moore, M. H. B. Donn, R. Khanna, and M. F. A'Hearn 1983. Studies of proton-irradiated ice mixtures. *Icarus*, **54**, 388-392.

Moore, M. H., and T. Tanabe 1990. Mass spectra of sputtered polyoxymethylene: Implications for comets. *Astrophys. J. Lett.* **365**, 39-42.

Mumma, M. J., H. A. Weaver, H. P. Larson, D. S. Davis, and M. Williams 1986. Detection of water vapor in Halley's comet. *Science* **232**, 1523-1528.

Mumma, M. J., W. E. Blass, H. A. Weaver, and H. P. Larson 1988. Measurements of the ortho-para ratio and nuclear spin temperature of water vapor in comets Halley and Wilson (1986l) and implications for their origin and evolution.. *Bull. Am. Astron. Soc.* **20**, 11.04.

Mumma, M. J., P. R. Weissman, and S. A. Stern 1993. Comets and the origin of the solar system: Reading the Rosetta stone. *Protostars and Planets III*, (E. H. Levy and J. I. Lunine, eds.), University of Arizona Press, Tuscson, Arizona.

Newburn, R., C. Acton, S. Bhaskaran, D. Brownlee, A. Cheauvront, T. Duxbury, M. Hanner, B. Semenov, S. Sandford, and P. Tsou 2004. Stardust imaging of comet Wild 2: First look *Lunar Planetary Inst. Conf. Abs.* **35**, 1437.

Nickolaisen, S. L., H. E. Cartland, and C. Wittig 1992. CO internal excitation from the reaction: H + CO_2 $\rightarrow$ CO + OH. *J. Chem. Phys.* **96**, 4378-4386.

Notesco, G., A. Bar-Nun, and T. Owen 2003. Gas trapping in water ice at very low deposition rates and implications for comets. *Icarus* **162**, 183-189.

Notesco, G., and A. Bar-Nun 2005. A $\sim$25 K temperature of formation for the submicron ice grains which formed comets. *Icarus* **175**, 546-550.

Okabe, H. 1978. *Photochemistry of Small Molecules.* John Wiley & Sons, New York.

Oldershaw, G. A., and D. A. Porter 1969. Direct determination of threshold energies for the reactions of hydrogen atoms with N_2O and CO_2. *Nature* **223**, 490-491.

Oppenheimer, M. 1975. Gas phase chemistry in comets. *Astrophys. J.* **196**, 251-259.

Pierce, D. M., and M. F. A'Hearn 2003. Formation of carbon monoxide in the near-nucleus coma of comets. *Bull. Am. Astron. Soc.* **35**, 28.07.

Press, W. H., W. T. Vetterling, S. A. Teukolsky, and B. P. Flannery (Eds.) 1992. *Numerical Recipes in FORTRAN: The Art of Scientific Computing, Second Edition.* Cambridge University Press, New York.

Renner, R. 1934. *Z. Phys.* **92**, 172. (As referenced in Herzberg 1950).

Rice, J. K., and A. P. Baronavski 1991. Nonstatistical CO product distributions from the hot H-atom reaction, H + CO_2 → OH + CO. *J. Chem. Phys.* **94**, 1006-1019.

Rodgers, S. D., and S. B. Charnley 1998. HNC and HCN in comets. *Astrophys. J. Lett.* **501**, 227-230.

Rodgers, S. D., and S. B. Charnley 2001. On the origin of HNC in comet Lee. *Mon. Not. R. Astron. Soc.* **323**, 84-92.

Rodgers, S. D., and S. B. Charnley 2005. Suprathermal chemical reactions driven by fast hydrogen atoms in cometary comae. *Mon. Not. R. Astron. Soc.* **356**, 1542-1548.

Samarasinha, N. H., and M. J. S. Belton, 1994. The nature of the source of CO in comet P/Halley. *Icarus* **108**, 103-111.

Schleicher, D. G. and M. F. A'Hearn 1983. The fluorescence of cometary OH. *Astrophys. J.* **331**, 1058-1077.

Sekanina, Z. 1976. A probability of encounters with interstellar comets and the likelihood of their existence. *Icarus* **27**, 123-133.

Shimanouchi, T. Molecular vibrational frequencies. *NIST Chemistry WebBook, NIST Standard Reference Database Number 69*, P. J. Linstrom and W. G. Mal-

lard, eds. June 2005. National Institute of Standards and Technology, Gaithersburg, MD, USA (http://www.webbook.nist.gov).

Shimizu, M. 1975. Ion chemistry in the cometary atmosphere. *Astrophys. and Space Science* **36**, 353-361.

Skorov, Y. V., and H. Rickman 1998. Simulation of gas flow in a cometary Knudsen layer. *Planet. Space Sci.* **46**, 975-996.

Skorov, Y. V., and H. Rickman 1999. Gas flow and dust acceleration in a cometary Knudsen layer. *Planet. Space Sci.* **47**, 935-949.

Stern, S. A. 2003. The evolution of comets in the Oort cloud and the Kuiper belt. *Nature* **424**, 639-642.

Stern, S. A., and J. M. Shull 1988. The influence of supernovae and passing stars on comets in the Oort cloud. *Nature*, **332**, 407-411.

Stoer, J., and R. Bulirsch 1980. *Introduction to Numerical Analysis*, Springer-Verlag, New York.

Streit, G. E., C. J. Howard, A. L. Schmeltekopf, J. A. Davidson, and H. I. Schiff 1976. Temperature dependence of $O(^1D)$ rate constants for reactions with O_2, N_2, CO_2, O_3, and H_2O. *J. Chem. Phys.* **65**, 4761-4764.

Swings, P. 1943. Reports on the progress of astronomy: Cometary spectra. *Mon. Not. Royal Astron. Soc.* **103**, 86-87.

Talbi, D., and E. Herbst 2002. The gas-phase destruction of interstellar carbon dioxide: Calculations on the reactions between CO_2 and H_2 and between CO_2 and H. *Astron. Astrophys.* **386**, 1139-1142.

Tozzi, P., P. D. Feldman, and M. C. Festou 1998. Origin and production of C(^{1}D) atoms in cometary comae. *Astron. Astrophys.* **330**, 753-763.

Tully, J. C. 1975. Reactions of O(^{1}D) with atmospheric molecules. *J. Chem. Phys.* **62**, 1893-1898.

Weaver, H. A., P. D. Feldman, M. C. Festou, and M. F. A'Hearn 1981. Water production models for comet Bradfield /1979 X/. *Astrophys. J.* **251**, 809-819.

Weaver, H. A., P. D. Feldman, J. B. McPhate, M. F. A'Hearn, C. Arpigny, and T. E. Smith 1994. Detection of CO Cameron band emission in comet P/Hartley 2 (1991 XV) with the Hubble Space Telescope. *Astrophys. J.* **422**, 374-380.

Womack, M., A. Homich, M. C. Festou, J. Magnum, W. T. Uhl, and S. A. Stern 1999. Maps of HCO^+ Emission in C/1995 O1 (Hale-Bopp). *Earth, Moon, Planets* **77**, 259-264.

Woodney, L. M. 2000 *Chemistry in Comets Hale-Bopp and Hyakutake*, Ph.D. Thesis, University of Maryland.

Woodney, L. M., J. McMullin, and M. F. A'Hearn 1997. Detection of OCS in comet Hyakutake (C/1996 B2). *Planet. Space Sci.* **45**, 717-719.

Woods, T. N., P. D. Feldman, K. F. Dymond, and D. J. Sahnow 1986. Rocket ultraviolet spectroscopy of comet Halley and abundance of carbon monoxide and carbon. *Nature* **324**, 436-438.

Wu, C. Y. R., and F. Z. Chen 1993. Velocity distributions of hydrogen atoms and hydroxyl radicals produced through solar photodissociation of water. *J. Geophys. Res.* **98**, 7145-7435.

Wurm, K. 1943. Die Natur dur Kometen. *Mitt. Hamburg. Sternw.*, **8(51)**, 57-92. (As referenced in Festou et al. 2004, p.5.)

Wyckoff, S., R. S. Heyd, and R. Fox 1999. Unidentified molecular bands in the plasma tail of comet Hyakutake (C/1996 B2). *Astrophys. J. Lett.* **512**, 73-76.

Xie, X., and M. J. Mumma 1996a. Monte Carlo simulation of cometary atmospheres: Application to comet P/Halley at the time of the *Giotto* spacecraft encounter. I. Isotropic model. *Astrophys. J.* **464**, 442-456.

Xie, X., and M. J. Mumma 1996b. Monte Carlo simulation of cometary atmospheres: Application to comet P/Halley at the time of the *Giotto* spacecraft encounter. II. Axisymmetric model. *Astrophys. J.* **464**, 457-475.